OBSERVING AND MODELING
URBAN THUNDERSTORM MODIFICATION DUE TO
LAND SURFACE AND AEROSOL EFFECTS

by

Paul Edward Schmid

A Dissertation

Submitted to the Faculty of Purdue University

In Partial Fulfillment of the Requirements for the degree of

Doctor of Philosophy

Department of Earth, Atmospheric, and Planetary Sciences

West Lafayette, Indiana

May 2020

THE PURDUE UNIVERSITY GRADUATE SCHOOL
STATEMENT OF COMMITTEE APPROVAL

Dr. Dev Niyogi, Chair, Advisor
Department of Earth, Atmospheric, and Planetary Sciences

Dr. Daniel Aliaga
Department of Computer Science

Dr. Alexander Gluhovsky
Department of Earth, Atmospheric, and Planetary Sciences

Dr. Venkatesh Merwade
Department of Civil Engineering

Dr. J. Marshall Shepherd
Department of Geography, University of Georgia

Dr. Udaysankar Nair
Department of Atmospheric Science, University of Alabama in Huntsville

Approved by:
Dr. Daniel J. Cziczo

Dedicated to Paige Emily and I guess Stacey too.

ACKNOWLEDGMENTS

The work performed for this dissertation was funded with grants: NASA Earth System Science Fellowship (NESSF) NNX12AO03H, NSF AGS-1902642, NSF OAC-1835739, NSF AGS-1522494, NSF CBET 1250232, NSF AGS 0847472, and Purdue University Discretionary Funds. Parts of the research have been published in *Journal of Applied Meteorology and Climatology, Geophysical Research Letters,* and *Earth Interactions* with additional work being submitted to *Urban Climate*. A special thanks also to members of the committee without whose advising, this work would not be possible. I also thank Drs. Jon Harbor and Harshvardhan for their prior work with me as members of my committee for my preliminary examinations. Finally, I thank the staffs and students of the EAPS and Agronomy departments, the Land Surface research group, as well as the Purdue Graduate School for aiding me in reaching this point.

TABLE OF CONTENTS

LIST OF TABLES

LIST OF FIGURES

ABSTRACT

Urban meteorology has developed in parallel to other sub-fields in the science, but in many ways remains poorly described. In particular, the study of urban rainfall modification remains behind compared to other comparable features. Urban rainfall modification refers to the change of a precipitation feature as it crosses an urban area. Typically, this manifests as rainfall initiation, local suppression, local invigoration, and/or storm morphology changes. Research in the prior decades have shown urban rainfall modification to arise from a combination of land-atmosphere and aerosol-cloud interaction. Urban areas create a greater surface roughness, which produces local convergence and divergence, modifying local thunderstorm inflow and morphology. The land surface also generates vertical velocity perturbations which can act to initiate or modify existing convection. Urban aerosols act as CCN to perturb existing cloud and precipitation characteristics. Higher CCN narrows the cloud droplet distribution, creating more smaller cloud droplets, and initially reducing precipitation efficiency by keeping more liquid water in the cloud than what would form into rain. The CCN-cloud interaction eventually increasing heavy rainfall production as graupel riming is enhanced by the narrower cloud droplet distribution, leading to more larger raindrops and higher rain in areas.

This dissertation addresses the observation and modeling of urban thunderstorm interaction from both the land surface and aerosol perspective. It reassesses the original urban rainfall anomaly: The La Porte Anomaly. First analyzed in the late 1960s, the La Porte Anomaly was ultimately dismissed by 1980 as either a temporary, biased, or otherwise unexplainable observation, as the process level understanding had yet to be explained. The contemporary analysis utilizes all existing data and objective optimal interpolation to show that a rainfall anomaly downwind of Chicago has indeed existed at least since the 1930s. The current rainfall anomaly exists as a broad region of warm season rainfall downwind of Chicago that is 20-30% greater than the regional average. Using synoptic parameters, the rainfall anomaly is shown to be independent of wind direction and most closely associated with local land surface forcing. Weekdays, where local aerosol loading has been measured at 40% or more greater than weekends, have up to 50% more warm season rainfall than weekends. The analysis is able to show that there is a land surface and aerosol contribution to the rainfall anomaly, but cannot unambiguously separate them.

In order to separate the land surface and aerosol effects on urban rainfall distribution, a numerical model was improved to better handle urban weather interaction. The Regional Atmospheric Modeling System (RAMS 6.0) was chosen for its base land surface and cloud physics parameterization. The Town Energy Budget (TEB) urban canopy model was coupled to RAMS to handle the urban land surface. The Simple Photochemical Module (SPM) was coupled with the cloud physics to handle conversion of surface emissions to CCN. The model utilized an external traffic simulation to create a realistic diurnal and weekly cycle of surface emissions, based on human behavior. The new Urban RAMS was used to study the land surface sensitivity of city size and of aerosol loading in two studies using the Real Atmosphere Idealized Land surface (RAIL) method, by which all non-urban features of the land surface are removed to isolate the urban effects. The city size study determined that the land surface of a given city eventually has a maximum effect on thunderstorm modifying potential, and that rainfall does not continue to increase or decrease locally for cities larger than a certain size based on that storm's own motion. The aerosol-cloud analysis corroborated previous observations on the non-linear effects of aerosol loading on clouds. It also demonstrated that understanding the aerosol effect in an urban environment requires high resolution observations of precipitation change. In a single thunderstorm, regions can be both impacted by local rainfall rate increases and decreases from urban aerosols, leading to little total change in precipitation. But the rainfall rate changes can significantly affect soil moisture and drought potential in and around urban areas.

Following the idealized studies, the historical and current La Porte Anomaly was simulated to separate the land surface from the aerosol factors near the Chicago area. The Urban RAMS model was deployed on a real land surface with full model physics. Simulations with 1932, 1962, 1992, and 2012 land covers were run over an exceptionally wet Aug. 2007 to approximate the rain variability for an entire summer season. Surface emissions were also varied in the 2012 land cover for variable aerosol loading. The simulations successfully reproduced the location of the downwind rainfall anomaly in each land cover scenario: farther east toward La Porte in 1932, moving southwestward to its current location by 2012. Doubling surface emissions eliminated the downwind anomaly, as was observed during the highest pollution decade of the 1970s. Eliminating surface emissions also decreased the downwind anomaly. As the land cover at the upwind edge of Chicago became more connected from the 1932 to 2012 land cover scenarios, a local upwind rainfall anomaly developed, moving westward with urban expansion. The results of these simulations enabled the conclusions that a) at the upwind edge, the land surface dominates urban rainfall modification, b) the aerosol loading sustains and increases the locally downwind rainfall increase, and c) that the total modification distance is static on given day and given urban footprint. A more expansive city does not produce a rainfall anomaly more distantly downwind, but rather the distance of rainfall modification moves to where the upwind edge of the city begins.

The modeling work ends with a two-city simulation in the southeast United States, of a bow-echo forming near Memphis, TN and crossing Birmingham, AL before splitting. Simulations were performed on different surface emissions rates, land covers where Birmingham did not exist, and a novel approach with two inner emitting grids over both Birmingham and Memphis. A storm tracking algorithm enabled one-to-one comparisons of point simulated storm characteristics between scenarios. The results of most scenarios only corroborated previous research, showing how increased aerosol loading changes cloud and rainfall characteristics until the highest aerosol loading shuts down riming and rainfall enhancement. However, the two most accurate simulations, where the storm forms and splits over Birmingham, were a non-urban higher rural aerosol scenario and the scenario with Memphis also emitting pollution. In order to split the storm over Birmingham, the upwind cloud characteristics were primed by higher upwind aerosols, either from a realistic city upwind or unrealistically high rural aerosols. The conclusions produced by this study demonstrated the importance of aerosol cloud interaction, perhaps equal with land surface, but also the need for far upwind information for a storm in a given city. Memphis and Birmingham are separated by over 300km, far exceeding the threshold thought to connect two cities by mutual rainfall modification.

The overall conclusions of the research presented in this dissertation shows a more unified approach to the effects of urban rainfall modification. The upwind edge of a city is a fixed location, and a thunderstorm begins modifying at that point. The thunderstorm usually produces a local rainfall maximum at the upwind edge, due to the vertical velocity of the urban land surface. The urban aerosols proceed to narrow the cloud droplet distribution, locally reducing rainfall as the storm passes over the urban area. Eventually the enhanced rainfall from enhanced riming produces a maximum somewhere downwind. However, “downwind” is a location relative to the storm’s motion and could exist anywhere over the urban footprint or downwind in a rural region. The climatological location of increased rainfall is an average of every storm in a season and beyond. The results of each part of the study provide a way to continue the research presented here.

CHAPTER 1. INTRODUCTION

What is urban thunderstorm modification? Simply put, the observed features of a thunderstorm may change as they pass over a city, compared to a similar storm that does not. Observable features of an individual storm may increase or decrease: rainfall rate, cloud height, storm duration, lightning frequency, and many others. And when the seasonal total of thunderstorm changes is considered, an urban area can broadly change local climate through the regional variability in rainfall. Urban areas may increase the risk of local flash flooding, but in some cases can exacerbate regional drought. It is commonly cited that over 50% of the Earth's population lives on the "less than 2%" of the land surface that is developed (i.e. urban)[1], and that number is growing (Snow et al. 2012). One cannot understate the importance of understanding localized urban effects on thunderstorms and rainfall.

Urban thunderstorm interaction is forced primary from a combination of land-atmosphere and cloud-aerosol interaction. But understanding its features involves a multidisciplinary approach from within atmospheric sciences and the broader scientific community. The mechanisms by which an individual thunderstorm changes can be understood through the mesoscale dynamics of that thunderstorm. Both the land surface and the cloud-aerosol interaction impact these dynamics. The individual processes of each of these atmospheric specialties require the use of numerical weather models. Outside the immediate realm of atmospheric sciences, inadvertent weather modification in the built environment is a fundamentally human problem, given that over 50% of the population lives on such a small part of the surface. The built environment can be considered both through the lens of how it changes its local environment and how it was created in the first place – e.g. through urban planning and architecture. Human activity links the land surface with cloud physics through pollution generated on the surface which later perturbs clouds. Urban aerosols cannot exist without the people in the built environment generating through there activity. And it is ultimately the people who are impacted by localized flooding or changes in agriculture due to changes in the greater urban envelope.

[1] New research presented in Chapter 4 of this dissertation shows that the fraction of developed land on the Earth's surface is closer to 0.6% than 2%.

Finally, the study of urban thunderstorms, as a complex system within urban weather, can only be studied in the context of its own history. The first urban rainfall studies began in the 1960s. However, the processes necessary to explain observations of urban thunderstorm modification and, urban weather in general, may have not existed at the time certain studies were performed. The understanding itself is surrounded by the history of how that understanding evolved (Figure 1). The earliest studies of urban weather may be better explained by processes first researched decades later, but our contemporary research must be guided by the details of the earliest studies. This introduction is presented as a survey of our contemporary understanding of urban weather (1.2), through more fundamental processes (1.3), but always guided by the history of how it was discovered (1.1).

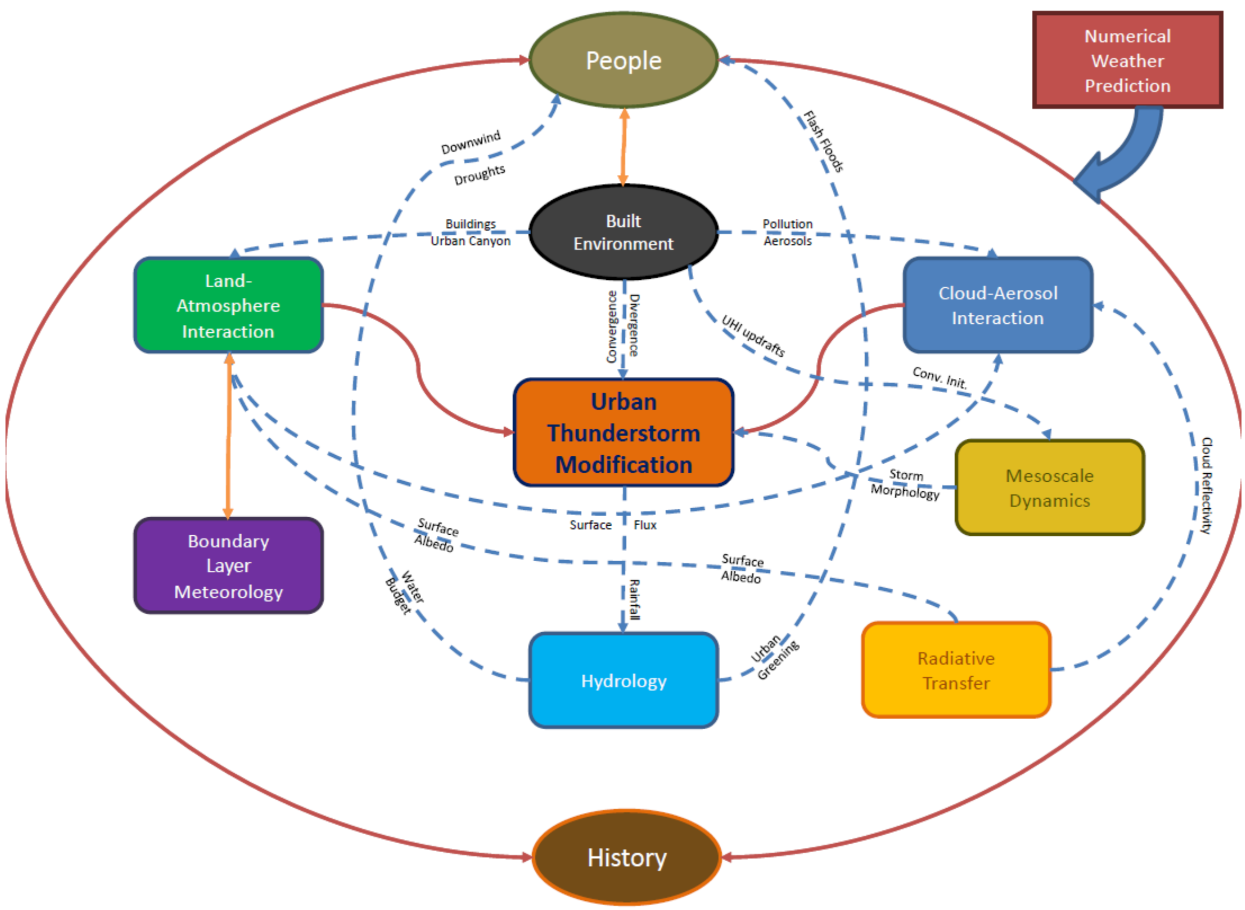

Figure 1. Conceptual flowchart of scientific disciplines in the complex system of urban thunderstorm modification.

1.1 History of Urban Rainfall Modification (pre-1900 – 2000)

The possibility that cities could impact thunderstorms and precipitation patterns was described as early as 1921 (Horton). However, the study of urban weather evolved with the innovation of meteorology as an independent science. The urban heat island (UHI), wherein the center of a city is observably warmer than its surrounding, especially at night, was first studied in detail by Luke Howard in 1833 (Mills 2008). *The Climate of London* became the first in-depth study of urban weather, however the UHI phenomenon had been at least qualitatively for centuries. In particular, Benjamin Franklin made limited observations of the effect in Philadelphia in 1752 (Meyer 1991), and it is possible that the notion of cities being warmer than surrounding areas was reported for nearly as long as cities have existed, potentially noted by Aristotle in *Politics*[2]. The bibliographies in reviews by Mills (2014) and Stewart (2019) provide a historical timeline of observational UHI research leading up to the first precipitation experiments.

From the 1920s to the 1960s, urban weather research focused mostly on temperature and UHI effects. However, there was a select few observations and experiments which noted potentially significant rainfall variability around urban areas. Changnon's 1968 "The La Porte Weather Anomaly – Fact or Fiction" (Changnon 1968) was the first scientific study that noted 1) a significant difference in rainfall across an urban area and 2) attributed cause – increased cloud water due to urban aerosols. The results were controversial because of the possibility that the increased rainfall was due to observer bias at a single site. Subsequent debate ensued as to whether the rainfall increase was "Fallacy" (Holzman 1971) or "Fact" (Changnon 1971). The increased rainfall downwind of Chicago was inconsistent from year to year and appeared to disappear entirely during the 1970s (Changnon and Huff 1977), leading to the conclusion that the rainfall feature was merely temporary (Changnon 1980a,b). Even as research on the anomaly itself concluded, debate remained as to whether it was due to observer Err (Clark 1979) or a significant urban meteorological feature (Rao 1980).

Research on La Porte, along with earlier concerns of urban areas affecting heavy rainfall (Huff and Changnon 1960) prompted the METROpolitan Meteorological EXperiment (METROMEX) (Changnon et al. 1971) to investigate urban rainfall effects outside of St. Louis.

[2] It's unclear if Aristotle was referring to literal warmth in cities, or if it was a metaphor for human personality traits.

METROMEX found that warm precipitation downwind of St. Louis increased 20-40% compared to rural areas (Dettwiller and Changnon 1976). Studies noted that weekday rain was increased compared to weekend and that the increased seasonal rainfall primarily manifested as increased heavy rainfall (Huff and Changnon 1972). Increased hail downwind and lightning over the entire urban environment was also noted (Huff and Changnon 1973; Huff 1975). METROMEX concluded that urban areas created increased rainfall downwind due to *unspecified* interactions between the urban land surface and the atmosphere and urban aerosols with clouds (Changnon et al. 1976). Much of the continued skepticism (Eichenlaub 1972; Clark 1979; Braham 1979; Dirks 1983) of the results or existence of urban rainfall modification was due to the limited scope and lack of detail into the individual atmospheric processes in METROMEX (Lowry 1998). Because of changing research priorities in the United States, METROMEX represented the high point of urban research for nearly 30 years, with most subsequent urban studies analyzing the limited data collected during the campaign (Ackerman 1985; Changnon and Huff 1986; Hjelmfelt 1982; Vukovich and King 1980). Some other studies from the time did probe urban effects on rainfall in London (Atkinson 1968), Mumbai (Khemani and Murty 1973), Washington (Harnack et al. 1975), Hungary (Lowry et al. 1978), and Tokyo (Yonetani 1982), but none with results as widely discussed as METROMEX. Lowry's 1998 "Urban Effects on Precipitation Amount" (Lowry 1998) provides a review of research to that point as well as recommendations for the future – namely designed, replicable experiments and consistency in data collection.

As noted by Lowry and reiterated by Shepherd (2005), the apparent failures of the first golden age of urban rainfall research was the inability to attribute causation of observed effects. In part, the processes behind the effect had not yet been described (see 1.3). But even if they had, the complex system of urban thunderstorm modification could not fully be described because the effects were overlapping and non-linear. While numerical weather models existed at the time (i.e. Myrup 1969), they lacked the complexity necessary to separate each factor at play in the urban climate system. By the early 21st century, computer power and weather model complexity had sufficiently evolved to begin to study the causation of observed urban rainfall patterns. But skepticism from the apparent disappearance[3] of the La Porte anomaly to the shortcomings of METROMEX ultimately resulted in its principal researchers, Stanley Changnon and Floyd Huff,

[3] Note: The anomaly did not disappear. See Chapter 2.

to never speak again. And the residual skepticism toward urban weather modification persists in the atmospheric science community over 50 years after their results were first reported (Mills 2020, personal conversation).

1.2 Contemporary Understanding of Urban Rainfall Effects (2000 – present)

From the early 2000s, our understanding of both observations and processes affecting urban rainfall variability has continued to evolve. The contemporary understanding of urban rainfall interaction is of a complex synergy between the urban land surface and urban aerosols (Grimmond et al. 2010). Our understanding is sufficient to describe the interactions but conclusions have been slow to change in the past 40 years (Mills 2014). For individual rainfall events, urban areas modify storms in one or more of the following ways:

a) Storm initiation (Ashley et al. 2011; Han and Baik 2008)
b) Local rainfall enhancement (Kishtawal et al. 2010; Yang et al. 2014; Ganeshan et al. 2013)
c) Local rainfall suppression (Rosenfeld 2000; Alpert et al. 2008; Kawecki et al. 2016)
d) Storm morphological modification, such as splitting (Bornstein and Lin 2000; Villarini et al. 2009)

Individual storms may experience both rainfall enhancement and suppression over the same urban area. And the dynamics forcing urban rainfall modification are a complex interplay between land-atmosphere interaction and urban aerosol-cloud interaction.

The urban land surface has a significant effect on local precipitation (Pielke et al. 2011). The effects of the urban heat island on rainfall result from the UHI either initiating convection or perturbing existing convection (Bornstein and Lin 2000). While the temperature increase in the UHI is strongest at night (Hu et al. 2016), the day-time UHI creates a deeper planetary boundary layer over and downwind (Han and Baik 2008) of an urban center. Similar to a land-sea breeze, the UHI creates vertical circulations across the urban land surface (Ryu et al. 2013), which initiates convection at the upwind boundary (Zhang et al. 2009), but generally suppresses moist convection over the center of large urban areas (Schmid and Niyogi 2013; Oke 1973). The urban circulations are more intense, wider, deeper vertically, and drier than those upwind in rural areas (Baik et al.

2001). Because the UHI dries the urban boundary layer, the UHI initiates moist convection (e.g. resulting in rain) only if there is a sufficiently moist upwind boundary layer (Dixon and Mote 2003; Miao et al. 2011). The bulk UHI effects produce near surface horizontal divergence upwind and convergence downwind (Bornstein and Lin 2000; Zhong and Yang 2015b), combined with competing vertical divergence at urban edges and convergence at the urban center (Lo et al. 2007). Synoptic conditions determine how these UHI features affect an existing convective system (Snow et al. 2012): Stronger external forcing favors horizontal upwind divergence which weakens or splits existing convection producing a rainfall minimum over the city and increased rainfall downwind. Weaker external forcing favors the vertical convergence which produces a precipitation maximum near the center, but would advect rainfall from initiated convection to the downwind edge. Given that many of the UHI processes were described earlier and independent of aerosol processes, it is possible that the strength and significance of urban land surface effects were misattributed to processes dominantly controlled by aerosols (Schmid and Niyogi 2017).

Different aerosol-cloud processes have the ability to change the rainfall amount, intensity, and variability in and around the urban environment (Tao et al. 2012). Increased aerosols in the urban environment yield higher cloud condensation nuclei (CCN) concentration. More concentrated CCN values yield a larger number of smaller cloud droplets in a narrower cloud droplet distribution (Twomey and Twomey 1977; Twohy et al. 2005). These small droplets reduce the efficiency of droplet growth by collision-coalescence ("warm rain" process) and reduce the number of raindrops formed at temperatures above freezing (Givati and Rosenfeld 2004) and initially suppress rainfall (Rosenfeld 2000). However, a cloud with these properties has an increased lifetime (Albrecht 1989) and deeper mixed layer (Koren 2005). Because of the smaller droplets, more supercooled liquid water exists in the mixed phase region of the cloud (Rosenfeld and Woodley 2000). This enhances graupel and hail formation by riming of ice crystals (Rosenfeld et al. 2008). The increased number of larger frozen hydrometeors eventually results in larger rain drops and thus increased rain rates and amount at the surface (Han et al. 2012). The riming enhancement is non-linear and non-monotonic (Li et al. 2008). With very high aerosol loading, the liquid cloud droplet distribution becomes so narrow that riming is decreased compared to clean-air values (Saleeby et al. 2016), resulting in decreased precipitation (Khain et al. 2011). The same riming enhancement in the mixed phase region of the cloud results in increased lightning flash density (Orville et al. 2001; Stallins et al. 2013), detectable both in individual storms and in the lightning climatology across an urban area (Bell et al. 2008). The weekly cycle of lightning (Bell et al. 2009) provides conclusive evidence of urban aerosol impacts on convective processes and may extend to hail and tornadoes (Rosenfeld and Bell 2011). Aerosol interactions are able to invigorate dynamic convection at the mesoscale (Ntelekos et al. 2009; Kawecki et al. 2016), which further enhances rainfall via increased moisture ingestion into the cloud (Lee 2012), and can prompt thunderstorm morphological changes such as splitting (Khain and Lynn 2009).

Giant CCN have an opposite impact on precipitation – enhancing the warm rain process by increased drizzle nucleation, and suppressing cold rain (Feingold et al. 1999). GCCN may form in the urban environment as large carbon aerosols, normally hydrophobic, are coated in smaller hygroscopic aerosols (Andreae and Rosenfeld 2008). Outside of cloud interaction, urban aerosols can change the intensity of the UHI: sulfate and nitrate aerosols scatter sunlight, decreasing UHI intensity (Wang et al. 2012); carbon aerosols absorb heat, increasing UHI intensity (Wang 2007). The urban aerosol interaction can be detected via a weekly cycle in rainfall intensity (Jin et al. 2005; Tuttle and Carbone 2011). While rainfall intensity increases, total rainfall from an individual storm may be unchanged or decrease due to the competing aerosol effects which reduce precipitation efficiency outside the context of riming (Li et al. 2009; Yang et al. 2011). Aerosol perturbation produce more spatially variable rainfall because of different regions of a system being preferentially enhanced or suppressed (Altaratz et al. 2014; Shi et al. 2017). The consensus on the relation between aerosols and rainfall is still evolving, but agrees that precipitation increases when aerosols increase cloud condensation: in moist environments with moderate external forcing (Khain et al. 2008). As non-local forcing increases, there must be a higher aerosol loading to produce the same effect as a more locally forced system (Carrió and Cotton 2011).

Isolating the individual urban aerosol effects on rainfall is especially difficult operationally or even in field studies because the hypothesized processes are not regularly measured (Feingold 2009). Urban aerosols also coexist in a highly non-linear interplay with the urban land surface (Deng et al. 2016) with each produces compounding or opposing effects on rainfall. Some studies thus conclude that there is no detectable relation between urban aerosols and precipitation (Jin et al. 2005; Jin and Shepherd 2008) or that the apparent aerosol effect is more related to covarying synoptic features (Storer et al. 2010; Fan et al. 2009). Other studies find a significant (Lacke et al.

2009; Berg et al. 2008) or even dominant (Zhong et al. 2015; Kawecki et al. 2016; Schmid and Niyogi 2017) effect of urban aerosols on precipitation.

Quantifying the contribution of individual land surface and aerosol effects requires the use of numerical weather models (van den Heever and Cotton 2007). Numerical models have evolved with parallel cooperative research to urban-rainfall theory (Shepherd 2005). Models are particularly useful isolating the individual land surface and aerosol sensitivities leading to rainfall modification (Shepherd et al. 2010; Chen et al. 2012; Li et al. 2013). Specific modeling studies have been undertaken in Houston (Burian and Shepherd 2005; Carrió et al. 2010), Washington-Baltimore (Zhang et al. 2011a; Ryu et al. 2016), New York (Hosannah and Gonzalez 2014), Atlanta (Dixon and Mote 2003; Shem and Shepherd 2009), Indianapolis (Niyogi et al. 2011), St. Louis (Rozoff et al. 2003), Mexico City (Ochoa et al. 2015), Tokyo (Takahashi et al. 2011), the Pearl River delta (Lo et al. 2007; Wang et al. 2014), the Yangtze River valley (Wan et al. 2013), Mumbai (Lei et al. 2008), and multiple Indian cities (Kishtawal et al. 2010). The results have led to a particular interesting in advancing urban hydrology (Chen et al. 2012), given that urban areas tend to increase heavy rainfall and are constructed of impervious surfaces more prone to flash flooding (Smith et al. 2002). Urban rainfall modification makes cities more uniquely prone to flash flooding (Villarini et al. 2009; Wright et al. 2012), especially in locally forced events (Smith et al. 2016). Recent studies on aerosol variability indicate that aerosols are the mechanism behind an increased flash flood risk (Fan et al. 2015; Zhong and Yang 2015a). But smart planning via understanding of urban hazards can help mitigating the flooding risk in both current and future climates (Yang et al. 2016).

1.3 Structure of Original Research Presented

In order to understand the individual processes behind urban rainfall variability, numerical weather models are required. Rather than present the research in the order in which it was undertaken, this dissertation is presented from the steps needed to gain a greater understanding of urban thunderstorm modification:

- Chapter 2: Observations of the La Porte Anomaly – This chapter confirms the historic and continued existence of the first well-studied urban rainfall feature (see 1.1), and uses innovative analysis to show what processes behind urban thunderstorm modification require the most attention.

- Chapter 3: Numerical Model Development – This chapter discusses the parameterizations and features used in the numerical model for the remainder of the research.
- Chapter 4: Idealized Simulations of Urban Thunderstorm Modification – This chapter presents two published studies of simulations from the model on an idealized land surface, in order to isolate urban from non-urban effects.
- Chapter 5: Modeling the Historic and Current La Porte Anomaly – This chapter shows the simulation of the La Porte Anomaly to demonstrate the sensitivity of the observed features to hypothesized processes.
- Chapter 6: A Multicity Simulation of a Thunderstorm Impacting Birmingham, Alabama – This chapter expands the urban environment to a superregional setting to show that two seemingly separated urban areas can be reconnected through by a modified thunderstorm.

Chapter 7 presents a synthesis of the results and conclusions from the prior research chapters, highlighting what new innovations have come from it. Given the human element of the urban weather system, and the growing the urban population, it ends with recommendations of where this research can proceed in the future.

1.4 References

Ackerman, B., 1985: Temporal March of the Chicago Heat Island. *J. Clim. Appl. Meteorol.*, **24**, 547–554, doi:10.1175/1520-0450(1985)024<0547:TMOTCH>2.0.CO;2.

Albrecht, B. A., 1989: Aerosols, cloud microphysics, and fractional cloudiness. *Science*, **245**, 1227–1230, doi:10.1126/science.245.4923.1227.

Alpert, P., N. Halfon, and Z. Levin, 2008: Does Air Pollution Really Suppress Precipitation in Israel? *J. Appl. Meteorol. Climatol.*, **47**, 933–943, doi:10.1175/2007JAMC1803.1.

Altaratz, O., I. Koren, L. A. Remer, and E. Hirsch, 2014: Review: Cloud invigoration by aerosols—Coupling between microphysics and dynamics. *Atmos. Res.*, **140**–**141**, 38–60, doi:10.1016/j.atmosres.2014.01.009.

Andreae, M. O., and D. Rosenfeld, 2008: Aerosol–cloud–precipitation interactions. Part 1. The nature and sources of cloud-active aerosols. *Earth-Science Rev.*, **89**, 13–41, doi:10.1016/j.earscirev.2008.03.001.

Ashley, W. S., M. L. Bentley, and J. A. Stallins, 2011: Urban-induced thunderstorm modification in the Southeast United States. *Clim. Change*, doi:10.1007/s10584-011-0324-1.

Atkinson, B. W., 1968: A Preliminary Examination of the Possible Effect of London's Urban Area on the Distribution of Thunder Rainfall 1951-60. *Trans. Inst. Br. Geogr.*, **44**, 97, doi:10.2307/621751.

Baik, J.-J., Y.-H. Kim, and H.-Y. Chun, 2001: Dry and Moist Convection Forced by an Urban Heat Island. *J. Appl. Meteorol.*, **40**, 1462–1475, doi:10.1175/1520-0450(2001)040<1462:DAMCFB>2.0.CO;2.

Bell, T. L., D. Rosenfeld, K.-M. Kim, J.-M. Yoo, M.-I. Lee, and M. Hahnenberger, 2008: Midweek increase in U.S. summer rain and storm heights suggests air pollution invigorates rainstorms. *J. Geophys. Res.*, **113**, 1–22, doi:10.1029/2007JD008623.

Bell, T. L., D. Rosenfeld, and K.-M. Kim, 2009: Weekly cycle of lightning: Evidence of storm invigoration by pollution. *Geophys. Res. Lett.*, **36**, 1–5, doi:10.1029/2009GL040915.

Berg, W., T. L'Ecuyer, and S. van den Heever, 2008: Evidence for the impact of aerosols on the onset and microphysical properties of rainfall from a combination of satellite observations and cloud-resolving model simulations. *J. Geophys. Res.*, **113**, 1–15, doi:10.1029/2007JD009649.

Bornstein, R., and Q. Lin, 2000: Urban heat islands and summertime convective thunderstorms in Atlanta: three case studies. *Atmos. Environ.*, **34**, 507–516, doi:10.1016/S1352-2310(99)00374-X.

Braham, R. R., 1979: Comments on "Urban, Topographic and Diurnal Effects on Rainfall in the St. Louis Region." *J. Appl. Meteorol.*, **18**, 371–375, doi:10.1175/1520-0450(1979)018<0371:COTADE>2.0.CO;2.

Burian, S. J., and J. M. Shepherd, 2005: Effect of urbanization on the diurnal rainfall pattern in Houston. *Hydrol. Process.*, **19**, 1089–1103, doi:10.1002/hyp.5647.

Carrió, G. G., and W. R. Cotton, 2011: Urban growth and aerosol effects on convection over Houston. Part II: Dependence of aerosol effects on instability. *Atmos. Res.*, **102**, 167–174, doi:10.1016/j.atmosres.2011.06.022.

Carrió, G. G., W. R. Cotton, and W. Y. Y. Cheng, 2010: Urban growth and aerosol effects on convection over Houston. Part I: The August 2000 Case. *Atmos. Res.*, **96**, 560–574, doi:10.1016/j.atmosres.2010.01.005.

Changnon, S. A., 1968: The La Porte weather anomaly - Fact or fiction? *Bull. Am. Meteorol. Soc.*, **49**, 4–11.

Changnon, S. A., 1971: La Porte Anomaly. *Science (80-.).*, **172**, 987–988, doi:10.1126/science.172.3987.987-a.

Changnon, S. A., 1980a: More on the La Porte Anomaly: A Review. *Bull. Am. Meteorol. Soc.*, **61**, 702–711, doi:10.1175/1520-0477(1980)061<0702:MOTLPA>2.0.CO;2.

Changnon, S. A., 1980b: Evidence of Urban and Lake Influences on Precipitation in the Chicago Area. *J. Appl. Meteorol.*, **19**, 1137–1159, doi:10.1175/1520-0450(1980)019<1137:EOUALI>2.0.CO;2.

Changnon, S. A., and F. A. Huff, 1977: La Porte Again: A New Anomaly. *Bull. Am. Meteorol. Soc.*, **58**, 1069–1072.

Changnon, S. A., and F. A. Huff, 1986: The Urban-related Nocturnal Rainfall Anomaly at St. Louis. *J. Clim. Appl. Meteorol.*, **25**, 1985–1995, doi:10.1175/1520-0450(1986)025<1985:TURNRA>2.0.CO;2.

Changnon, S. A., F. A. F. Huff, and R. G. Semonin, 1971: METROMEX: an Investigation of Inadvertent Weather Modification. *Bull. Am. Meteorol. Soc.*, **52**, 958–968, doi:10.1175/1520-0477(1971)052<0958:MAIOIW>2.0.CO;2.

Changnon, S. A., R. G. Semonin, and F. A. Huff, 1976: A Hypothesis for Urban Rainfall Anomalies. *J. Appl. Meteorol.*, **15**, 544–560, doi:10.1175/1520-0450(1976)015<0544:AHFURA>2.0.CO;2.

Chen, F. and Coauthors, 2012: Research priorities in observing and modeling urban weather and climate. *Bull. Am. Meteorol. Soc.*, **93**, 120306091314009, doi:10.1175/BAMS-D-11-00217.1.

Clark, R. R., 1979: A Hydrologic Reanalysis of the La Porte Anomaly. *Bull. Am. Meteorol. Soc.*, **60**, 415–421, doi:10.1175/1520-0477(1979)060<0415:AHROTL>2.0.CO;2.

Deng, J., H. Xu, and L. Zhang, 2016: Nonlinear effects of anthropogenic aerosol and urban land surface forcing on spring climate in eastern China. *J. Geophys. Res. Atmos.*, **121**, 4581–4599, doi:10.1002/2015JD024377.

Dettwiller, J., and S. A. Changnon, 1976: Possible Urban Effects on Maximum Daily Rainfall at Paris, St. Louis and Chicago. *J. Appl. Meteorol.*, **15**, 517–519, doi:10.1175/1520-0450(1976)015<0518:PUEOMD>2.0.CO;2.

Dirks, R. A., 1983: Progress in weather modification research: 1979–1982. *Rev. Geophys.*, **21**, 1065, doi:10.1029/RG021i005p01065.

Dixon, P. G., and T. L. Mote, 2003: Patterns and Causes of Atlanta's Urban Heat Island–Initiated Precipitation. *J. Appl. Meteorol.*, **42**, 1273–1284, doi:10.1175/1520-0450(2003)042<1273:PACOAU>2.0.CO;2.

Eichenlaub, V., 1972: The La Porte Weather Anomaly: Its Controversies and Implications. *Sch. Sci. Math.*, **72**, 208–213, doi:10.1111/j.1949-8594.1972.tb08842.x.

Fan, J. and Coauthors, 2009: Dominant role by vertical wind shear in regulating aerosol effects on deep convective clouds. *J. Geophys. Res.*, **114**, 1–9, doi:10.1029/2009JD012352.

Fan, J., D. Rosenfeld, Y. Yang, C. Zhao, L. R. Leung, and Z. Li, 2015: Substantial contribution of anthropogenic air pollution to catastrophic floods in Southwest China. *Geophys. Res. Lett.*, **42**, 6066–6075, doi:10.1002/2015GL064479.

Feingold, G., 2009: Cloud-aerosol interactions from the micro to the cloud scale. *Clouds Perturbed Clim. Syst. Their Relatsh. to Energy Balanc. Atmos. Dyn. Precip.*, 319–338.

Feingold, G., W. R. Cotton, S. M. Kreidenweis, J. T. Davis, and J. A. T. D. Avis, 1999: The Impact of Giant Cloud Condensation Nuclei on Drizzle Formation in Stratocumulus: Implications for Cloud Radiative Properties. *J. Atmos. Sci.*, **56**, 4100–4117, doi:10.1175/1520-0469(1999)056<4100:TIOGCC>2.0.CO;2.

Ganeshan, M., R. Murtugudde, and M. L. Imhoff, 2013: A multi-city analysis of the UHI-influence on warm season rainfall. *Urban Clim.*, **6**, 1–23, doi:10.1016/J.UCLIM.2013.09.004.

Givati, A., and D. Rosenfeld, 2004: Quantifying Precipitation Suppression Due to Air Pollution. *J. Appl. Meteorol.*, **43**, 1038–1056, doi:10.1175/1520-0450(2004)043<1038:QPSDTA>2.0.CO;2.

Grimmond, C. S. B. and Coauthors, 2010: Climate and More Sustainable Cities: Climate Information for Improved Planning and Management of Cities (Producers/Capabilities Perspective). *Procedia Environ. Sci.*, **1**, 247–274, doi:10.1016/j.proenv.2010.09.016.

Han, J.-Y., and J.-J. Baik, 2008: A Theoretical and Numerical Study of Urban Heat Island–Induced Circulation and Convection. *J. Atmos. Sci.*, **65**, 1859–1877, doi:10.1175/2007JAS2326.1.

Han, J.-Y., J.-J. Baik, and A. P. Khain, 2012: A Numerical Study of Urban Aerosol Impacts on Clouds and Precipitation. *J. Atmos. Sci.*, **69**, 504–520, doi:10.1175/JAS-D-11-071.1.

Harnack, R. P., H. E. Landsberg, R. P. Harnack, and H. E. Landsberg, 1975: Selected Cases of Convective Precipitation Caused by the Metropolitan Area of Washington, D.C. *J. Appl. Meteorol.*, **14**, 1050–1060, doi:10.1175/1520-0450(1975)014<1050:SCOCPC>2.0.CO;2.

van den Heever, S. C., and W. R. Cotton, 2007: Urban Aerosol Impacts on Downwind Convective Storms. *J. Appl. Meteorol. Climatol.*, **46**, 828–850, doi:10.1175/JAM2492.1.

Hjelmfelt, M. R., 1982: Numerical Simulation of the Effects of St. Louis on Mesoscale Boundary-Layer Airflow and Vertical Air Motion: Simulations of Urban vs Non-Urban Effects. *J. Appl. Meteorol.*, **21**, 1239–1257, doi:10.1175/1520-0450(1982)021<1239:NSOTEO>2.0.CO;2.

Holzman, B. G., 1971: La Porte Precipitation Fallacy. *Science (80-.).*, **171**, 847–847, doi:10.1126/science.171.3974.847.

Horton, R. E., 1921: Thunderstorm Breeding Spots. *Mon. Weather Rev.*, **49**, 193–193, doi:10.1175/1520-0493(1921)49<193a:TS>2.0.CO;2.

Hosannah, N., and J. E. Gonzalez, 2014: Impacts of Aerosol Particle Size Distribution and Land Cover Land Use on Precipitation in a Coastal Urban Environment Using a Cloud-Resolving Mesoscale Model. *Adv. Meteorol.*, **2014**, 1–17, doi:10.1155/2014/904571.

Hu, X.-M. and Coauthors, 2016: Analysis of Urban Effects in Oklahoma City using a Dense Surface Observing Network*. *J. Appl. Meteorol. Climatol.*, **55**, 723–741, doi:10.1175/JAMC-D-15-0206.1.

Huff, F. a., and S. a. Changnon, 1973: Precipitation Modification By Major Urban Areas. *Bull. Am. Meteorol. Soc.*, **54**, 1220–1232, doi:10.1175/1520-0477(1973)054<1220:PMBMUA>2.0.CO;2.

Huff, F. A., 1975: Urban effects on the distribution of heavy convective rainfall. *Water Resour. Res.*, **11**, 889–896, doi:10.1029/WR011i006p00889.

Huff, F. A., and S. A. Changnon, 1960: Distribution of excessive rainfall amounts over an urban area. *J. Geophys. Res.*, **65**, 3759–3765, doi:10.1029/JZ065i011p03759.

Huff, F. A., and S. A. Changnon, 1972: Climatological Assessment of Urban Effects on Precipitation at St. Louis. *J. Appl. Meteorol.*, **11**, 823–842, doi:10.1175/1520-0450(1972)011<0823:CAOUEO>2.0.CO;2.

Jin, M., and J. M. Shepherd, 2008: Aerosol relationships to warm season clouds and rainfall at monthly scales over east China: Urban land versus ocean. *J. Geophys. Res.*, **113**, 1–12, doi:10.1029/2008JD010276.

Jin, M., J. M. Shepherd, and M. D. King, 2005: Urban aerosols and their variations with clouds and rainfall: A case study for New York and Houston. *J. Geophys. Res.*, **110**, 1–12, doi:10.1029/2004JD005081.

Kawecki, S., G. M. Henebry, A. L. Steiner, S. Kawecki, G. M. Henebry, and A. L. Steiner, 2016: Effects of Urban Plume Aerosols on a Mesoscale Convective System. *J. Atmos. Sci.*, **73**, 4641–4660, doi:10.1175/JAS-D-16-0084.1.

Khain, a., D. Rosenfeld, A. Pokrovsky, U. Blahak, and A. Ryzhkov, 2011: The role of CCN in precipitation and hail in a mid-latitude storm as seen in simulations using a spectral (bin) microphysics model in a 2D dynamic frame. *Atmos. Res.*, **99**, 129–146, doi:10.1016/j.atmosres.2010.09.015.

Khain, a. P., N. BenMoshe, A. Pokrovsky, J. Of, and T. H. E. Atmospheric, 2008: Factors Determining the Impact of Aerosols on Surface Precipitation from Clouds: An Attempt at Classification. *J. Atmos. Sci.*, **65**, 1721–1748, doi:10.1175/2007JAS2515.1.

Khain, A., and B. Lynn, 2009: Simulation of a supercell storm in clean and dirty atmosphere using weather research and forecast model with spectral bin microphysics. *J. Geophys. Res.*, **114**, doi:10.1029/2009JD011827.

Khemani, L. T., and B. V. R. Murty, 1973: Rainfall Variations in an Urban Industrial Region. *J. Appl. Meteorol.*, **12**, 187–194, doi:10.1175/1520-0450(1973)012<0187:RVIAUI>2.0.CO;2.

Kishtawal, C. M., D. Niyogi, M. Tewari, R. a. Pielke, and J. M. Shepherd, 2010: Urbanization signature in the observed heavy rainfall climatology over India. *Int. J. Climatol.*, **30**, 1908–1916, doi:10.1002/joc.2044.

Koren, I., 2005: Aerosol invigoration and restructuring of Atlantic convective clouds. *Geophys. Res. Lett.*, **32**, 4–7, doi:10.1029/2005GL023187.

Lacke, M. C., T. L. Mote, and J. M. Shepherd, 2009: Aerosols and associated precipitation patterns in Atlanta. *Atmos. Environ.*, **43**, 4359–4373, doi:10.1016/j.atmosenv.2009.04.022.

Lee, S. S., 2012: Effect of Aerosol on Circulations and Precipitation in Deep Convective Clouds. *J. Atmos. Sci.*, **69**, 1957–1974, doi:10.1175/JAS-D-11-0111.1.

Lei, M., D. Niyogi, C. Kishtawal, R. a. Pielke, A. Beltrán-Przekurat, T. E. Nobis, and S. S. Vaidya, 2008: Effect of explicit urban land surface representation on the simulation of the 26 July 2005 heavy rain event over Mumbai, India. *Atmos. Chem. Phys.*, **8**, 5975–5995, doi:10.5194/acp-8-5975-2008.

Li, D. and Coauthors, 2013: Modeling Land Surface Processes and Heavy Rainfall in Urban Environments: Sensitivity to Urban Surface Representations. *J. Hydrometeorol.*, **14**, 1098–1118, doi:10.1175/JHM-D-12-0154.1.

Li, G., Y. Wang, and R. Zhang, 2008: Implementation of a two-moment bulk microphysics scheme to the WRF model to investigate aerosol-cloud interaction. *J. Geophys. Res.*, **113**, D15211, doi:10.1029/2007JD009361.

Li, G., Y. Wang, K.-H. Lee, Y. Diao, and R. Zhang, 2009: Impacts of aerosols on the development and precipitation of a mesoscale squall line. *J. Geophys. Res.*, **114**, 1–18, doi:10.1029/2008JD011581.

Lo, J. C. F., A. K. H. Lau, F. Chen, J. C. H. Fung, and K. K. M. Leung, 2007: Urban Modification in a Mesoscale Model and the Effects on the Local Circulation in the Pearl River Delta Region. *J. Appl. Meteorol. Climatol.*, **46**, 457–476, doi:10.1175/JAM2477.1.

Lowry, W. P., 1998: Urban effects on precipitation amount. *Prog. Phys. Geogr.*, **22**, 477–520, doi:10.1177/030913339802200403.

Lowry, W. P., F. Probald, W. P. Lowry, and F. Probald, 1978: An Attempt to Detect the Effects of a Steelworks on Precipitation Amounts in Central Hungary. *J. Appl. Meteorol.*, **17**, 964–975, doi:10.1175/1520-0450(1978)017<0964:AATDTE>2.0.CO;2.

Meyer, W. B., 1991: Urban Heat Island and Urban Health: Early American Perspectives. *Prof. Geogr.*, **43**, 38–48, doi:10.1111/j.0033-0124.1991.00038.x.

Miao, S., F. Chen, Q. Li, and S. Fan, 2011: Impacts of Urban Processes and Urbanization on Summer Precipitation: A Case Study of Heavy Rainfall in Beijing on 1 August 2006. *J. Appl. Meteorol. Climatol.*, **50**, 806–825, doi:10.1175/2010JAMC2513.1.

Mills, G., 2008: Luke Howard and The Climate of London. *Weather*, **63**, 153–157, doi:10.1002/wea.195.

Mills, G., 2014: Urban climatology: History, status and prospects. *Urban Clim.*, **10**, 479–489, doi:10.1016/j.uclim.2014.06.004.

Myrup, L. O., 1969: A Numerical Model of the Urban Heat Island. *J. Appl. Meteorol.*, **8**, 908–918, doi:10.1175/1520-0450(1969)008<0908:ANMOTU>2.0.CO;2.

Niyogi, D. and Coauthors, 2011: Urban Modification of Thunderstorms: An Observational Storm Climatology and Model Case Study for the Indianapolis Urban Region *. *J. Appl. Meteorol. Climatol.*, **50**, 1129–1144, doi:10.1175/2010JAMC1836.1.

Ntelekos, A. A., J. A. Smith, L. Donner, J. D. Fast, W. I. Gustafson, E. G. Chapman, and W. F. Krajewski, 2009: The effects of aerosols on intense convective precipitation in the northeastern United States. *Q. J. R. Meteorol. Soc.*, **135**, 1367–1391, doi:10.1002/qj.476.

Ochoa, C. a., A. I. Quintanar, G. B. Raga, and D. Baumgardner, 2015: Changes in Intense Precipitation Events in Mexico City. *J. Hydrometeorol.*, 150327085005006, doi:10.1175/JHM-D-14-0081.1.

Oke, T. R., 1973: City size and the urban heat island. *Atmos. Environ.*, **7**, 769–779, doi:10.1016/0004-6981(73)90140-6.

Orville, R. E. and Coauthors, 2001: Enhancement of cloud-to-ground lightning over Houston, Texas. *Geophys. Res. Lett.*, **28**, 2597, doi:10.1029/2001GL012990.

Pielke, R. A. and Coauthors, 2011: Land use/land cover changes and climate: modeling analysis and observational evidence. *Wiley Interdiscip. Rev. Clim. Chang.*, **2**, 828–850, doi:10.1002/wcc.144.

Rao, A. R., 1980: Stochastic Analysis of Annual Rainfall Affected by Urbanization. *J. Appl. Meteorol.*, **19**, 41–52, doi:10.1175/1520-0450(1980)019<0041:SAOARA>2.0.CO;2.

Rosenfeld, D., 2000: Suppression of Rain and Snow by Urban and Industrial Air Pollution. *Science (80-.).*, **287**, 1793–1796, doi:10.1126/science.287.5459.1793.

Rosenfeld, D., and W. L. Woodley, 2000: Deep convective clouds with sustained supercooled liquid water down to -37.5 °C. *Nature*, **405**, 440–442, doi:10.1038/35013030.

Rosenfeld, D., and T. L. Bell, 2011: Why do tornados and hailstorms rest on weekends? *J. Geophys. Res.*, **116**, 1–14, doi:10.1029/2011JD016214.

Rosenfeld, D. and Coauthors, 2008: Flood or drought: how do aerosols affect precipitation? *Science (80-.).*, **321**, 1309–1313, doi:10.1126/science.1160606.

Rozoff, C. M., W. R. Cotton, and J. O. Adegoke, 2003: Simulation of St. Louis, Missouri, Land Use Impacts on Thunderstorms. *J. Appl. Meteorol.*, **42**, 716–738, doi:10.1175/1520-0450(2003)042<0716:SOSLML>2.0.CO;2.

Ryu, Y.-H., J.-J. Baik, and J.-Y. Han, 2013: Daytime urban breeze circulation and its interaction with convective cells. *Q. J. R. Meteorol. Soc.*, **139**, 401–413, doi:10.1002/qj.1973.

Ryu, Y.-H., J. A. Smith, E. Bou-Zeid, M. L. Baeck, Y.-H. Ryu, J. A. Smith, E. Bou-Zeid, and M. L. Baeck, 2016: The Influence of Land Surface Heterogeneities on Heavy Convective Rainfall in the Baltimore–Washington Metropolitan Area. *Mon. Weather Rev.*, **144**, 553–573, doi:10.1175/MWR-D-15-0192.1.

Saleeby, S. M., S. C. van den Heever, P. J. Marinescu, S. M. Kreidenweis, and P. J. DeMott, 2016: Aerosol effects on the anvil characteristics of mesoscale convective systems. *J. Geophys. Res. Atmos.*, **121**, 10,880-10,901, doi:10.1002/2016JD025082.

Schmid, P. E., and D. Niyogi, 2013: Impact of city size on precipitation-modifying potential. *Geophys. Res. Lett.*, **40**, 5263–5267, doi:10.1002/grl.50656.

Schmid, P. E., and D. Niyogi, 2017: Modeling Urban Precipitation Modification by Spatially Heterogeneous Aerosols. *J. Appl. Meteorol. Climatol.*, **56**, 2141–2153, doi:10.1175/JAMC-D-16-0320.1.

Shem, W., and M. Shepherd, 2009: On the impact of urbanization on summertime thunderstorms in Atlanta: Two numerical model case studies. *Atmos. Res.*, **92**, 172–189, doi:10.1016/j.atmosres.2008.09.013.

Shepherd, J. M., 2005: A Review of Current Investigations of Urban-Induced Rainfall and Recommendations for the Future. *Earth Interact.*, **9**, 1–27, doi:10.1175/EI156.1.

Shepherd, J. M. J., J. A. J. Stallins, M. L. M. Jin, and T. L. Mote, 2010: Urbanization: Impacts on clouds, precipitation, and lightning. *Urban Ecosyst. Ecol.*, 1–28, doi:10.2134/agronmonogr55.c1.

Shi, P. and Coauthors, 2017: Urbanization and air quality as major drivers of altered spatiotemporal patterns of heavy rainfall in China. *Landsc. Ecol.*, **32**, 1723–1738, doi:10.1007/s10980-017-0538-3.

Smith, B. K., J. Smith, and M. L. Baeck, 2016: Flash flood-producing storm properties in a small urban watershed. *J. Hydrometeorol.*, JHM-D-16-0070.1, doi:10.1175/JHM-D-16-0070.1.

Smith, J. A., M. L. Baeck, J. E. Morrison, P. Sturdevant-Rees, D. F. Turner-Gillespie, and P. D. Bates, 2002: The Regional Hydrology of Extreme Floods in an Urbanizing Drainage Basin. *J. Hydrometeorol.*, **3**, 267–282, doi:10.1175/1525-7541(2002)003<0267:TRHOEF>2.0.CO;2.

Snow, J. T., X. Zeng, P. Klein, S. E. Sarnat, J. M. Shepherd, and E. M. Stanley, 2012: *Urban Meteorology: Forecasting, Monitoring, and Meeting Users' Needs*. National Academies Press, Washington, D.C., 4 pp.

Stallins, J. A., J. Carpenter, M. L. Bentley, W. S. Ashley, and J. A. Mulholland, 2013: Weekend–weekday aerosols and geographic variability in cloud-to-ground lightning for the urban region of Atlanta, Georgia, USA. *Reg. Environ. Chang.*, **13**, 137–151, doi:10.1007/s10113-012-0327-0.

Stewart, I. D., 2019: Why should urban heat island researchers study history? *Urban Clim.*, **30**, 100484, doi:10.1016/j.uclim.2019.100484.

Storer, R. L., S. C. van den Heever, G. L. Stephens, and F. Collins, 2010: Modeling Aerosol Impacts on Convective Storms in Different Environments. *J. Atmos. Sci.*, **67**, 3904–3915, doi:10.1175/2010JAS3363.1.

Takahashi, H., Y. Nakamura, and H. Suzuki, 2011: Frequency Distribution of Intense Rainfall in the Wards of Tokyo and Its Relationship with the Spatial Structure of Building Heights. *J. Geogr. (Chigaku Zasshi)*, **120**, 359–381, doi:10.5026/jgeography.120.359.

Tao, W.-K., J.-P. Chen, Z. Li, C. Wang, and C. Zhang, 2012: Impact of aerosols on convective clouds and precipitation. *Rev. Geophys.*, **50**, doi:10.1029/2011RG000369.

Tuttle, J. D., and R. E. Carbone, 2011: Inferences of weekly cycles in summertime rainfall. *J. Geophys. Res.*, **116**, 1–13, doi:10.1029/2011JD015819.

Twohy, C. H., M. D. Petters, J. R. Snider, B. Stevens, W. Tahnk, M. Wetzel, L. Russell, and F. Burnet, 2005: Evaluation of the aerosol indirect effect in marine stratocumulus clouds: Droplet number, size, liquid water path, and radiative impact. *J. Geophys. Res.*, **110**, D08203, doi:10.1029/2004JD005116.

Twomey, S., and S. Twomey, 1977: The Influence of Pollution on the Shortwave Albedo of Clouds. *J. Atmos. Sci.*, **34**, 1149–1152, doi:10.1175/1520-0469(1977)034<1149:TIOPOT>2.0.CO;2.

Villarini, G., J. A. Smith, F. Serinaldi, J. Bales, P. D. Bates, and W. F. Krajewski, 2009: Flood frequency analysis for nonstationary annual peak records in an urban drainage basin. *Adv. Water Resour.*, **32**, 1255–1266, doi:10.1016/J.ADVWATRES.2009.05.003.

Vukovich, F. M., and W. J. King, 1980: A Theoretical Study of the St. Louis Heat Island: Comparisons Between Observed Data and Simulation Results on the Urban Heat Island Circulation. *J. Appl. Meteorol.*, **19**, 761–770, doi:10.1175/1520-0450(1980)019<0761:ATSOTS>2.0.CO;2.

Wan, H., Z. Zhong, X. Yang, and X. Li, 2013: Impact of city belt in Yangtze River Delta in China on a precipitation process in summer: A case study. *Atmos. Res.*, **125–126**, 63–75, doi:10.1016/j.atmosres.2013.02.004.

Wang, C., 2007: Impact of direct radiative forcing of black carbon aerosols on tropical convective precipitation. *Geophys. Res. Lett.*, **34**, doi:10.1029/2006GL028416.

Wang, X., J. Liao, J. Zhang, C. Shen, W. Chen, B. Xia, and T. Wang, 2014: A Numeric Study of Regional Climate Change Induced by Urban Expansion in the Pearl River Delta, China. *J. Appl. Meteorol. Climatol.*, **53**, 346–362, doi:10.1175/JAMC-D-13-054.1.

Wang, Y., Y. Yang, N. Zhao, C. Liu, and Q. Wang, 2012: The magnitude of the effect of air pollution on sunshine hours in China. *J. Geophys. Res.*, **117**, 1–9, doi:10.1029/2011JD016753.

Wright, D. B., J. A. Smith, G. Villarini, and M. L. Baeck, 2012: Hydroclimatology of flash flooding in Atlanta. *Water Resour. Res.*, **48**, doi:10.1029/2011WR011371.

Yang, H.-L., H. Xiao, and Y.-C. Hong, 2011: A numerical study of aerosol effects on cloud microphysical processes of hailstorm clouds. *Atmos. Res.*, **102**, 432–443, doi:10.1016/j.atmosres.2011.09.007.

Yang, L., F. Tian, J. A. Smith, and H. Hu, 2014: Urban signatures in the spatial clustering of summer heavy rainfall events over the Beijing metropolitan region. *J. Geophys. Res. Atmos.*, n/a-n/a, doi:10.1002/2013JD020762.

Yang, L., J. Smith, M. L. Baeck, B. Smith, F. Tian, and D. Niyogi, 2016: Structure and evolution of flash flood producing storms in a small urban watershed. *J. Geophys. Res. Atmos.*, 1–19, doi:10.1002/2015JD024478.

Yonetani, T., 1982: Increase in Number of Days with Heavy Precipitation in Tokyo Urban Area. *J. Appl. Meteorol.*, **21**, 1466–1471, doi:10.1175/1520-0450(1982)021<1466:IINODW>2.0.CO;2.

Zhang, D.-L., Y.-X. Shou, and R. R. Dickerson, 2009: Upstream urbanization exacerbates urban heat island effects. *Geophys. Res. Lett.*, **36**, 1–5, doi:10.1029/2009GL041082.

Zhang, D.-L., Y.-X. Shou, R. R. Dickerson, and F. Chen, 2011: Impact of Upstream Urbanization on the Urban Heat Island Effects along the Washington–Baltimore Corridor. *J. Appl. Meteorol. Climatol.*, **50**, 2012–2029, doi:10.1175/JAMC-D-10-05008.1.

Zhong, S., and X.-Q. Yang, 2015a: Mechanism of urbanization impact on a summer cold frontal rainfall process in the Great Beijing Metropolitan Area. *J. Appl. Meteorol. Climatol.*, 150312130123006, doi:10.1175/JAMC-D-14-0264.1.

Zhong, S., and X. Q. Yang, 2015b: Ensemble simulations of the urban effect on a summer rainfall event in the Great Beijing Metropolitan Area. *Atmos. Res.*, **153**, 318–334, doi:10.1016/j.atmosres.2014.09.005.

Zhong, S., Y. Qian, C. Zhao, R. Leung, and X. Yang, 2015: A case study of urbanization impact on summer precipitation in the Greater Beijing Metropolitan Area: Urban heat island versus aerosol effects. *J. Geophys. Res. Atmos.*, **120**, 10,903-10,914, doi:10.1002/2015JD023753.

CHAPTER 2. OBSERVATIONS OF THE LA PORTE ANOMALY

Following the historical discussion in Chapter 1, it is important to reiterate here that the La Porte Anomaly was the *first* urban precipitation feature to be described and studied in detail (Changnon 1968, 1971). It apparently manifested as a region of precipitation, centered in La Porte, Indiana, 80 km downwind of Chicago, where warm-season rainfall at one station was over 50% greater than upwind. The increased total warm-season rainfall (Dettwiller and Changnon 1976) was primarily due to more frequent heavy rain downwind of the city (Changnon et al. 1976), and it was accompanied by increased hail and more frequent lightning (Huff and Changnon 1973). The original research indicated that the La Porte anomaly existed at least as early as the 1930s, persisted through the mid-1960s, but by the 1970s it had apparently disappeared (Changnon 1980a; Rao 1980). This chapter will present results of research using historical to contemporary data to demonstrate:

- The La Porte Anomaly indeed existed as originally observed.
- While the rainfall anomaly downwind of Chicago disappeared during the 1970s, it reappeared and persists to today in seasonal precipitation.
- The rainfall variability is most prominent under locally forced conditions, demonstrating they are an urban modification.
- The urban rainfall changes exist independent of wind direction and influences from Lake Michigan.
- From 2005 – present, the summer rainfall downwind of Chicago is 30% greater than upwind and the downwind weekday rainfall is over 50% greater than on weekdays – a characteristic indicator that urban aerosols influence the local variability.

2.1 Data and Methodology

Critiques of the original studies of the La Porte anomaly almost universally focus on data and methodological quality (Lowry 1998; Changnon 1992). The data and methods for this chapter rely on objective and multi-sensor observations, with robust, statistically significant analyses.

2.1.1 Historical Data and Methods

The precipitation from 1930 – 2000 was gridded at 9-km spacing in the 90,000 km^2 (30 × 30 grids) region around Chicago using an optimal interpolation technique (Gandin 1966; Bellerby 2013). Irregularly spaced surface precipitation observations from the Global Historical Climatology Network (GHCN)(Peterson et al. 1998; Menne et al. 2012), which include weather service and cooperative sites, were interpolated over a background field of a hydrological reanalysis (Livneh et al. 2013), chosen for its minimal urban signature. The optimal analysis field $\mathbf{P^A}$ is computed by weighting ($\mathbf{w}$) the difference between the point observations $\mathbf{P^O}$ and the background reanalysis $\mathbf{P^B}$.

$$\mathbf{P^A} = \mathbf{P^B} + \mathbf{w}(\mathbf{P^O} - \mathbf{P^B})$$

The weights are computed based observation point distances from the center of each grid, with the observational error computed as the difference between individual observational monthly variance and observational-background covariance. The **S** matrix represents the Gaussian distance (D^g) of each site from the center of the grid (b), and the **R** matrix represents the Gaussian distances of each site from each other. Correlation length (c_{len}), at which two sites would be considered identical, was defined as 600 m.

$$D^g = \exp\left(-\frac{D^2}{c_{len}^2}\right)$$

$$\mathbf{R} = \begin{bmatrix} D_{11}^g & D_{12}^g & \cdots \\ D_{21}^g & D_{22}^g & \cdots \\ \vdots & \vdots & \ddots \end{bmatrix} \qquad \mathbf{S} = \begin{bmatrix} D_{b1}^g \\ D_{b2}^g \\ \vdots \end{bmatrix}$$

$$\mathbf{E} = var(\mathbf{P^O}) - \mathbf{C_{OB}}\mathbf{R}^{-1}\mathbf{C_{OB}^T} \qquad \text{where} \qquad \mathbf{C_{OB}} = \begin{bmatrix} cov(\mathbf{P^B}, \mathbf{P_1^O}) \\ cov(\mathbf{P^B}, \mathbf{P_2^O}) \\ \vdots \end{bmatrix}$$

$$\mathbf{w} = (\mathbf{R} + \mathbf{IE})^{-1}\mathbf{S^T}$$

For grids with zero or one point observations, the optimal analysis was the background or the average of the background and point with maximum expected error respectively. Optimal interpolation provides a sufficient precipitation analysis because seasonal rainfall values are temporally independent – i.e. the observed rainfall in the 1960s is not significantly dependent on the observed values in the 1950s.

2.1.2 Contemporary Data and Methods

From 2005 – present, this study used in situ raingauge observations and the 4km, Advanced Hydrologic Prediction Service Multisensor Precipitation Reanalysis (MPR) (Nelson et al. 2010) available from 2005 to assess the warm season rainfall. The 4-km grid spacing of the product is sufficient to analyze specifically urban rainfall features (Paul et al. 2018). The MPR, like any gridded precipitation analysis, may differ from individual rain gauges but the errors are greatest at the smallest temporal and spatial scales (hourly or sub 1-km). These errors become acceptably small at the daily time scale and greater (Wu et al. 2012).

The errors in the gridded precipitation product continue to decrease as the time scale of evaluation becomes larger. The root mean square error (RMSE) between n individual rain gauges and the AHPS analysis, bilinearly interpolated to the gauge, defined as:

$$RMSE = \sqrt{\frac{\sum_n \left(\overline{R_{AHPS}} - R_{gauge}\right)^2}{n}}$$

At a daily time scale, over the study region, the average daily RMSE = 3.6 mm·day-1, lower but comparable to the values found in other studies(Wu et al. 2012) (4.5 mm·day^{-1}). At the seasonal and 10-year scale, the RMSE are an order of magnitude less than their daily values - $RMSE_{season}$ = 0.61 mm·day^{-1}, and $RMSE_{10\text{-}yr}$ = 0.43 mm·day^{-1}.

The MPR has been used in the operational and research communities for over a decade (McEnery et al. 2005). In particular, it has been used to quantitatively diagnose rainfall(Zhang et al. 2011b), operationally assess flash flooding (Zhang et al. 2014), and seasonally analyze drought severity (McRoberts et al. 2012; Cumbie-Ward and Boyles 2016) with these acknowledged errors – RMSE ≈ 100% per day. Recent studies have noted how radar alone could diagnose urban rainfall anomalies at a climatological scale (Hamidi et al. 2016; Fabry et al. 2017), and that incorporating rain gauges improves the skill of a precipitation analysis. While the daily RMSE between MPR product and rain gauges is near 100%, it decreases to 18% when reassessed at a seasonal scale and 9.9% at 10-years. Given that the La Porte anomaly manifests as a seasonal to climatological feature with a magnitude of 40% greater than the regional average, the MPR is able to quantitatively describe and analyze it.

The North American Regional Reanalysis (NARR) was used to categorize rain events (Mesinger et al. 2006)– separating storms by mean regional wind direction (see) and regional storm speed, CAPE, and PBL height (see 2.6). To produce Fig. 3, individual daily rainfall totals were transformed into a generalized upwind-downwind coordinate centered through downtown Chicago. Daily rainfalls directly upwind and downwind of the center of Chicago were sampled in swaths 40 km perpendicular to the storm motion and 300km parallel to storm motion with a 2-km grid sample radius, with a minimum of 10 days at each angle of storm motion. The storm motions across Fig. 3 represent 92% of summer days and 98.7% of summer rainfall. To determine the location of "peak" rainfall, a three-point boxcar average was applied to the gridded rainfall data to remove highly variable outlier points. The "relative anomaly" was computed as a percent difference between the average precipitation in a 30-km radius surround the peak anomaly rainfall and the average precipitation of the entire domain. The urban footprint overlaid in the figure uses the MODIS land cover product from 2010 (Friedl et al. 2002; Friedl and Sulla-Menashe 2015).

The urban effects presented at different storm motion vectors were objectively classified by assessing a hybrid clustering (Bernard et al. 2013) of the principal components (PCA) (Cheng et al. 2010) of the rainfall in the upwind, central, and downwind regions. Due to the correlation, the first principal component was representative of mean rainfall, but the 2nd and 3rd PC captured the rainfall variability to cluster the angles into distinct, related classes.

The methods to detect if rainfall regimes are "different" follow a series of non-parametric statistical tests because rainfall, even in very large sample sizes, rarely follows a known or consistent distribution (Wilks 2011). To test the significance of the difference between two regions of rainfall (i.e. upwind vs downwind), the Mann-Whitney *U* test was used. The Mann-Whitney *U*-test is the non-parametric alternative to the sample *t*-test to determine if two samples arise from independent distributions (Gabriel 2002; Lamptey 2008). For three or more sets, the Mann-Whiney was supplemented with the Kruskal-Wallis one-way analysis of variance to determine if data arise from the same or distinct distributions (Maia et al. 2007). Spatial trends along a transect (Fig. 3) were calculated using the non-parametric Mann-Kendall trend analysis to determine how significantly and monotonically an trend could be detected (De et al. 2005; Chen et al. 2013).

The relative anomaly is assessed with respect to the NARR domain average values of storm velocity (independent of direction), PBL height, CAPE, and convective fraction. The independent variables are distributed into bins: ranges of values and the rainfall is averaged over the set of days corresponding with each value, with at least 10 days of data required. The daily domain mean storm motion was assessed in two bin sizes: 1° reported in the results, and 10° noted in Table S2. A least squares linear regression, weighted by the number of days in each bin, was performed on the highly correlated variables to assess their relation and the significance

2.2 The Contemporary Rainfall Anomaly

The contemporary "La Porte" anomaly is shown in Figure 2 as a broad region of rainfall, centered near (41N, -87W), greater than the summertime regional average. The rainfall anomaly in NWI emerges as a 'hotspot' with values 100 – 120 mm greater than the regional average (a 30-40% increase). This rainfall anomaly is climatologically downwind of Chicago: the mean summer storm motion vector is from the NW (156°), while the rainfall-weighted mean storm motion is from the WNW (124°). A positive rainfall anomaly also exists from near downtown Chicago, extending east into Lake Michigan. The increased rainfall is especially notable, given that Lake Michigan itself reduces warm season rainfall compared to locations far from the lake (Notaro et al. 2013). Northwest of the Chicago urban area receives climatologically more precipitation during the summer. Thus, there is a local reduction in precipitation at the upwind edge, which gradually increases across the urbanized area, extending into a broad region of increased rainfall downwind of the city.

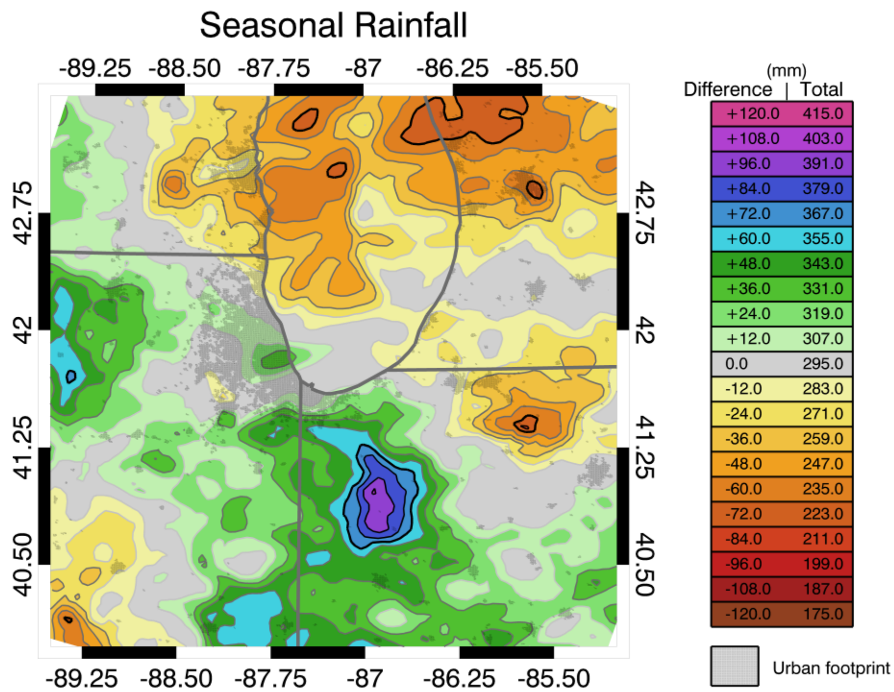

Figure 2. 2005 – 2016 climatology of summertime (JJA) rainfall in the Chicago region, and anomalies with respect to the regional mean. The non-linear scale highlights the location and extent of the anomaly downwind of Chicago in NWI.
Locations labeled: * - anomaly location, V – Valparaiso, L – La Porte, C – downtown Chicago, R – Rockford.

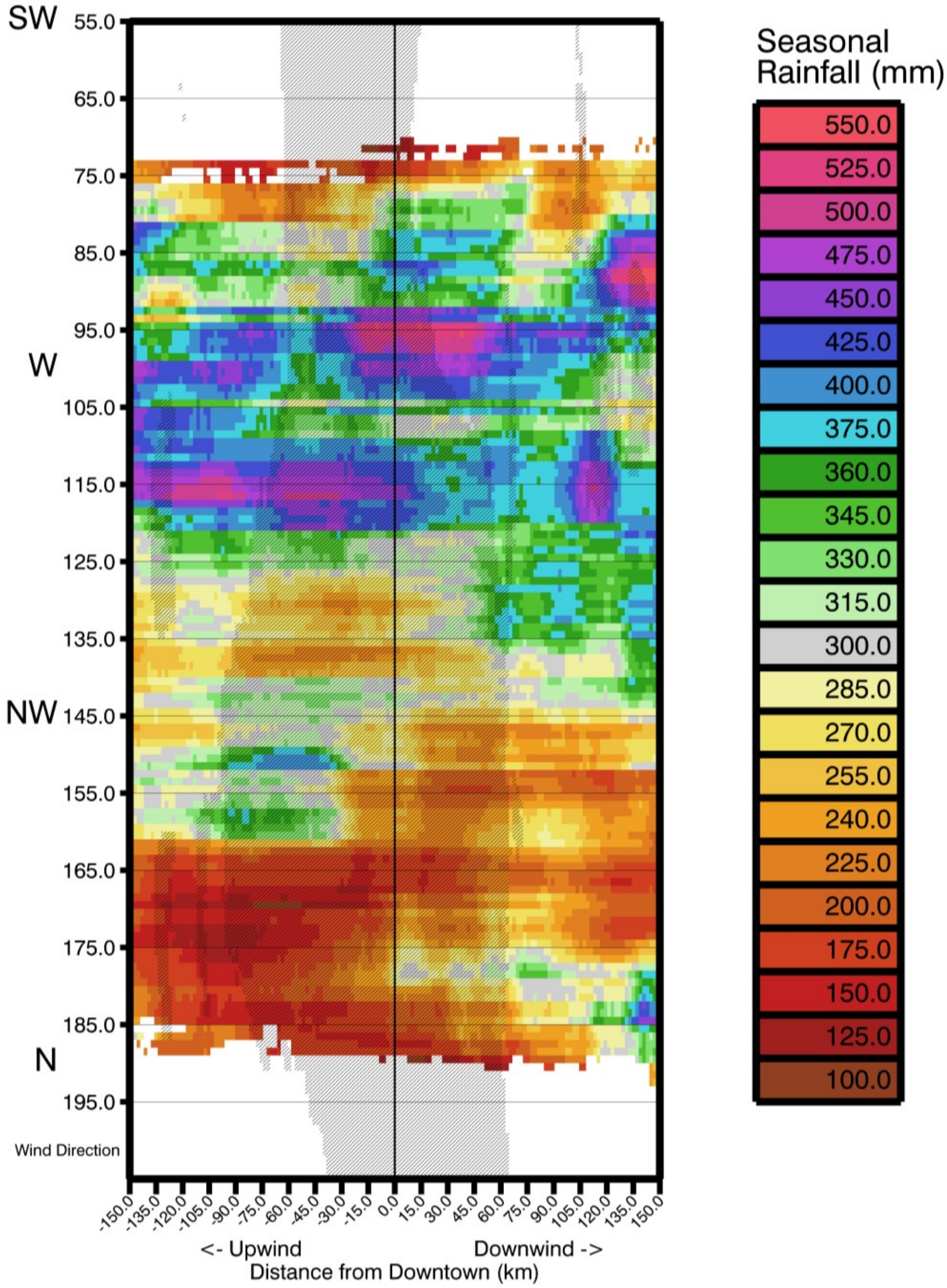

Figure 3. Seasonal, regional rainfall transformed into a generalized upwind/downwind vs storm motion coordinate system. The extent of the Chicago urban footprint is overlaid. Precipitation from all angles were scaled to represent seasonal rainfall if all summer precipitation occurred at a given angle. The wind angles displayed represent 92% of all summer days, and 98.7% of total summer precipitation during the 2005 – 2016 study period. The mean storm motion angle is 156.9° overall, and 124.7° when weighted by precipitation intensity. The weighted storm motion vs precipitation average explains the precipitation maximum at 41.0N, -87.0W (80 km downwind). Table 1 summarizes the statistical significance of upwind/urban/downwind difference, demonstrating most angles are $p < 0.01$.

Figure 3 displays a Hovmöller-like diagram of scaled, seasonal precipitation in a generalized upwind-downwind coordinate. The rainfall with sufficient data to analyze all upwind and downwind rainfall (70° – 190°) represent 76.1% of summer days, and 93% of seasonal rainfall. The urban effects were analyzed for different storm motions in three regions: upwind, central (urbanized), and downwind. The urban effects were objectively separated using a cluster analysis which yielded the following regimes:

- *Cluster 1*. Storms moving from south of due west (< 90°), those from WNW to NW (120° – 145°), and those within a few degrees of due north (180°) demonstrate an abrupt decrease in rainfall at the upwind boundary, then a gradual increase across the central urban area extending downwind.
- *Cluster 2*. Storms from the W and WNW (90° – 120°) show a *gradual* decrease across the urban boundary, then increased rainfall downwind.
- *Cluster 3*. Storms from the NW and NNW (145° – 165°) show an abrupt increase at the upwind boundary, then gradual decrease across the central region, followed by a slight increase downwind.
- *Cluster 4*. Systems moving from north of 165° exhibit generally low rainfall values, but decrease upwind, increase across the center, then decrease downwind.

The rainfall of *Clusters 1* and *2* exhibits the "classic" urban rainfall pattern of an abrupt decrease at the upwind boundary followed by a gradual increase over the urban area to downwind. Notably, storms from the WNW (120-145°) account for 22.9% of days, and 33.1% of seasonal rainfall, and are largely responsible for the location and shape of the climatological precipitation anomaly downwind of Chicago. The narrow downwind enhancement in storms from near due north (*Cluster 4*) is possibly due to the lake-land boundary, rather than urban-rural. In all days with sufficient data to analyze a complete upwind/downwind path, the downwind rain is greater than the upwind and central or trending upward in 54.8% of days, representing 62% of seasonal rainfall.

2.3 Rainfall Variability is Due to the Urban Area

A Kruskal-Wallis test between all three regions showed that the rainfall distribution is statistically distinct between all three groups ($p < 0.01$) for almost every 1° bin of storm motion vectors. A Mann-Whitney test was performed to compare the pairs of each of the three regions. There is less distinction between the upwind and central rainfall distributions for storms with west-to-east motion (90°-105°) where the $p > 0.01$. The central-downwind distributions are statistically distinct except for storms from a more NW-SE motion (145°), where there is also less distinction between all three regions. The same tests, when performed over the adjacent rural area with arbitrary boundaries, show no significant difference in precipitation distribution over the same transect lengths. Therefore, the precipitation distribution differences across the urban transects indicate an urban modification.

Analysis of Figure 3 demonstrates the existence of distinct urban rainfall patterns and the modes of urban modification of storms originating from different directions. Thunderstorm motion also represents a proxy of differential exposure to urban land cover because of the non-circular shape of the Chicago urban footprint. However, despite that the cross section of urban footprint varies from 70–170km, there is no significant or monotonic relation between urban extent and rainfall modification. This indicates that the Chicago urban area is large enough to "fully modify" incipient thunderstorms causing climatological signature (Schmid and Niyogi 2013).

The direction of storm propagation can act as a proxy for thunderstorm morphology and how different storm types respond to urban modification. For example, in the Chicago area during the summer, linear storm morphologies (e.g. squall lines, bow echoes) typically move from the NW or N, while single-cell convection is more likely to move from the SW or W (Niyogi et al. 2011). *Cluster 1* represents weak cellular (from SW) or quasi-linear (from NW) convection which is weakened by the upwind urban-rural boundary. The UHI circulation suppresses convection while the urban aerosol plume perturbs the cloud, which initially reduces convective rainfall. The UHI-convergence over the city along with aerosol-cloud interaction gradually intensifies the storm, leading to enhanced precipitation downwind. *Cluster 2* represents stronger cellular and linear convection. Strong individual cellular convection still experiences an abrupt upwind boundary, while linear convection may erode both the land surface and aerosol pre-storm boundaries. Thus the linear storms of *Cluster 2* do not show a significant upwind change. The strong external forcing present in *Cluster 2* storms likely dampens the urban effects. *Cluster 3* and *4* represent weakly forced linear convective or non-convective (stratiform) systems. At the upwind edge, convection may be initiated by the UHI circulation, or enhanced. Rainfall at the boundary could also be enhanced by a faster convective response to the aerosol-interactions or general enhancement of non-convective precipitation, where greater cloud water can increase stratiform rainfall. However, in all cases, these observations alone cannot distinguish the land-surface from the urban aerosol effects in upwind and central regions and need to be considered as the total urban impact on the thunderstorms

2.4 Day-of-week as a proxy for urban aerosol loading

In Chicago, weekend pollutants are typically only 40-50% of their weekday values (Blanchard et al. 2008). These difference in urban aerosols produce a remarkable effect on observed precipitation (Figure 4). A summer season comprised entire of weekday precipitation events would receive 15% more precipitation (40 mm) across the entire domain than weekend events. The difference is most pronounced in the downwind anomaly region, where the maximum weekday-weekend difference is coincident with the maximum seasonal anomaly. Locales downwind of Chicago, receive nearly 50% more rainfall on weekdays than weekends. The weekday-weekend difference also eliminates what influences urban land boundaries and Lake Michigan have on regional rainfall variability leaving only the urban aerosol forcing. While most of the study area receives more weekday precipitation, on weekends there is an increase at the upwind boundary. The statistical distributions of weekday and weekend urban rainfall are distinct for most of the domain. A Mann-Whitney test for each grid shows that weekday precipitation is statistically distinct from weekend for approximately 87% of the domain ($p < 0.01$). However, *all* downwind grids are distinct to this level of significance. There is less distinction in the upwind grids, suggesting an urban aerosol influence on the rain anomaly.

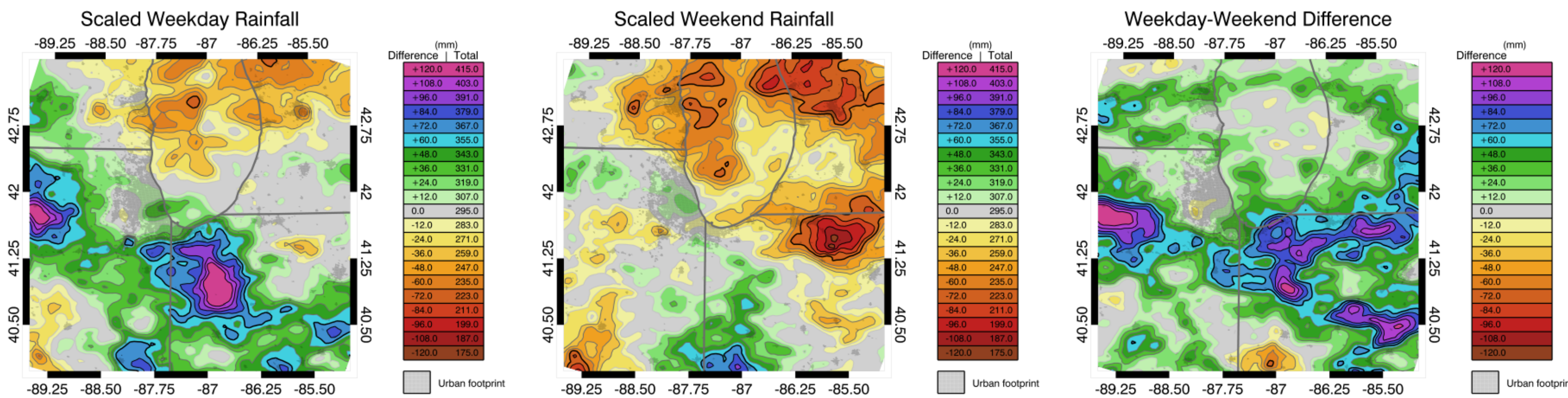

Figure 4. 2005 – 2016 summertime precipitation, scaled to the same seasonal total in Fig. 1, for a) weekdays (Tues. – Fri.) and b) weekend (Sat. – Mon.) days, with the c) weekend – weekday difference between (b) and (a). For the entire region, 60.6% of seasonal precipitation falls on weekdays, which comprise only 57.2% of days. For the downwind anomaly region, the weekday contribution to total seasonal precipitation rises to 63.0%. The largest difference between weekdays and weekends is located near the peak overall downwind anomaly at 40.9N, -86.8W (80 km downwind).

The weekday-weekend cycle of precipitation can show both the aerosol and land-surface contribution to precipitation modification. The aerosol field is approximately coterminous with the urban land cover at the upwind edge, but it can advect far downwind of the city. When a storm initially approaches the city, it encounters the edge of the urban land cover and urban aerosol field concurrently. However, a storm will remain in the downwind aerosol field far from the urban land itself. On weekdays, an approaching storm ingests a heavier aerosol load at the city edge, which can initially suppress convective precipitation as seen in the rainfall reduction at the upwind edge of the city but increases precipitation downwind. On weekends, the aerosol loading is decreased, and a system is prone to a greater contribution from the land surface. The UHI-induced circulation, strongest at the urban edge, invigorates the storm updraft and produces more intense rainfall at the city edge. The lower aerosol load modifies precipitation processes more slowly, so there is still a positive rainfall anomaly downwind.

2.5 Historical Variability of the Anomaly

The combined land-surface and aerosol interactions synergistically explain the climatological variability of the location and strength of the downwind anomaly. The original studies (Changnon 1971, 1968, 1980a) explained the observational history of the La Porte anomaly until 1980. The NWI rainfall began to increase at least by 1920, peaking during the 1950s. From the mid-1950s to 1970, the peak anomaly migrated southwestward 40 km, from near the La Porte observation station to near Valparaiso. By 1980, the anomaly had apparently disappeared. The studies during that time utilized only limited observations, which excluded many cooperative sites. They utilized non-objective analyses (i.e. hand-analyzed maps), fueling the controversy over its existence.

An optimal interpolation method was employed to assemble all historical data, including cooperative sites not in the original studies. The optimally interpolated rainfall anomaly for the Chicago region at 9-km spacing from 1930-2000 is shown in Figure 5. Each map shows the average summertime rainfall anomaly relative to the decadal mean over the ten-year period of each decade. By the 1930s, there was a consistent positive precipitation anomaly in NWI, downwind of Chicago. During the 1940s and 1950s, it intensified and migrated eastward toward La Porte. A peak seasonal anomaly of 120 mm (a 40% enhancement) occurred in 1959, in the grid containing the La Porte station. It is possible that observer bias was responsible for the magnitude of the anomaly, however, the surrounding region also shows a consistent positive anomaly throughout the time. During the 1960s, the rainfall anomaly in La Porte had weakened, or possibly migrated far to the southeast of the urban area. In the 1970s, the anomaly seemingly disappeared, and led to scientific debates regarding the urban rainfall modification (Holzman 1971; Rao 1980). During the 1980s, the downwind anomaly began to return and persists to the present.

Given that the 1970s was the decade with the highest total aerosol output from Chicago (Lyons and Stedman 1991; Landis 1980), the “disappearance” of the anomaly may have been due to the nonlinear response of precipitation to very high aerosol loading (Rosenfeld et al. 2008). During the 1970s, the portion of heavy rain events downwind is historically low (less than 20% of rainfall), indicative of suppressed convection at the time. Despite a continued increase in metropolitan population and urban land cover extent, the implementation of the Clean Air Act (CAA) reduced Chicago’s pollution in the decades after the 1970s. During the 1980s, the anomaly began to “reappear” south and slightly west of its previous location. Along with increased regional rainfall in 1990s to the 2000s, consistent with other urban areas following the CAA (Diem 2013), the positive anomaly persisted and migrated from the east to the southeast of the city. The shift and broadening of the downwind anomaly coincided with a predominantly westward suburban expansion. The largest urban footprint influences a greater number of storms, producing a downwind anomaly over a larger location. When a storm is perturbed by urban effects at a more westward location, it completes the process to intensify surface precipitation at a more westward location. Therefore, the location of the precipitation anomaly shifted to its current location.

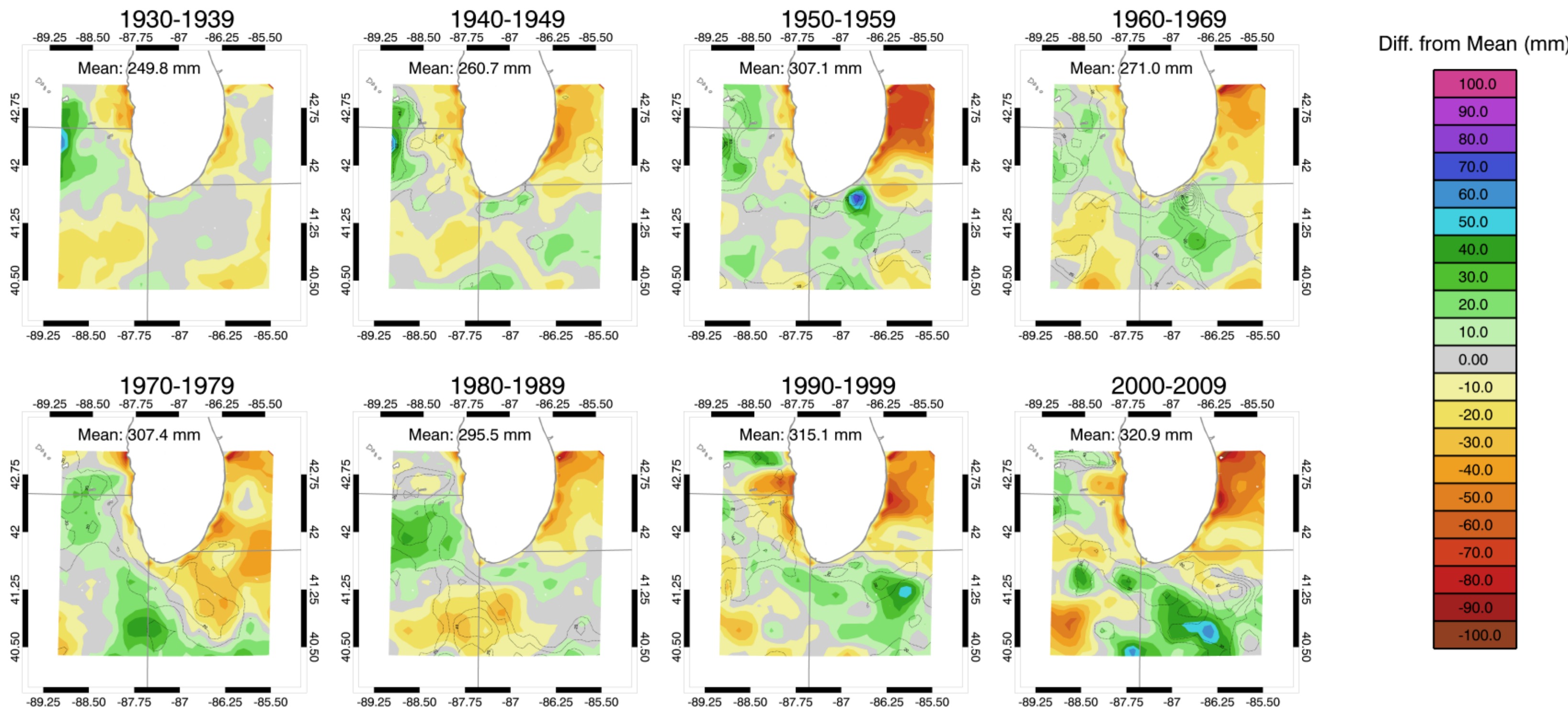

Figure 5. The relative precipitation anomaly to the regional mean for each decade from the 1930s to 2000s over the study region, as reconstructed using optimal interpolation of surface rainfall measurements. The peak anomaly magnitude in the 1950s may be due to observer bias. Its apparent disappearance during the 1970s is likely due to the extremely high aerosol loading suppressing precipitation in polluted areas. The general westward movement of the anomaly is explained by the preferential expansion of the Chicago urban footprint to the west. Individual storm systems in 2000 encounter the urban edge at a more westerly location, begin modification earlier, and produce increased rainfall at a more westerly location.

2.6 Continued Existence and Dependence on Synoptic Factors

While the overall downwind anomaly is a climatological feature, its location and intensity for any given event is dependent on external conditions. Figure 6 details how the anomaly varies depending on storm speed, synoptic instability (quantified through convectively available potential energy or CAPE), and the degree of local land-atmosphere coupling (represented by planetary boundary layer or PBL height). Results identify a significant linear relation between maximum rainfall location and storm speed (Fig. 6a). Independent of latitudinal location, a weighted linear regression shows that for every 1 m·s^{-1} increase in storm velocity, the location of maximum rainfall moves approximately 10 km to the east. This indicates that the urban modification is time-

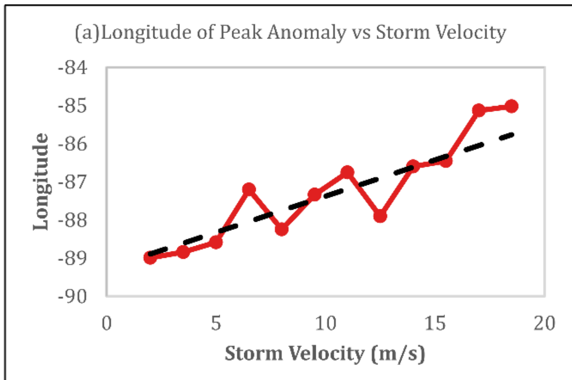

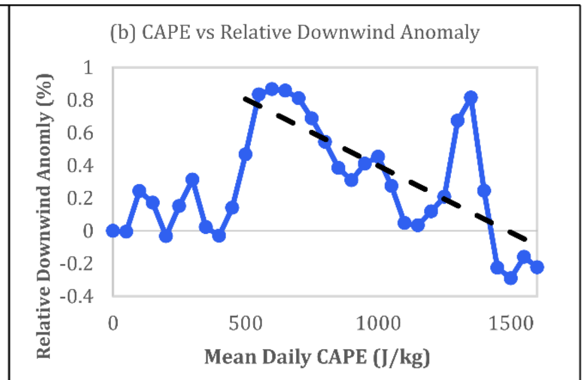

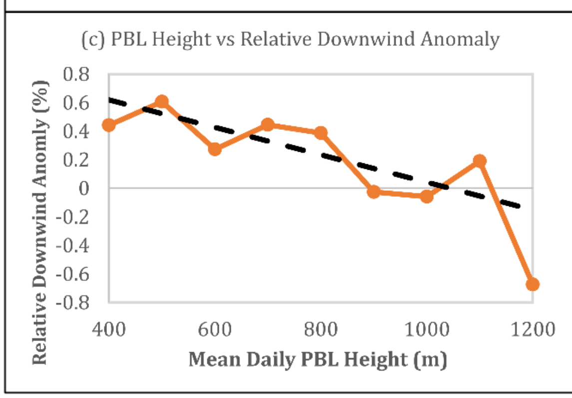

(d) Summary of Relevant Statistics

	n	*T*	r_1	m_1	R^2_1	p_1	r_2	m_2	R^2_2	p_2
Storm V	.99	.1.5	**.91**	**.19**	**.72**	**.00**	*.18*	*.03*	*.54*	*.65*
PBL H	.99	**62.4**	-.14	---	---	---	**-.86**	**-.10**	**.86**	**.03**
CAPE	.91	**30.1**	-.28	---	---	---	*.03*	*.00*	*.47*	*.26*
C < 500	*.58*	54.3	---	---	---	---	*.40*	*.05*	*.51*	*.06*
C >500	*.36*	20.0	---	---	---	---	**-.74**	**-.08**	**.82**	**.00**

n - Percent of days considered
T - Total seasonal rainfall trend (mm/characteristic value)
Subscripts
1- Variable compared to longitude
2- Variable compared to anomaly
r - Pearson correlation coefficient
m - Slope of linear regression
R^2 - closeness of fit to regression
p - Statistical significance of ANOVA for regression against observations.
Bold values indicate > 95% significance.

Figure 6. Graphs showing the relation between a) storm velocity and anomaly longitude, b) CAPE and downwind anomaly intensity, c) PBL height and downwind anomaly intensity, and d) Table summarizing relevant statistics and regression slopes and significances. In (d), regressions are not performed for insignificant relationships. The relation between the precipitation anomaly shows that a) faster moving storms produce an anomaly at a location farther downwind (more easterly), b) for storms within a regime sufficient for cold convective precipitation (CAPE > 500 J·kg-1), the more strongly forced storms decrease the relative intensity of the downwind anomaly, and c) the downwind anomaly is most intense on days with strong land-atmosphere coupling (i.e. low PBL height).

dependent. The surface heterogeneity and feedback from the urban environment modifies a storm to produce a downwind increase in rainfall after a "sufficient" time threshold, on the scale of cycling a surface perturbation throughout a storm (an hour or two). Faster storms have moved farther downwind than the slower ones thus the maximum anomaly is located farther to the east.

The relative intensity of the downwind anomaly (defined as the ratio of peak rainfall to the domain mean) is inversely related to synoptic forcing (Fig. 6b) and land-atmosphere coupling (Fig. 6c). The total domain precipitation increases monotonically for both increased CAPE (10% per 100 J/kg) and higher PBL heights (20% per 100 m), but the relative anomaly decreases. Meanwhile, the relative anomaly decreases by 10% for every 100 m increase in PBL height, further highlighting that the anomaly is due to the coupling between the land surface and atmosphere. CAPE has a non-linear impact on the prominence of the downwind anomaly. On stable days (CAPE < 500 $J \cdot kg^{-1}$), there is no detectable relation. But for higher values, the relative downwind anomaly decreases by 8.2% per 100 $J \cdot kg^{-1}$ of added CAPE. This indicates that the downwind rainfall anomaly is created by the modification of convective precipitation and is most prominent on days with moderate but not high instability.

2.7 Discussion

Considering the results from this study, a paradigm by which thunderstorm modify in the urban environment is possible:

1) An incipient storm encounters the land-cover and aerosol boundary at the upwind urban edge. Both effects simultaneously perturb the storm, but the variable aerosol effects can be seen in the weekday-weekend difference. Weekend precipitation increases only at the upwind edge. In environments with the weakest forcing, the upwind UHI may initiate convection, but the upwind effect for most storms is rainfall reduction. In the most strongly forced environments, the storm weakens more gradually, due to dampened urban effects.

2) The storm continues to ingest urban aerosols and weak surface perturbations from the urban surface as it crosses. For most convection, a system will modify to eventually produce enhanced rainfall. Depending on the speed of a storm and synoptic forcing, this enhancement may occur while the system is still over the urbanized area. In systems with

the strongest external forcing, the total urban modification is realized only as a gradual reduction in rainfall, with possibly no further enhancement.

3) Downwind the aerosols maintain an "urban thunderstorm" well past the edge of the urban land. The land surface no longer directly provides urban perturbations, but the rainfall enhancement may exist downwind, dependent on storm velocity. The location of the downwind anomaly depends on where a storm begins modification upwind with its speed.

Across all events, the relative anomaly is most prominent in locally forced, highly coupled storms, further confirming that urban environments significantly modify rainfall climatology. This modification can be detected in observational climatology when the data are reviewed with consideration of urban dynamics and aerosol-cloud processes. While the effects of the urban land surface and aerosols both impact a system, the magnitude of the weekday-weekend rainfall difference compared to measures of land-atmosphere coupling, along with the process understanding of aerosol-cloud interaction, indicate that the aerosol-cloud modification can be a *dominant mechanism* by which urban rainfall modification occurs. The urban land effects forcing is secondary, however, the land is reason that the aerosols are elevated into the cloud via UHI circulation and the reason the aerosol exist in the first place via human activity.

2.8 References

Bellerby, T. J., 2013: Ensemble Representation of Uncertainty in Lagrangian Satellite Rainfall Estimates. *J. Hydrometeorol.*, **14**, 1483–1499, doi:10.1175/JHM-D-12-0121.1.

Bernard, E., P. Naveau, M. Vrac, O. Mestre, E. Bernard, P. Naveau, M. Vrac, and O. Mestre, 2013: Clustering of Maxima: Spatial Dependencies among Heavy Rainfall in France. *J. Clim.*, **26**, 7929–7937, doi:10.1175/JCLI-D-12-00836.1.

Blanchard, C., S. Tanenbaum, and D. Lawson, 2008: Differences between Weekday and Weekend Air Pollutant Levels in Atlanta; Baltimore; Chicago; Dallas–Fort Worth; Denver; Houston; New York; Phoenix; Washington, DC; and Surrounding Areas. *J. Air Waste Manage. Assoc.*, **58**, 1598–1615, doi:10.3155/1047-3289.58.12.1598.

Changnon, S. A., 1968: The La Porte weather anomaly - Fact or fiction? *Bull. Am. Meteorol. Soc.*, **49**, 4–11.

Changnon, S. A., 1971: La Porte Anomaly. *Science (80-.).*, **172**, 987–988, doi:10.1126/science.172.3987.987-a.

Changnon, S. A., 1980: More on the La Porte Anomaly: A Review. *Bull. Am. Meteorol. Soc.*, **61**, 702–711, doi:10.1175/1520-0477(1980)061<0702:MOTLPA>2.0.CO;2.

Changnon, S. A., 1992: Inadvertent Weather Modification in Urban Areas: Lessons for Global Climate Change. *Bull. Am. Meteorol. Soc.*, **73**, 619–627, doi:10.1175/1520-0477(1992)073<0619:IWMIUA>2.0.CO;2.

Changnon, S. A., R. G. Semonin, and F. A. Huff, 1976: A Hypothesis for Urban Rainfall Anomalies. *J. Appl. Meteorol.*, **15**, 544–560, doi:10.1175/1520-0450(1976)015<0544:AHFURA>2.0.CO;2.

Chen, Y.-R., B. Yu, and G. Jenkins, 2013: Secular Variation in Rainfall Intensity and Temperature in Eastern Australia. *J. Hydrometeorol.*, **14**, 1356–1363, doi:10.1175/JHM-D-12-0110.1.

Cheng, C. S., G. Li, Q. Li, H. Auld, C. S. Cheng, G. Li, Q. Li, and H. Auld, 2010: A Synoptic Weather Typing Approach to Simulate Daily Rainfall and Extremes in Ontario, Canada: Potential for Climate Change Projections. *J. Appl. Meteorol. Climatol.*, **49**, 845–866, doi:10.1175/2010JAMC2016.1.

Cumbie-Ward, R. V., and R. P. Boyles, 2016: Evaluation of a High-Resolution SPI for Monitoring Local Drought Severity. *J. Appl. Meteorol. Climatol.*, **55**, 2247–2262, doi:10.1175/JAMC-D-16-0106.1.

De, S. J., E. F. Wood, and S. J. Déry, 2005: Observed twentieth century land surface air temperature and precipitation covariability. *Geophys. Res. Lett.*, **32**, 1–4, doi:10.1029/2005GL024234.

Dettwiller, J., and S. A. Changnon, 1976: Possible Urban Effects on Maximum Daily Rainfall at Paris, St. Louis and Chicago. *J. Appl. Meteorol.*, **15**, 517–519, doi:10.1175/1520-0450(1976)015<0518:PUEOMD>2.0.CO;2.

Diem, J. E., 2013: The 1970 Clean Air Act and termination of rainfall suppression in a U.S. urban area. *Atmos. Environ.*, **75**, 141–146, doi:10.1016/j.atmosenv.2013.04.041.

Fabry, F., V. Meunier, B. P. Treserras, A. Cournoyer, and B. Nelson, 2017: On the climatological use of radar data mosaics: Possibilities and challenges. *Bull. Am. Meteorol. Soc.*, **98**, 2135–2148, doi:10.1175/BAMS-D-15-00256.1.

Friedl, M., and D. Sulla-Menashe, 2015: MCD12Q1 MODIS/Terra+Aqua Land Cover Type Yearly L3 Global 500m SIN Grid V006 [Data set]. doi:10.5067/MODIS/MCD12Q1.006.

Friedl, M. . and Coauthors, 2002: Global land cover mapping from MODIS: algorithms and early results. *Remote Sens. Environ.*, **83**, 287–302, doi:10.1016/S0034-4257(02)00078-0.

Gabriel, K. R., 2002: Confidence Regions and Pooling—Some Statistics for Weather Experimentation. *J. Appl. Meteorol.*, **41**, 505–518, doi:10.1175/1520-0450(2002)041<0505:CRAPSS>2.0.CO;2.

Gandin, L. S., 1966: Objective analysis of meteorological fields. By L. S. Gandin. Translated from the Russian. Jerusalem (Israel Program for Scientific Translations), 1965. Pp. vi, 242: 53 Figures; 28 Tables. £4 1s. 0d. *Q. J. R. Meteorol. Soc.*, **92**, 447–447, doi:10.1002/qj.49709239320.

Hamidi, A., N. Devineni, J. F. Booth, A. Hosten, R. R. Ferraro, and R. Khanbilvardi, 2016: Classifying Urban Rainfall Extremes using Weather Radar Data: An Application to Greater New York Area. *J. Hydrometeorol.*, JHM-D-16-0193.1, doi:10.1175/JHM-D-16-0193.1.

Holzman, B. G., 1971: La Porte Precipitation Fallacy. *Science (80-.).*, **171**, 847–847, doi:10.1126/science.171.3974.847.

Huff, F. a., and S. a. Changnon, 1973: Precipitation Modification By Major Urban Areas. *Bull. Am. Meteorol. Soc.*, **54**, 1220–1232, doi:10.1175/1520-0477(1973)054<1220:PMBMUA>2.0.CO;2.

Lamptey, B. L., 2008: Comparison of Gridded Multisatellite Rainfall Estimates with Gridded Gauge Rainfall over West Africa. *J. Appl. Meteorol. Climatol.*, **47**, 185–205, doi:10.1175/2007JAMC1586.1.

Livneh, B., E. a. Rosenberg, C. Lin, B. Nijssen, V. Mishra, K. M. Andreadis, E. P. Maurer, and D. P. Lettenmaier, 2013: A Long-Term Hydrologically Based Dataset of Land Surface Fluxes and States for the Conterminous United States: Update and Extensions*. *J. Clim.*, **26**, 9384–9392, doi:10.1175/JCLI-D-12-00508.1.

Lowry, W. P., 1998: Urban effects on precipitation amount. *Prog. Phys. Geogr.*, **22**, 477–520, doi:10.1177/030913339802200403.

Lyons, C. E., and D. H. Stedman, 1991: *Remote Sensing Enhanced Motor Vehicle Emissions Control for Pollution Reduction in the Chicago Metropolitan Area: Siting and Issue Analysis*. 75p pp.

Maia, A. H. N., H. Meinke, S. Lennox, and R. Stone, 2007: Inferential, Nonparametric Statistics to Assess the Quality of Probabilistic Forecast Systems. *Mon. Weather Rev.*, **135**, 351–362, doi:10.1175/MWR3291.1.

McEnery, J. and Coauthors, 2005: NOAA'S ADVANCED HYDROLOGIC PREDICTION SERVICE. *Bull. Am. Meteorol. Soc.*, **86**, 375–386, doi:10.1175/BAMS-86-3-375.

McRoberts, D. B., J. W. Nielsen-Gammon, D. B. McRoberts, and J. W. Nielsen-Gammon, 2012: The Use of a High-Resolution Standardized Precipitation Index for Drought Monitoring and Assessment. *J. Appl. Meteorol. Climatol.*, **51**, 68–83, doi:10.1175/JAMC-D-10-05015.1.

Menne, M. J., I. Durre, R. S. Vose, B. E. Gleason, and T. G. Houston, 2012: An Overview of the Global Historical Climatology Network-Daily Database. *J. Atmos. Ocean. Technol.*, **29**, 897–910, doi:10.1175/JTECH-D-11-00103.1.

Mesinger, F. and Coauthors, 2006: North American Regional Reanalysis. *Bull. Am. Meteorol. Soc.*, **87**, 343–360, doi:10.1175/BAMS-87-3-343.

Nelson, B. R., D.-J. Seo, and D. Kim, 2010: Multisensor Precipitation Reanalysis. *J. Hydrometeorol.*, **11**, 666–682, doi:10.1175/2010JHM1210.1.

Niyogi, D. and Coauthors, 2011: Urban Modification of Thunderstorms: An Observational Storm Climatology and Model Case Study for the Indianapolis Urban Region *. *J. Appl. Meteorol. Climatol.*, **50**, 1129–1144, doi:10.1175/2010JAMC1836.1.

Notaro, M., K. Holman, A. Zarrin, E. Fluck, S. Vavrus, and V. Bennington, 2013: Influence of the Laurentian Great Lakes on Regional Climate. *J. Clim.*, **26**, 789–804, doi:10.1175/JCLI-D-12-00140.1.

Paul, S., S. Ghosh, M. Mathew, A. Devanand, S. Karmakar, and D. Niyogi, 2018: Increased Spatial Variability and Intensification of Extreme Monsoon Rainfall due to Urbanization. *Sci. Rep.*, **8**, 3918, doi:10.1038/s41598-018-22322-9.

Peterson, T. C., R. Vose, R. Schmoyer, and V. Razuvaëv, 1998: Global historical climatology network (GHCN) quality control of monthly temperature data. *Int. J. Climatol.*, **18**, 1169–1179, doi:10.1002/(SICI)1097-0088(199809)18:11<1169::AID-JOC309>3.0.CO;2-U.

Rao, A. R., 1980: Stochastic Analysis of Annual Rainfall Affected by Urbanization. *J. Appl. Meteorol.*, **19**, 41–52, doi:10.1175/1520-0450(1980)019<0041:SAOARA>2.0.CO;2.

Rosenfeld, D. and Coauthors, 2008: Flood or drought: how do aerosols affect precipitation? *Science (80-.).*, **321**, 1309–1313, doi:10.1126/science.1160606.

Schmid, P. E., and D. Niyogi, 2013: Impact of city size on precipitation-modifying potential. *Geophys. Res. Lett.*, **40**, 5263–5267, doi:10.1002/grl.50656.

Wilks, D. S., 2011: *Statistical methods in the atmospheric sciences*. Academic Press, 676 pp.

Wu, W., D. Kitzmiller, and S. Wu, 2012: Evaluation of Radar Precipitation Estimates from the National Mosaic and Multisensor Quantitative Precipitation Estimation System and the WSR-88D Precipitation Processing System over the Conterminous United States. *J. Hydrometeorol.*, **13**, 1080–1093, doi:10.1175/JHM-D-11-064.1.

Zhang, J. and Coauthors, 2011: National Mosaic and Multi-Sensor QPE (NMQ) System: Description, Results, and Future Plans. *Bull. Am. Meteorol. Soc.*, **92**, 1321–1338, doi:10.1175/2011BAMS-D-11-00047.1.

Zhang, J. and Coauthors, 2014: A Real-Time Algorithm for Merging Radar QPEs with Rain Gauge Observations and Orographic Precipitation Climatology. *J. Hydrometeorol.*, **15**, 1794–1809, doi:10.1175/JHM-D-13-0163.1.

CHAPTER 3. NUMERICAL MODEL DEVELOPMENT

Observations alone can identify urban precipitation patterns, and careful analysis can demonstrate the sum of potential forcings. But separating the individual factors contributing to urban thunderstorm modification absolutely requires the use of a robust numerical weather model (Shepherd 2005; Grimmond et al. 2010; Mills 2014). This chapter focuses on the numerical model features and innovations used in the simulations in the forthcoming chapters. The model developed is Urban RAMS: An implementation of the Regional Atmospheric Modeling System (RAMS, 3.1) coupled with the Town Energy Budget (TEB, 3.2.1) urban canopy model, the Simple Photochemical Module (SPM, 3.2.2) air quality and chemistry model, and using a urban procedural model derived schedule of surface emissions which incorporates simulated human activity into the weather system (3.2.3). The innovations used to improve this model represent a completely new contribution to the field and contain original published work (Schmid and Niyogi 2017, 2013).

3.1 The Regional Atmospheric Modeling System (RAMS)

RAMS is a non-hydrostatic, cloud-resolving model particularly suited to handling urban-atmospheric interactions (Cotton et al. 2003; Pielke et al. 1992). It is well suited for these types of numerical simulations because it is capable of resolving surface convection at a relative fine scale, and it utilizes a robust cloud microphysics scheme to handle cloud-aerosol interactions. It uses two-way interactive Arakawa C grid nesting, with few restrictions on the nest locations and ratios. The relatively forgiving grid geometry also enables multiple nests within one broader grid (Walko et al. 1995), providing enhanced potential for multicity simulations (see Chapter 6). It employs the Harrington 2-stream radiative parameterization (1997), the Kain-Fritsch (1993; Kain 2004) convective parameterization for grids with greater than 10-km spacing[4], Klemp and Wilhelmson lateral boundary conditions (1978), Mellor and Yamada turbulence closure (1982).

The model uses the LEAF-3 land surface parameterization (Walko et al. 2000; Walko and Tremback 2005). LEAF-3 parameterizes typical surface features such as soil and vegetation, using

[4] None of the simulations from Chapter 4-6 were in tropical locations. For tropical and some marine convection, parameterization should be employed in grids as fine as 4-km.

30 different land surface classes. It also can represent sub-grid variability in surface characteristics by divided model grid cells into patches. This makes it particularly well suited in a complex urban environment, as it can approximate the existence of urban trees or lakes without the need to define an entirely new land surface class. Along with being able to create features such as "greenness" (i.e. 95% urban, 5% trees) within an urban grid, the patch framework creates a more realistic urban-rural boundary by more transitioning from urban to rural over a few model grid cells. This type of transition prevents unrealistically large circulations at the boundary (e.g. more typical of a land-sea breeze).

RAMS cloud microphysics are particularly well-suited to handle urban aerosol-cloud interaction because the parameterization explicitly considers cloud nucleation (van den Heever and Cotton 2007). The microphysical parameterization uses the bin-emulating Colorado State University (CSU) scheme with eight two-moment water substance types, including six hydrometeor types representing two "bins" of small-mode/large-mode hydrometeors: drizzle/rain, graupel/hail, snow/aggregates. It includes explicitly nucleating aerosols (Saleeby et al. 2004; Meyers et al. 1997) with dry and wet deposition, and a hybrid-binned riming scheme for the formation of graupel and hail (Saleeby and Cotton 2008). The small (CCN) aerosols activate to form cloud droplets (Feingold et al. 1994), while the large (GCCN) aerosols nucleate directly to drizzle (Feingold et al. 1999). The bin-approximating approach of the CSU scheme is particularly useful for urban aerosol-cloud interaction because it parameterizes the hydrometeors important for both warm-rain and cold-rain modification. In particular, the riming scheme accurately simulates the cold-rain enhancement via autoconversion of snow to graupel via riming, then melting into large rain drops.

3.2 Development of Urban RAMS Parameterization

To create an urban version of RAMS, it needed the capacity to simulate the urban land surface through an urban canopy model (3.2.1) and a better way to handle urban aerosols (3.2.2, 3.2.3). The "out-of-the-box" model (RAMS 6.0) initializes CCN and GCCN homogeneously in space. Many previous RAMS studies (van den Heever and Cotton 2007; Carrió et al. 2010; Collins et al. 2012) varied concentrations over the entire domain. But the urban model required for this study required some way of capturing the spatial variability of an urban aerosol plume. Aerosols

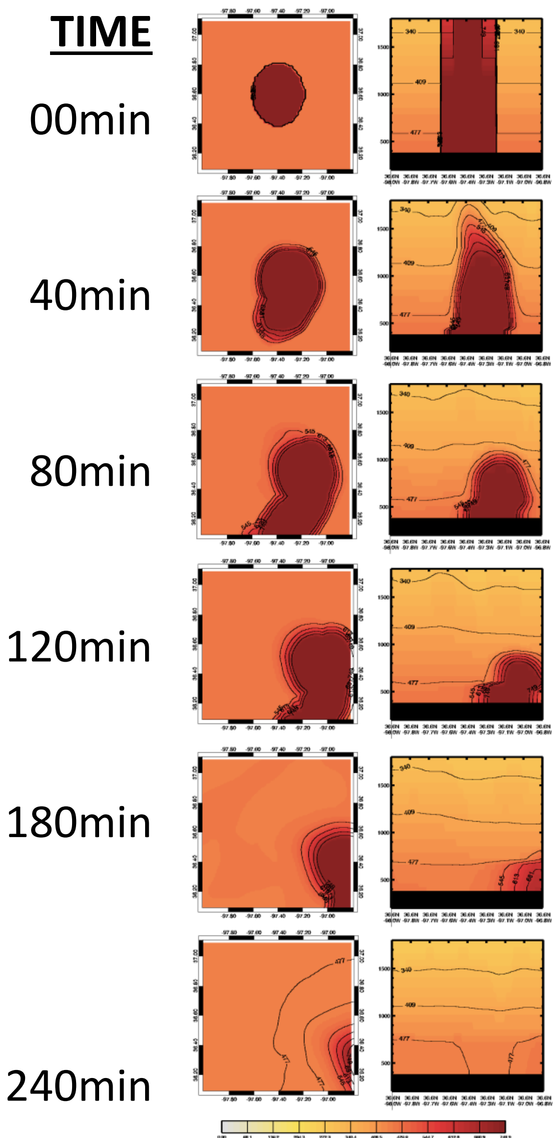

Figure 7. Six hour simulation of heterogeneous aerosol initialization. The aerosol column almost immediately disperses and leaves the domain.

(CCN) could be heterogeneously distributed in space at model initiation, but preliminary simulations showed that the column collapsed and left the domain within a few hours (Figure 7). In fact, without nudging, model CCN ultimately leave the entire domain after a few days of simulation time, which leads to a dry bias in long term RAMS simulations. The solution to this problem was to treat urban areas as aerosol sources in order to create variability and replenish the entire model's supply of cloud-nucleating aerosols.

3.2.1 The Town Energy Budget (TEB)

The Town Energy Budget (TEB) parameterization (Masson 2000) parameterizes the urban energy balance in the urban roughness sublayer. It replaces LEAF-3 for the roughness sublayer in urban grid squares in the model. It treats urban grids as a street canyon with mostly uniform geometry to calculate temperature, humidity, wind speed, and energy fluxes. Urban grids are still divided into patches near boundaries through LEAF-3, so different urban grids can contain different levels of urbanization. TEB simplifies the urban canyon to fluxes between a generic "wall", "roof", and "road", each with a prescribed albedo and emissivity. The street canyon geometry requires building height, building fraction, building roughness length, and overall roughness length (z_0). As long as there are model-realistic values for each of these parameters, any number of urban types (e.g. local climate zones Ching et al. 2018) can be defined. Table 1 shows the values used for this implementation of TEB. The population density and job density values are not simulated in RAMS, but rather in an external traffic model used to calculate surface emissions for each urban type. The "Downtown" climate zone is also not implemented in RAMS as it would populate so few model grid squares, that its inclusion was not warranted in simulations at or around 1-km grid spacing.

Table 1. TEB parameters defined for this implementation of RAMS. Note the population and job density values are not for a RAMS simulation but used in the external traffic model (3.2.3) to simulation time-dependent surface emissions.

	Old Urban	Suburban	Downtown
Building Height (m)	15	5	55
Building fraction	0.6	0.4	0.8
Building HL	0.75	0.50	3.00
Canyon Aspect Ratio	1.125	0.333	12
Building roughness	1.50	0.40	6.75
z0	0.92	0.19	5.41
Roof Albedo	0.18	0.15	0.13
Roof Emissivity	0.91	0.91	0.90
Road Albedo	0.16	0.18	0.15
Road Emissivity	0.95	0.95	0.90
Wall Albedo	0.20	0.20	0.25
Wall Emissivity	0.90	0.90	0.85
Pop. Density (km^{-2})	5,000	1,200	12,000
Job Density (km^{-2})	2,800	350	60,000

3.2.2 The Simple Photochemical Module (SPM)

Urban RAMS is coupled with the Simple Photochemical Module (SPM) (Freitas et al. 2005), which handles the atmospheric chemical species most important to air quality prediction. In particular, the SPM handles the formation and dispersion of sulfur dioxide. The SPM emits during each time-step on the innermost model grid from the urban land surfaces separate vehicular and industrial components of NO, NO_2, $PM_{2.5}$, SO_2, and VOCs, predicting their interactions and subsequent byproducts. Industrial emissions are temporally constant from the urban land grids while vehicular emissions vary with local time-of-day and day-of-week. Vehicular emissions are determined using results from an offline traffic simulator described in 3.2.3. On weekdays, the emissions show two daily maxima corresponding to traffic rush hours, while on weekends, there is a single maximum during midday (Figure 8). The timing of the traffic rush hour(s) of any urban area is determined by that area's day-of-week and local time zone, and it can also be changed to reflect non-traditional work or commuting practice.

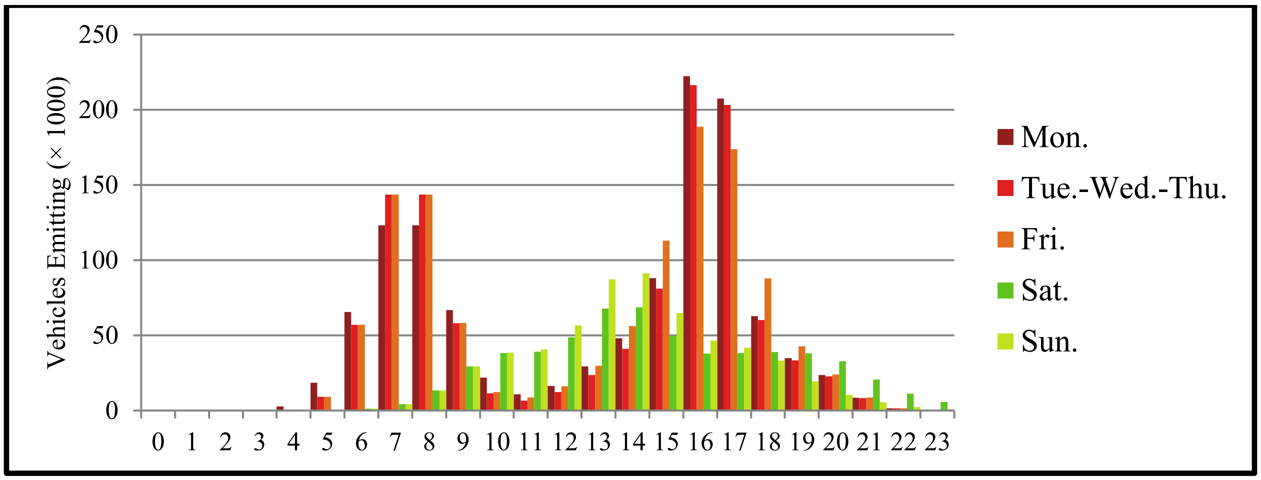

Figure 8. Comparison of weekday and weekend vehicular aerosol emission rates. Weekdays have a twice-daily rush hour with most of the day's emissions. Weekends have a broader emissions spectrum peaking from mid-day to evening local time.

SO_2 is necessary for the formation of the model hygroscopic urban CCN, ammonium hydroxide[5]. The formation of CCN from SO_2 in the model is approximated using a mass-balance approach based on measurements of nucleating sulfate formation made by Stevens et al. (2012). The Stevens et al. study found that 10^{17} to 10^{18} nucleating aerosol particles (0.01μm – 0.09μm radius) are formed per kilogram SO_2. The large range yields a formation efficiency (i.e. percent of SO_2 molecules becoming ammonium sulfate) of between 0.2% (if a kilogram of gas forms 10^{17} 0.01μm aerosols) to 14% (for 10^{18} 0.06μm aerosols). The simulated CCN are among the smaller particles assessed in the Stevens et al. study (0.02μm radius), and a series of simulations were

[5] CCN chemical speciation is a very poorly studied field as observations are almost non-existent. Cloud modification seems to be consistent with a sulfate dominant mode of nucleation. However, nitrates theoretically nucleate more rapidly, but into smaller droplets which only suppresses overall precipitation. Chapter 7 discusses this in further detail as one of the remaining levels of complexity in urban rainfall modeling.

performed to determine a formation efficiency consistent with previous measurements and modeling studies. A constant 0.8% particle formation efficiency was found to achieve the approximate urban aerosol concentrations used in prior thunderstorm interaction studies. A 0.8% efficiency produced peak cloud-free urban CCN concentrations of approximately 2000 cm^{-3} using SO_2 emission rates from Freitas et al. (2005). That urban concentrations are similar to previous modeling studies of urban aerosol-cloud interactions using RAMS (van den Heever and Cotton 2007) to represent aerosol concentrations measured during METROMEX urban field campaign (Changnon et al. 1976). For GCCN, the model assumes it is a large carbon particle coated in ammonium sulfate. A one-to-one mass balance of PM2.5 at concentration $25\mu g \cdot kg^{-1}$ (a mid-range urban concentration) equates to a number concentration of 0.1 cm^{-3} of carbon particles with mean $r = 3\mu m$ and density = $2.16 g \cdot cm^{-3}$ (80% carbon, 20% $(NH_4)_2SO_4$). Given that the mass balance produces the desired urban/rural CCN and GCCN concentration, no explicit new particle formation routine has been implemented yet.

3.2.3 Surface Emissions from Traffic Simulations

The SPM separates emission into traffic and industrial components. While the industrial component is held constant (i.e factories are always running at approximately the same level), the traffic component varies by time-of-day and by day-of-week. To simulate traffic aerosol loading, an offline traffic simulator was used (Garcia-Dorado et al. 2014, 2017). The traffic simulation used the population and job density from the TEB classes (Table 1) to simulate the behavior of up to 300,000 individual vehicles. The model can accommodate up to 360 km of roads either in a defined map or in an arbitrary configuration to simulate the behavior of the drivers of those vehicles traveling from home to work or on other trips. Drivers can be defined to make optimal travel, or a more realistic version wherein they do not take a perfect route from home to work.

Using The traffic model outputs vehicular carbon monoxide, which was used to scale the SPM traffic emissions. First traffic simulations used a 25 km radius circular city, with a 12 km inner radius of “Old Urban”, and a small 10 km^2 core of downtown (Figure 9). This setup was used in conjunction with the method described in 3.2.4 and results in Chapter 4. The traffic simulation produced emission patterns on weekdays which showed two peaks corresponding to morning and evening rush hours, and it produced a pattern on weekends with a broader mid-afternoon peak from non-work travel (Fig. 7). The weekend peak emissions value was slightly less than 50% that of weekday, corresponding to the few studies which measured vehicular emissions in time (CITE). The ultimate goal of this technique is to provide an explicitly simulated human feedback within the weather model – That is: aerosols from human behavior modify urban rainfall, it rains where it may have not rained before, human behavior changes due to the rain.

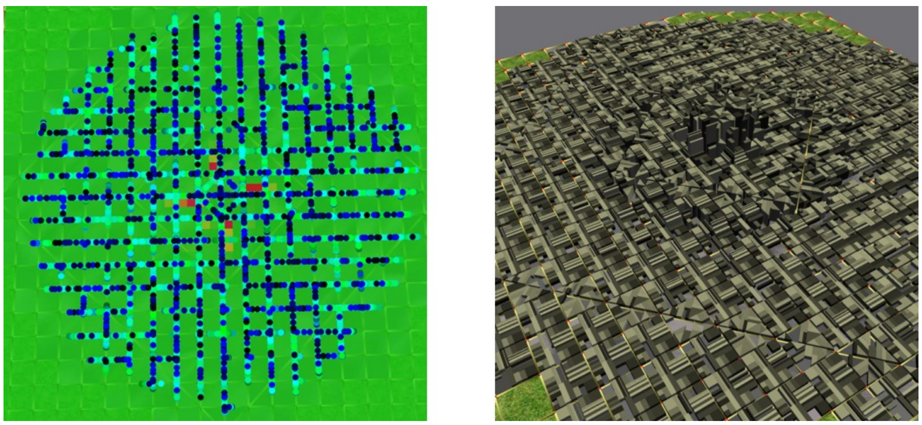

Figure 9. View of simulated circular (RAIL) city with point emissions from each individual vehicle.

3.2.4 The Real Atmosphere Idealized Land Method (RAIL)

Originally as a calibration tool for the SPM and vehicular emissions, the Real Atmosphere Idealized Land (RAIL) method found use as a way to isolate purely urban from non-urban factors in simulations. By removing heterogeneous non-urban features and topography, RAIL can help isolate urban feature for sensitivity studies (Schmid and Niyogi 2013, 2017). The RAIL method initializes the atmospheric component of a numerical model with 3D, heterogeneously variable data, but keeps the land component as simple as possible. In order to minimize non-urban effects, the terrain is completely flat (set to a mean value in the region simulated), and the only land surface types are the urban grids and crops. The "control" in RAIL studies uses a homogeneous, crop-only land surface. And to compare to the control, a circular urban area is subjectively placed in the path of a simulated thunderstorm to ensure the thunderstorm passes directly over the region of interest.

3.3 Caveats of Increased Model Complexity

The complexity of Urban RAMS represents a balance between operational-level speed and high-level parameterizations designed to optimally study one element of the urban modeling system. Any of all of the urban (or non-urban) parameterization schemes could be improved:

- The two urban climate zones in this adaptation of TEB can be adapted to a more robust LCZ scheme such as that provided by WUDAPT[6] (Ching et al. 2018; Mills et al. 2015).
- The fixed layer building scheme of TEB can evolve into a more robust building energy model (BEM) (Nie et al. 2016).
- RAMS cloud microphysics can evolve from the two-moment bin-approximating scheme into a very robust spectral bin microphysics (Khain et al. 2011).
- The model chemistry (SPM) could be improved or even replaced by a more robust model similar to WRF-Chem (Ntelekos et al. 2009).
- With the finer scale urban complexity provided by an LCZ scheme and BEM, the spatial resolution of the model can decrease to provide finer scale simulations.

The obvious caveats of "improving" any model parameterization is a loss of model skill. In many studies the increased complexity of a BEM decreases how realistically the model simulates urban features. This is because all of the parameterizations of any urban model and coupled and dependent on a balance of interconnected assumptions. RAMS cloud-aerosol interactions are based on measurements taken during METROMEX (1971). While contemporary studies (Nie et al., 2016) show the values to be correct, adding complexity in any part of the model requires the rest of it to be rebalanced in order to maintain reasonable atmospheric simulations. A lofty near-future goal in urban meteorology is to provide operational, 100-m simulations at the 2024 Paris Olympics (Masson et al. 2020).

[6] WUDAPT can likely be implemented within this adaptation of TEB without even a model recompile. The LCZ scheme would just require the TEB parameters.

3.4 References

Carrió, G. G., W. R. Cotton, and W. Y. Y. Cheng, 2010: Urban growth and aerosol effects on convection over Houston. Part I: The August 2000 Case. *Atmos. Res.*, **96**, 560–574, doi:10.1016/j.atmosres.2010.01.005.

Changnon, S. A., R. G. Semonin, and F. A. Huff, 1976: A Hypothesis for Urban Rainfall Anomalies. *J. Appl. Meteorol.*, **15**, 544–560, doi:10.1175/1520-0450(1976)015<0544:AHFURA>2.0.CO;2.

Ching, J. and Coauthors, 2018: World Urban Database and Access Portal Tools (WUDAPT), an urban weather, climate and environmental modeling infrastructure for the Anthropocene. *Bull. Am. Meteorol. Soc.*, BAMS-D-16-0236.1, doi:10.1175/BAMS-D-16-0236.1.

Collins, F., R. B. Seigel, and S. C. van den Heever, 2012: Dust Lofting and Ingestion by Supercell Storms. *J. Atmos. Sci.*, **69**, 1453–1473, doi:10.1175/JAS-D-11-0222.1.

Cotton, W. R. and Coauthors, 2003: RAMS 2001: Current status and future directions. *Meteorol. Atmos. Phys.*, **82**, 5–29, doi:10.1007/s00703-001-0584-9.

Feingold, G., B. Stevens, W. R. Cotton, and R. L. Walko, 1994: An explicit cloud microphysics/LES model designed to simulate the Twomey effect. *Atmos. Res.*, **33**, 207–233, doi:10.1016/0169-8095(94)90021-3.

Feingold, G., W. R. Cotton, S. M. Kreidenweis, J. T. Davis, and J. A. T. D. Avis, 1999: The Impact of Giant Cloud Condensation Nuclei on Drizzle Formation in Stratocumulus: Implications for Cloud Radiative Properties. *J. Atmos. Sci.*, **56**, 4100–4117, doi:10.1175/1520-0469(1999)056<4100:TIOGCC>2.0.CO;2.

Freitas, E. D. De, L. D. Martins, P. L. D. S. Dias, and M. D. F. Andrade, 2005: A simple photochemical module implemented in RAMS for tropospheric ozone concentration forecast in the metropolitan area of São Paulo, Brazil: Coupling and validation. *Atmos. Environ.*, **39**, 6352–6361, doi:10.1016/j.atmosenv.2005.07.017.

Garcia-Dorado, I., D. G. Aliaga, and S. V. Ukkusuri, 2014: Designing large-scale interactive traffic animations for urban modeling. *Comput. Graph. Forum*, **33**, 411–420, doi:10.1111/cgf.12329.

Garcia-Dorado, I., D. G. Aliaga, S. Bhalachandran, P. Schmid, and D. Niyogi, 2017: Fast Weather Simulation for Inverse Procedural Design of 3D Urban Models. *ACM Trans. Graph.*, **36**, 1–19, doi:10.1145/2999534.

Grimmond, C. S. B. and Coauthors, 2010: The International Urban Energy Balance Models Comparison Project: First Results from Phase 1. *J. Appl. Meteorol. Climatol.*, **49**, 1268–1292, doi:10.1175/2010JAMC2354.1.

Harrington, J. Y., 1997: The Effects of Radiative and Microphysical Processes on Simulated Warm and Transition Season Artic Stratus. Colorado State University, 289 pp.

van den Heever, S. C., and W. R. Cotton, 2007: Urban Aerosol Impacts on Downwind Convective Storms. *J. Appl. Meteorol. Climatol.*, **46**, 828–850, doi:10.1175/JAM2492.1.

Kain, J. S., 2004: The Kain–Fritsch Convective Parameterization: An Update. *J. Appl. Meteorol.*, **43**, 170–181, doi:10.1175/1520-0450(2004)043<0170:TKCPAU>2.0.CO;2.

Kain, J. S., and J. M. Fritsch, 1993: Convective parameterization for mesoscale models: The Kain-Fritsch scheme. *The Representation of Cumulus Convection in Numerical Models*, American Meteorological Society, 165–170.

Khain, a., D. Rosenfeld, A. Pokrovsky, U. Blahak, and A. Ryzhkov, 2011: The role of CCN in precipitation and hail in a mid-latitude storm as seen in simulations using a spectral (bin) microphysics model in a 2D dynamic frame. *Atmos. Res.*, **99**, 129–146, doi:10.1016/j.atmosres.2010.09.015.

Klemp, J. B., and R. B. Wilhelmson, 1978: The Simulation of Three-Dimensional Convective Storm Dynamics. *J. Atmos. Sci.*, **35**, 1070–1096, doi:10.1175/1520-0469(1978)035<1070:TSOTDC>2.0.CO;2.

Masson, V., 2000: A Physically-based Scheme for the Urban Energy Budget in Atmospheric Models. *Boundary-Layer Meteorol.*, **94**, 357–397, doi:10.1023/A:1002463829265.

Masson, V., E. de Coning, P. Steinle, R. Roberts, and R. S. Sokhi, 2020: WMO Research Demonstration Project: Paris Olympic Games 2024. *15th Symposium on the Urban Environment*, Boston, MA.

Mellor, G. L., and T. Yamada, 1982: Development of a turbulence closure model for geophysical fluid problems. *Rev. Geophys.*, **20**, 851, doi:10.1029/RG020i004p00851.

Meyers, M. P., R. L. Walko, J. Y. Harrington, and W. R. Cotton, 1997: New RAMS cloud microphysics parameterization. Part II: The two-moment scheme. *Atmos. Res.*, **45**, 3–39, doi:10.1016/S0169-8095(97)00018-5.

Mills, G., 2014: Urban climatology: History, status and prospects. *Urban Clim.*, **10**, 479–489, doi:10.1016/j.uclim.2014.06.004.

Mills, G., J. Ching, L. See, B. Bechtel, J. Feddema, V. Masson, and G. J. Steeneveld, 2015: An Introduction to the WUDAPT project. *Proceedings of the ICUC9. Meteo France*, 6.

NIE, W., B. F. ZAITCHIK, G. NI, T. SUN, W. NIE, B. F. ZAITCHIK, G. NI, and T. SUN, 2016: Impacts of Anthropogenic Heat on Summertime Rainfall in Beijing. *J. Hydrometeorol.*, JHM-D-16-0173.1, doi:10.1175/JHM-D-16-0173.1.

Ntelekos, A. A., J. A. Smith, L. Donner, J. D. Fast, W. I. Gustafson, E. G. Chapman, and W. F. Krajewski, 2009: The effects of aerosols on intense convective precipitation in the northeastern United States. *Q. J. R. Meteorol. Soc.*, **135**, 1367–1391, doi:10.1002/qj.476.

Pielke, R. A. and Coauthors, 1992: A comprehensive meteorological modeling system?RAMS. *Meteorol. Atmos. Phys.*, **49**, 69–91, doi:10.1007/BF01025401.

Saleeby, S. M., and W. R. Cotton, 2008: A Binned Approach to Cloud-Droplet Riming Implemented in a Bulk Microphysics Model. *J. Appl. Meteorol. Climatol.*, **47**, 694–703, doi:10.1175/2007JAMC1664.1.

Saleeby, S. M., W. R. Cotton, and F. Collins, 2004: A Large-Droplet Mode and Prognostic Number Concentration of Cloud Droplets in the Colorado State University Regional Atmospheric Modeling System (RAMS). Part I: Module Descriptions and Supercell Test Simulations. *J. Appl. Meteorol.*, **43**, 182–195, doi:10.1175/1520-0450(2004)043<0182:ALMAPN>2.0.CO;2.

Schmid, P. E., and D. Niyogi, 2013: Impact of city size on precipitation-modifying potential. *Geophys. Res. Lett.*, **40**, 5263–5267, doi:10.1002/grl.50656.

Schmid, P. E., and D. Niyogi, 2017: Modeling Urban Precipitation Modification by Spatially Heterogeneous Aerosols. *J. Appl. Meteorol. Climatol.*, **56**, 2141–2153, doi:10.1175/JAMC-D-16-0320.1.

Shepherd, J. M., 2005: A Review of Current Investigations of Urban-Induced Rainfall and Recommendations for the Future. *Earth Interact.*, **9**, 1–27, doi:10.1175/EI156.1.

Stevens, R. G. and Coauthors, 2012: Nucleation and growth of sulfate aerosol in coal-fired power plant plumes: sensitivity to background aerosol and meteorology. *Atmos. Chem. Phys.*, **12**, 189–206, doi:10.5194/acp-12-189-2012.

Walko, R. L., and C. J. Tremback, 2005: *Modifications for the Transition From LEAF-2 to LEAF-3*. PO Box 19195. Boulder, CO, 80308, 13 pp.

Walko, R. L., C. J. Tremback, R. A. Pielke, and W. R. Cotton, 1995: An Interactive Nesting Algorithm for Stretched Grids and Variable Nesting Ratios. *J. Appl. Meteorol.*, **34**, 994–999, doi:10.1175/1520-0450(1995)034<0994:AINAFS>2.0.CO;2.

Walko, R. L. and Coauthors, 2000: Coupled Atmosphere–Biophysics–Hydrology Models for Environmental Modeling. *J. Appl. Meteorol.*, **39**, 931–944, doi:10.1175/1520-0450(2000)039<0931:CABHMF>2.0.CO;2.

CHAPTER 4. IDEALIZED SIMULATIONS OF URBAN THUNDERSTORM MODIFICATION

This chapter discusses the results of two sets of quasi-idealized simulations (RAIL) to determine the specific sensitivities of 4.1: city footprint size and 4.2: urban aerosol generation on the susceptibility to thunderstorm modification. The concept of urban footprint shape is discussed in 4.3, noting that while shape could theoretically matter, the question is perhaps moot, as every urban area on Earth not bound by coastline or topography is relatively circular.

4.1 Sensitivity of Thunderstorm Modification to City Size

The goal of this study was to provide a framework by which cities most prone to thunderstorm modification could be evaluated. Given that no two cities, even within the same region could be impacted by the exact same system, the RAIL modeling framework enables this kind of sensitivity study to be performed. The study investigated whether there was a minimum or maximum urban land cover, in a certain configuration, that would impact how a given storm developed as it crossed the urban envelope.

4.1.1 Model Setup

Using the Urban RAMS model described in Chapter 3 with SPM emissions disabled, this study simulated a series of weak linear convection events over the eastern Great Plains from 7-11 May 2010. In a RAIL framework, a set of three nested grids 12 km – 3km – 0.75 km were centered at (37.5N, -95.5W) in SE Kansas, with a constant model elevation of 300 m. The central location was chosen to assure the simulated precipitation passed directly over the center of the inner grid. Table 2 details the size, location, and parameterizations used on each grid. For this study, the blank terrain is considered to be the control to which each urban scenario is compared. Cities with a radius of 5, 10, 15, 20, 25, 30, and 40 km were created in the center of the inner domain to simulate the sensitivity of city size to the urban rainfall modifying effects. The model was initialized from NAM reanalysis and nudged at the lateral boundaries every 12 hours. Given this study was originally for model calibration, the scenarios were also run on a 16 km – 4km – 1km nest to verify the results.

4.1.2 Results

Table 2. Details of model grids and parameterizations.

Model Parameter	Grid 1	Grid 2	Grid 3
Number points (nx,ny)	114 x 114	122 x 122	102 x 102
Grid spacing (Δx, Δy)	12km	3km	0.75km
Time step	20s	5s	1s
Domain center	City Center	E. of City	City Center
Num. Vert. levels (nz)	48	48	48
Vertical spacing (Δz)	40m	40m	40m
Vertical stretch	1.08	1.08	1.08
Max. Δz	1000m	1000m	1000m
Nudging time	12h	12h	12h
Rel. nudging weight	1	0.8	0.5
Cumulus parameterization	Kain-Fritsch	none	none
Microphysics	Meyers et al., 1997		
Cloud Aerosols	Saleeby and Cotton, 2004		
Boundary conditions	Klemp and Wilhelmson, 1978		
Radiation parameterization	Harrington 1997		
Eddy Diffusion	Mellor and Yamada, 1982		

Before simulated precipitation arrived at the cities, the local urban effects can be assessed. The average maximum heat island ΔT over the urban area increases linearly with city size to maximum of approximately 1ºC at a 20 km radius city. The heat island intensity does not continue to increase for larger cities (Oke 1973). The "dry island" moisture deficit in the urban area decreases the dewpoint linearly with increasing city size. Due to the high moisture content of the surrounding rural air, the dewpoint continues to decrease linearly with larger cities. Figure 10 shows the average daily urban heat island values (difference between city and no city) for temperature increase and dewpoint decrease for each city. Also shown is the morning (12UTC) maximum equivalent temperature difference, which increases linearly to a city of 20km then remains more constant for larger cities.

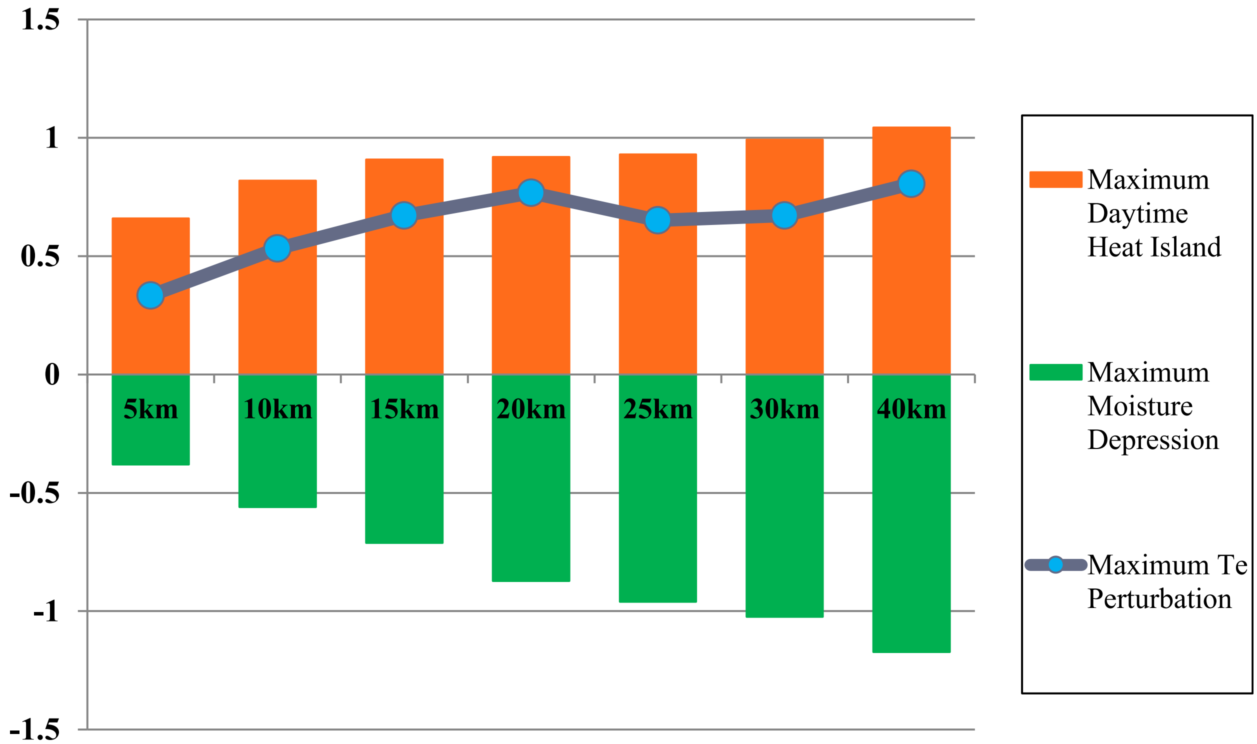

Figure 10. Average daily maximum simulated urban heat island (difference of city temperature and control), moisture depression, and equivalent temperature perturbation (in K).

The control simulation produced a line of precipitating storms, with a maximum simulated dBZ of 50-55, in grids with no convective parameterization. While the line propagated west-to-east, the individual updrafts composing the multicellular line propagated from the southwest-to-northeast. Figure 11a shows the distribution of precipitation at the surface for control Grid 2. Surface precipitation values of 1-3cm are common throughout the domain with values of 5-6cm in the eastern portion of Grid 2.

The addition of cities had a consistent precipitation-modifying effect on the simulated storms. Relative to the individual updrafts (SW-to-NE), there was a decrease in precipitation compared to the control. However, relative to the overall line motion (W-to-E) there was an increase in precipitation. The updrafts which passed directly over the city produced storms with less precipitation than with no city present. The updrafts which did not pass over the city land surface but did encounter the downwind aerosol field were invigorated and produced more precipitation than with no city. Figure 11b-e shows the change in precipitation in Grid 2 as a percent of control. While there are regions of increased and decreased precipitation downwind of

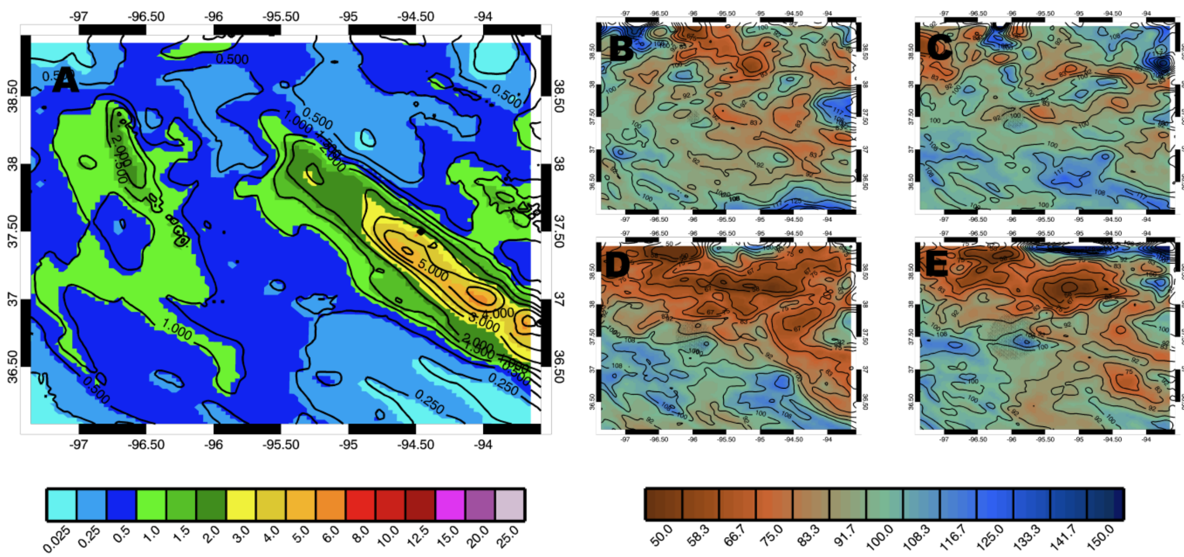

Figure 11. Simulated precipitation and differences for a) control precipitation (cm) displayed for Grid 2 domain, and precipitation difference as a percent of a) for b) 10 km city, c) 20 km city, d) 30 km city, and e) 40 km city.

the city, as the city size grows, there is a consistent reduction in precipitation across the overall domain. There was no consistent pattern of precipitation increase or decrease in the city center, due to the variable location of the urban circulation in the cities of different sizes.

As with the heat-island and moisture depression effects, the precipitation modification (either suppression or invigoration) increases linearly with city size up to a city of 20 km in radius (Figure 12). Maximum suppression downwind was 1.2 cm and maximum downwind invigoration was 0.8 cm for a city of 25 km in size. The 30 and 40 km cities showed slightly smaller suppression and invigoration, but the values were approximately constant with the 25 km city size. Figure 11 shows the maximum downwind suppression and invigoration for both northeast and southeast of the city. For the largest cities, precipitation decreases compared to the control more so southeast of the city due to heavy rain from invigoration effects.

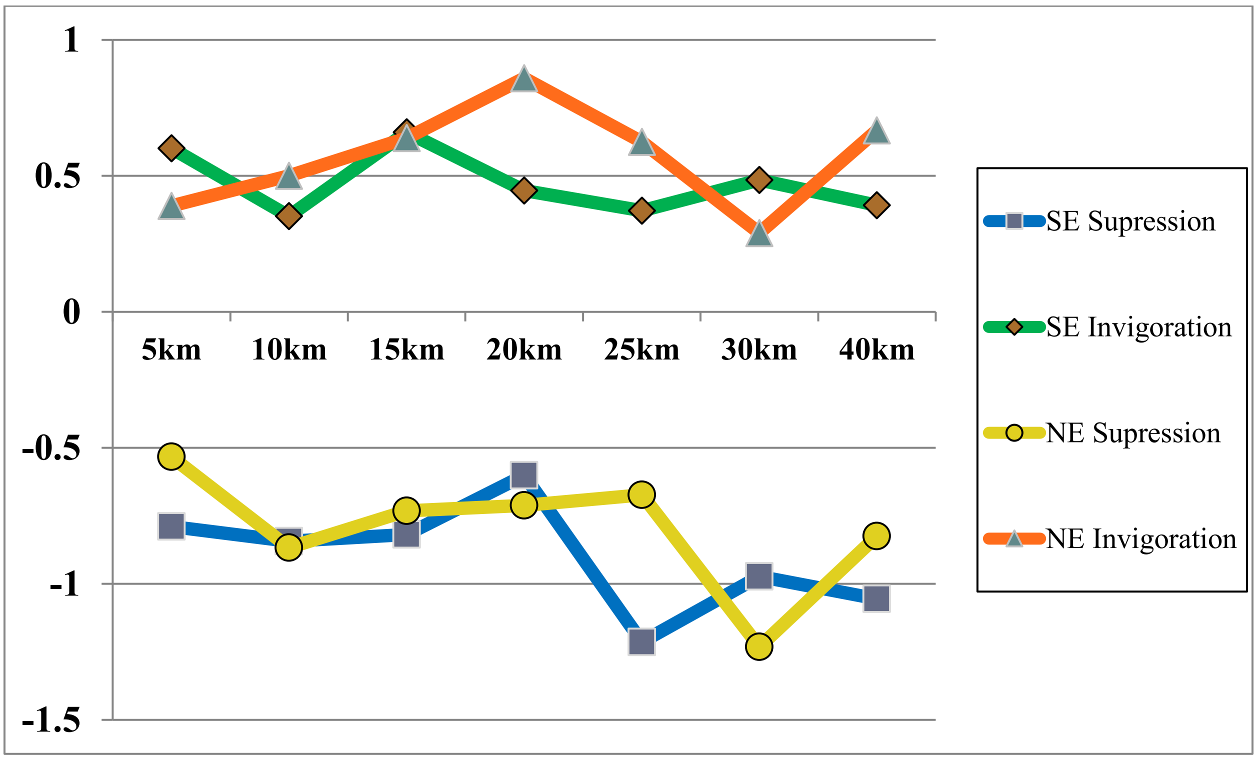

Figure 12. Maximum downwind precipitation suppression and invigoration (cm) for downwind regions northeast and southeast of circular city center for cities of different sizes.

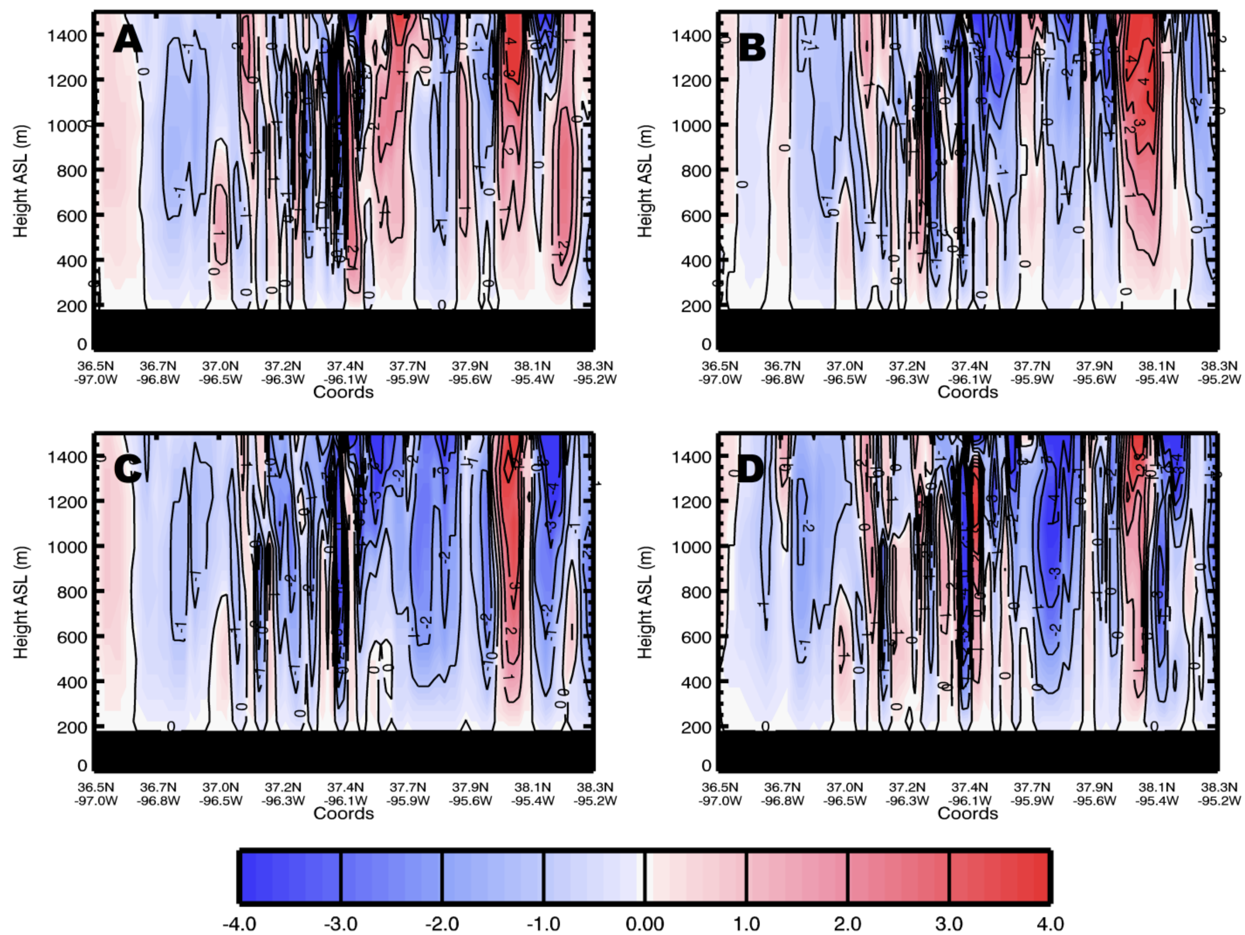

Figure 13. Cross section across city (SW to NE) of simulated difference in vertical velocity (cm s-1) between control land surface and a) 10 km city, b) 20 km city, c) 30 km city, and d) 40 km city.

4.1.3 Discussion

The specific location of the suppression and invigoration zones of precipitation is due to the specific characteristics of the simulated storm. The urban heat island creates a vertical circulation with a downward node near the urban-rural boundary. For an approaching updraft, this decreases vertical velocity in the storm. The moisture deficit in the city center advects toward the southwest via the storm inflow. The combined effects of the downward circulation and moisture deficit lead to precipitation reduction upwind of the city. In the city center, there is no consistent trend of suppression or invigoration. As the city size increases, the specific orientation of the urban circulation does not change linearly. Figure 13 shows a cross section of vertical velocity differences for increasing city size. Urban updrafts do not increase in radius with increased city size, but they become more numerous. The size (radius) of an urban circulation couplet is the same size as a dry convective updraft outside the city: dependent on relative humidity and local synoptic instability. The northeast side of the city shows a large downdraft of increasing velocity with larger city size. This broad downdraft helps suppress precipitation immediately downwind of the city.

The size threshold of 20 km for maximum urban thunderstorm modification potential can be explained by the characteristic size of the city, storm, and velocity of the updraft. Typical average values for the forward motion (V), depth (H), and updraft velocity (W) of a thunderstorm are 20 $m \cdot s^{-1}$ (60 $km \cdot hr^{-1}$), 10 km, and 10 $m \cdot s^{-1}$. A thunderstorm moving at 20 $m \cdot s^{-1}$ will take 2000 s to cross a city 20 km in radius. It also takes 2000 s for a complete updraft/downdraft transit of storm 10 km deep at 10 m s^{-1}. A surface perturbation put forth by land-surface heterogeneity will be communicated to the full thunderstorm at that time scale, so it will take that amount of time for a thunderstorm to modify in the presence of land-surface heterogeneity. So, *for this spcific case*, a very average thunderstorm, it becomes fully modified from a city of 20 km in radius and does not modify further for larger cities. So for this case, a city with radius 20 km is where the modification from the land surface reaches its maximum and does not continue to increase for larger cities, because the time the land surface perturbation takes to be communicated through the storm updraft (t_1) is equal to the time it takes for the storm to cross the urban area (t_2).

$$t_1 = 2H \cdot W^{-1} \qquad t_2 = 2R \cdot V^{-1} \qquad t_1 = t_2$$

For the nested grids of 16 km-4 km-1 km, the threshold of a 20 km radius city was also found, indicating that the result is not necessarily dependent on grid spacing. Faster moving storms would theoretically require a larger city to produce modification, but such storms may not follow the trend noted here. However, faster storms typically have stronger synoptic forcing and are less susceptible to urban modification.

This study utilized a simplified land surface, the RAIL method, to study the impact of city size on potential thunderstorm modification. A weak linear convection case was simulated over circular cities varying in radius from 5 km to 40 km. When the storms passed over the cities, an increase in precipitation was noted downwind of the city relative to line motion, while a decrease in precipitation was noted downwind and slightly upwind in the direction of updraft motion. The magnitude of precipitation modification increased linearly with city size up to a 20 km city, where it became more consistent with increasing city size. *The 20 km city threshold exists as it is the minimum size of a city for the simulated thunderstorm to communicate surface perturbation throughout the storm.*

Note that, the distribution of precipitation modification for just a single case is similar to seasonal to climatological time scales. Based on other studies in the vicinity of Indianapolis and St. Louis (Changnon et al. 1976; Niyogi et al. 2011), there is a precipitation decrease in the direction of the updrafts and increase for the updrafts which did not pass over the urban center. The land-surface discontinuity was the focus for this study, but aerosol effects in place in the model. Assessing their effects require a more realistic heterogeneous distribution in space (4.2). The RAIL method would remain useful to assess the heterogeneously initialized aerosol problem, as well as the problem of urban production.

4.2 Sensitivity of Thunderstorm Modification to Aerosol Loading

4.2.1 Model Setup

The RAIL method, with all model parameters from Chapter 3, was used to simulate this study. The model was initialized from North American Model (NAM) reanalysis of a low pressure system crossing the Southern Great Plains beginning at 1200UTC 11 May 2013. The model simulated conditions for 144 hours that included 96 hours of rain-free conditions (to assess CCN formation and dispersion), and 48 hours wherein a low pressure system with mixed precipitation crosses the model domain. The location most subject to cold and warm rain was 36.6N, 97.4W (north central Oklahoma, near the ARM SGP site), so it was selected as the center of the model domain, with a constant 300 m elevation. The base run produced a reasonable simulation of the low-pressure system: deep convective rain passes from west to east beginning at Hour 100, followed by stratiform rain from east to west from Hours 120-140, comparable to observations. A 25 km radius city (the critical size for a system with this motion based on 4.1.3) was subjectively placed there to investigate the urban impacts, with the remainder of the domain being crops.

Six scenarios, representing different SPM emission rates, were simulated. The "Control" for this study was with the 25km radius city with no active emissions and homogeneous CCN concentrations of 1000 cm^{-3} throughout the domain. It was compared with each of the emitting scenarios to demonstrate the pure effect of modified aerosol concentrations. The four emission scenarios contain an identical land surface to the Control, but varied the total SPM emissions rate, to yield characteristic values of peak clear-air urban CCN concentration.

- X1 corresponds to 1000 cm^{-3}
- X2 corresponds to 2000 cm^{-3}: the METROMEX values and typical for a large, Midwestern city.
- X3 corresponds to 3000 cm^{-3}
- X4 corresponding to 4000 cm^{-3}

In each of the emitting scenarios, the rural concentration far upwind of the city was initialized at 500 cm^{-3}. The peak CCN concentrations occur during the morning rush hour, when the urban boundary layer is low such that they are accumulated near the surface, then disperse upwards and downwind. Figure 14 shows the simulated CCN values at simulation Hour 74 (local 9am) forming from rush hour emissions, and dispersing by Hour 78 (local 1pm) in the X1 scenario. A final simulation (NoUrban) was conducted with all rural land and rural CCN, to assess the land surface component of this study. It is cautioned that the setup and corresponding results are by design to understand the specific urban feedbacks and require simplifications. Transferring the results into a real urban environment requires consideration of other local factors and uncertainties.

For the Control and each scenario, the model uses three nested grids with 16km – 4km – 1km spacing, with respective time steps of 24s – 6s – 1.5s, in horizontal domains of 102×88, 98×102, and 114×114, respectively. The NAM reanalysis of temperature, moisture, and wind was downscaled to create the initial conditions and the outermost (16km) grid was nudged every 12 hours. All grids used 52 vertical levels, stretched from 40m spacing at the surface to a maximum of 1000m spacing, near the top of the model. The modules and parameterizations described in Chapter 3 were used in each model level applicable. The SPM emissions, and subsequent CCN formation, are only processed on the innermost model grid, then upscaled to the other grids, to preserve mass balance.

4.2.2 Results

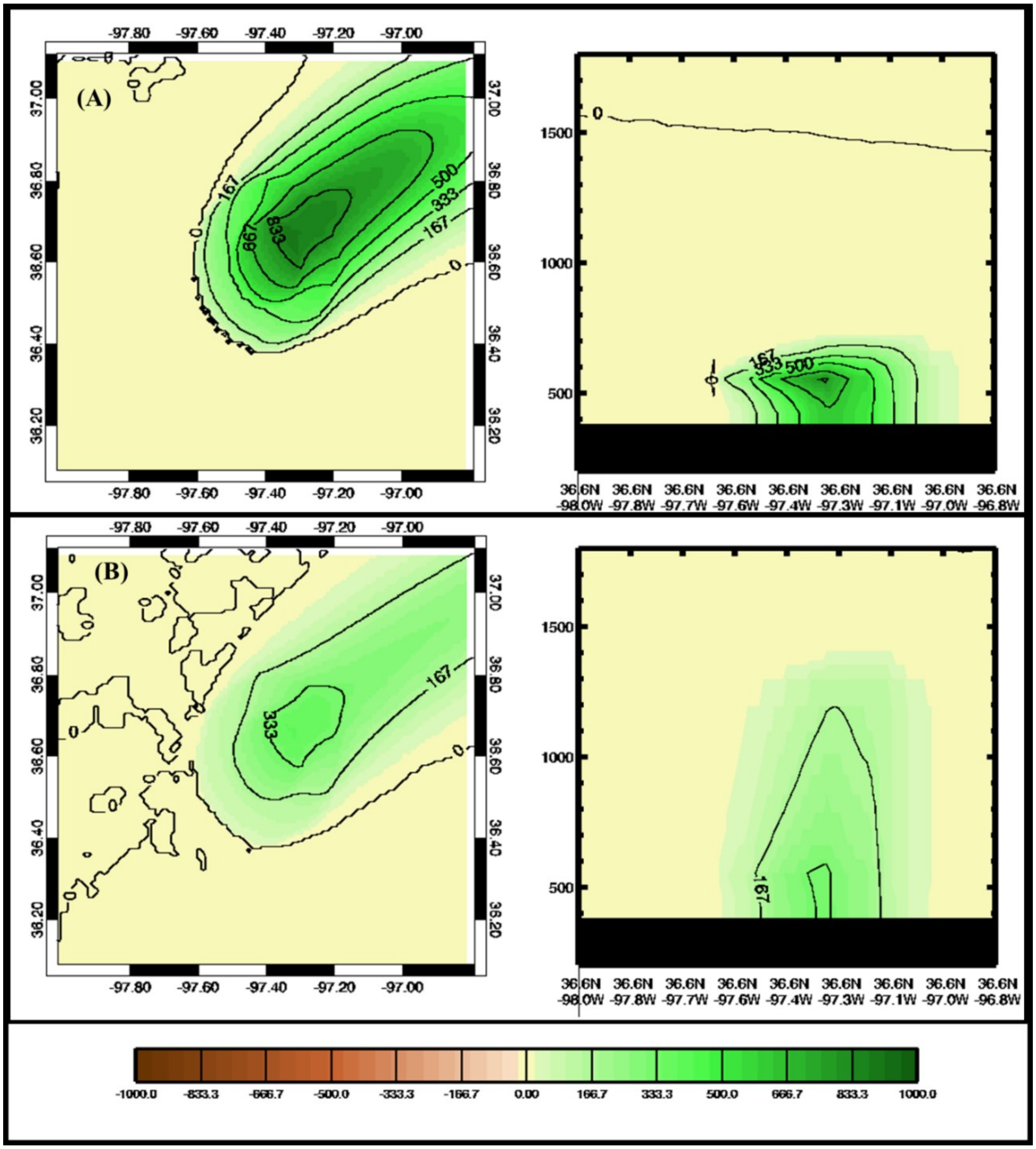

Figure 14. Simulated model CCN values in the horizontal (left) and vertical (right) directions for the X1 emission scenario at a) Hour 74 (9am Monday local time) – morning rush hour, and b) Hour 78 (1pm Monday local time) – midday. The morning CCN is maximum during the morning rush hour at a value of approximate 1000 cm-3, half of the METROMEX values (typical of X2).

The pre-storm environment for this simulation encompasses the 96 hours between model spin up and the arrival of precipitation in the innermost domain: Hour 4 to Hour 100. *Figure 15* shows the diurnal progression of (a) CCN differences between the control and each scenario, and (b) vertical velocity differences between each scenario and the control, averaged over the area within 10km of the city center, to show potential effects on storm microphysics and surface dynamics respectively. Simulation Hour 0 is 7am local time on a Saturday, so emissions are less than for a weekday. At Hour 48 (local 7am, Monday morning), the rush-hour dependent emission cycle is noted. CCN concentrations are greatest during the morning hours (Hours 48, 72, 96) because along with the rush hour emissions, the PBL is shallow, and aerosols do not mix vertically as extensively. As the PBL grows during the day, the vertical mixing and thermals cause aerosols to mix out and lower the peak concentrations. The concentrations increase again after 7pm local

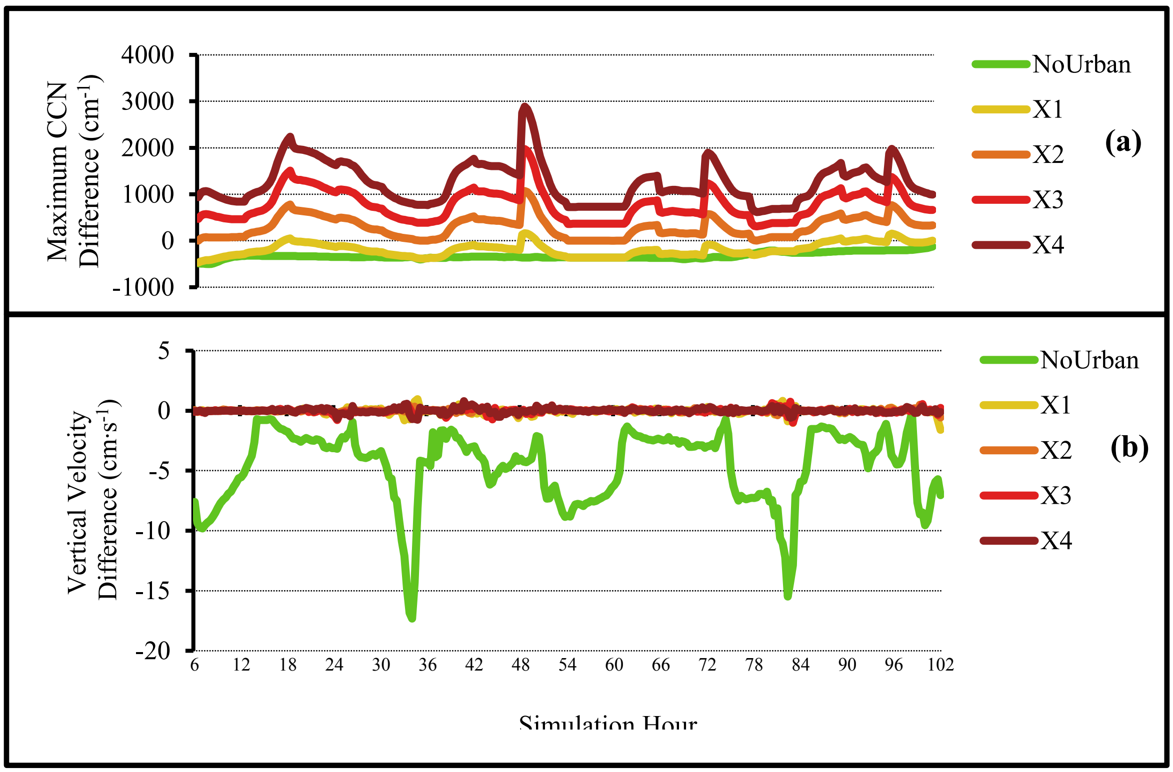

Figure 15. Comparison of a) aerosol loading (number·cm-3) and b) vertical velocity (cm·s-1) in the pre-storm environment compared to the control. Peak aerosol concentrations occur during the morning rush-hour when the PBL is shallow. There are broadly decreased values with no city present (NoUrban), but the changes due to aerosol direct effects (i.e. reflection) is orders of magnitude less.

time (Hours 60, 84), due to evening rush-hour emissions and the collapse in the PBL height after sunset.

The increased urban CCN concentrations during this time period do not significantly impact clouds, because the model atmosphere is too dry to form clouds at the top of the PBL. The completely homogeneous NoUrban scenario has vertical velocities of 0.05 to 0.15m·s^{-1} less than the urban land-surface scenarios, representing the magnitude of the pure UHI-induced circulation. Figure 16 shows the UHI circulation as depicted as the difference between the Control and NoUrban vertical velocities at Hour 57 (4pm local time). The most intense UHI circulation, corresponding to the most vigorous vertical mixing is at the urban/rural boundary and at the intraurban boundary between the two TEB urban climate zones. These edge circulations extend 1-3km vertically, indicative of deep mixing of urban CCN. Smaller urban thermals exist across the urban footprint, but are an order of magnitude less than the edge circulations. Downwind of the city, the vertical velocity perturbations propagate as bounded vertical waves.

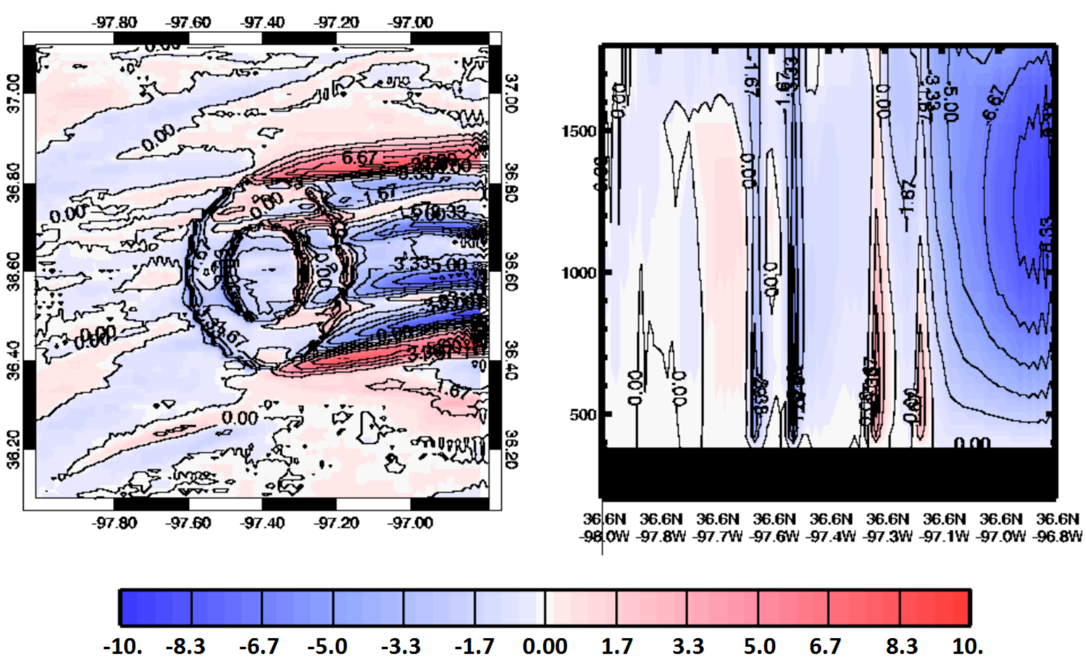

Figure 16. Map (left) and cross section (right) of the difference between the Control and NoUrban vertical velocity (cm·s-1) at Hour 57. While land surface in both simulations contain updrafts and downdrafts due to daytime heating of the surface, the pure urban land surface effect is shown here. Maximum vertical motion occurs at the city edge and transition from one urban zone to the other, noted as concentric circles at the approximate location of these features.

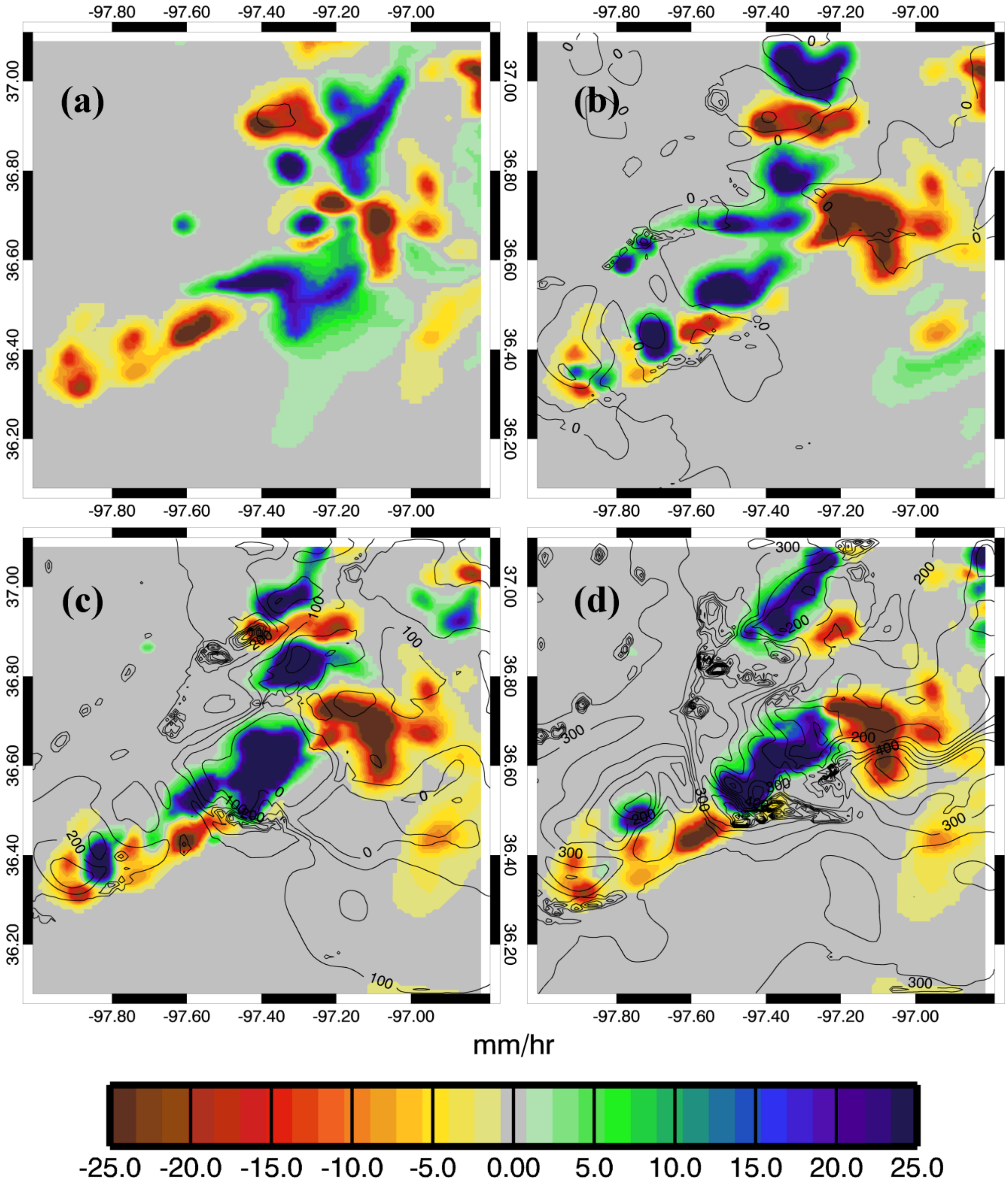

Figure 17. Change in instantaneous precipitation rate for a) X1, b) X2, c) X3, and d) X4 aerosol scenarios at simulation hour 106, compared to the control. There is a similar aerosol-induced invigoration effect as the precipitation reaches the urban aerosol field. Table 1 notes the differing times of invigorated precipitation arrival. Note for the X1 scenario, hour 106 is the maximum precipitation, but not the time of its initial arrival.

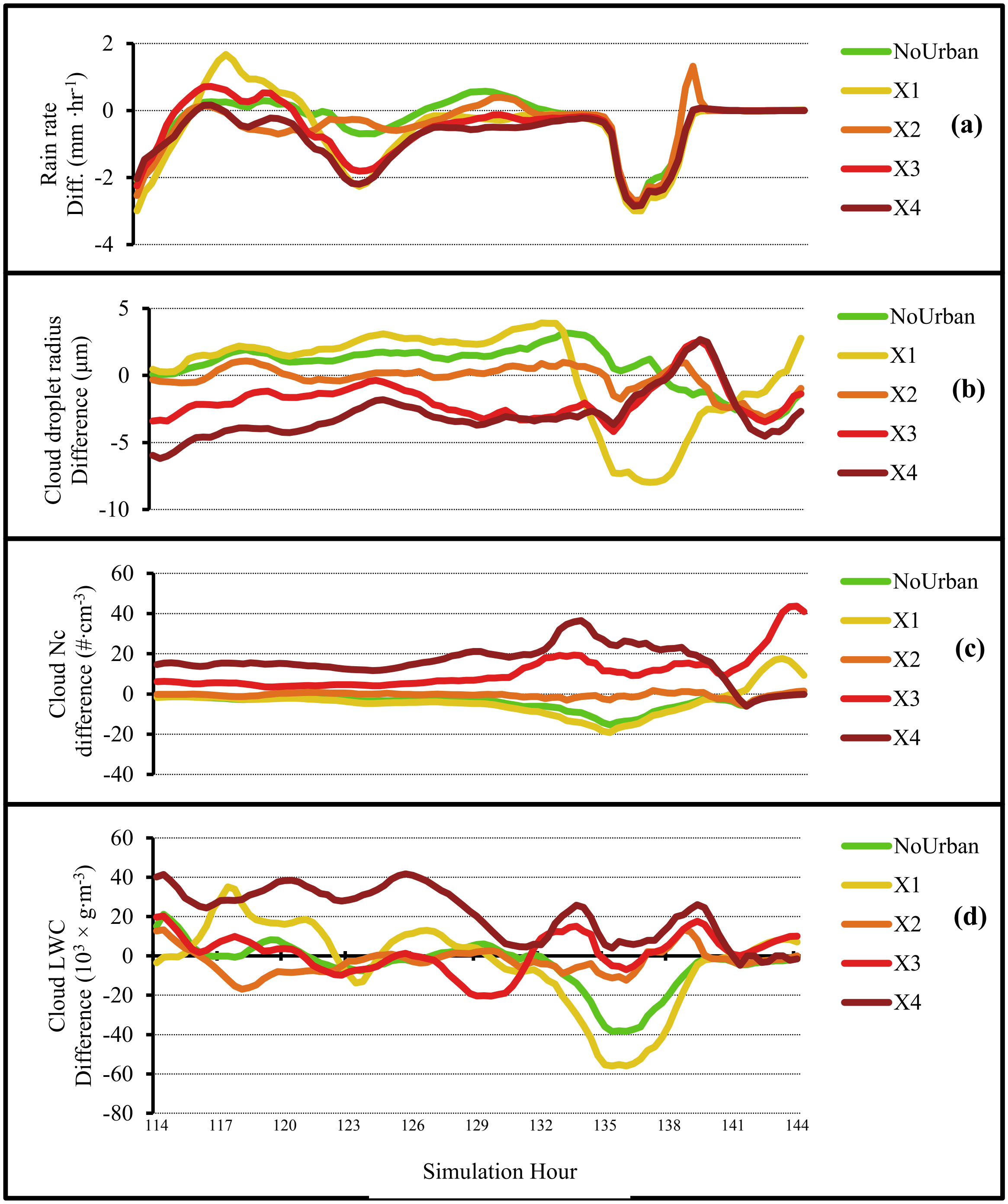

Figure 18. Differences between each scenario and the control at 20 minute intervals for a) Domain average precipitation rate (mm·hr-1), b) Non-urban cloud droplet radius (µm), c) Non-urban cloud number concentration (number·cm-3), and d) Domain average cloud liquid water content (g·m-3 × 103) During this time, aerosol loading suppresses the warm rain process. Thus, the NoUrban case exhibits a small increase in precipitation compared to the control.

For the control and each scenario, frontal convective precipitation associated with a synoptic low enters the innermost domain from the east at simulation Hour 103 (2pm local time). When the cloud system is perturbed by urban aerosol field of the emission scenarios, precipitation rate increases compared to the control. In particular, the X3 scenario simulated rain rates of over $70\mathrm{mm{\cdot}hr^{-1}}$ greater than the control during all three 20-minute outputs at Hours 105.6 – 106.3, characteristic of potential flash flooding. Figure 17 shows the difference in precipitation rate overlaid with the CCN differences at Hour 106. The NoUrban precipitation is decreased by 20 $\mathrm{mm{\cdot}hr^{-1}}$, compared to the control, during Hours 107-108. Figure 18 shows the differences in maximum precipitation rate and time of arrival over the city center for each of the scenarios, with maximum differences highlighted. The increased aerosol loading delays the arrival of maximum precipitation but increases the heaviest rain rates.

Table 3. Percent changes to total precipitation for different inner domain sectors. While the mean precipitation decreases for all aerosol loads, regions of invigorated maximum precipitation persist. The NoUrban scenario is left blank for urban land cover because it represents a change in two variables: land-cover and aerosols. The total precipitation is more spatially variable in scenarios with aerosols, and less variable in the NoUrban scenario.

Sector	Control (cm)	X1 (%)	X2 (%)	X3 (%)	X4 (%)	NoUrban
Mean Total	3.78	*-28.95*	*-36.65*	*-43.51*	*-47.18*	*-28.32*
Mean Rural	3.57	*-22.45*	*-33.13*	*-44.76*	*-48.24*	*-24.78*
Mean All Urban	5.62	*-63.83*	*-55.53*	*-36.80*	*-41.51*	---
Mean Suburban	5.76	*-63.84*	*-57.76*	*-40.14*	*-46.92*	---
Mean Downtown	5.25	*-63.81*	*-48.88*	*-26.82*	*-25.39*	---
Mean City Edge	6.01	*-65.21*	*-59.13*	*-46.21*	*-46.42*	---
Mean Downtown Edge	5.73	*-62.86*	*-52.25*	*-33.62*	*-39.55*	---
Max Total	10.90	**41.81**	**62.69**	**41.10**	**48.32**	**56.88**
Max Rural	10.90	**41.81**	**62.69**	**41.10**	**48.32**	**56.88**
Max All Urban	10.05	*-3.37*	**11.95**	**21.82**	**32.59**	---
Max Suburban	10.05	*-5.54*	**11.95**	**21.82**	**29.99**	---
Max Downtown	7.34	*-4.61*	**6.77**	**24.78**	**44.62**	---
Max City Edge	10.90	*-7.69*	**10.30**	-1.16	**27.10**	---
Max Downtown Edge	8.50	*-4.01*	**14.14**	**14.45**	**20.95**	---

After the passage of the heaviest rain by Hour 108, there is a dry, but cloudy period, during which surface aerosols vertically mix into the PBL, and ultimately modify the clouds. At Hour 114, shallower, more stratiform rain crosses the new urban aerosol field from east to west. For this event, the aerosols impact is opposite to that observed for heavy convective rain. Higher aerosol concentrations reduce precipitation, while the lowest concentration (NoUrban) produces slightly heavier rain rate (approximately 2 $mm \cdot hr^{-1}$). Figure 18 shows the domain average rain rates, aligned with non-urban cloud droplet radius, non-urban number concentration, and domain average cloud liquid water content. Note, these averaged differences are characteristically lower than single grid values as regions of the domain. Especially in rural upwind regions, there is negligible change because there is little difference in aerosol forcing. For each scenario, higher aerosol loading leads to higher concentration of smaller droplets and more water mass remains in the cloud as opposed to forming into rain.

The change in total precipitation with each scenario is most spatially variable around the city itself. Figure 19 shows the difference between the Control and each emission scenario. There is generally decreased precipitation with spatially heterogeneous aerosols, compared to the homogeneous Control. For the X1 scenario (Figure 19a), the urban center and nearby rural areas result in an almost universal decrease in rainfall compared to the Control, while the rural areas farther from the city edge show increased rain. As the aerosol loading progressively increases (Fig. 19bcd), the aerosol concentration at the urban edge upwind of the convective rain event (the southwest side) becomes sufficient to perturb the system. This manifests as a small area in the city with increased total rainfall, corresponding entirely to the enhanced rain rates as the system arrived (Fig. 17). For the highest aerosol loading (Fig. 19d), there is a pronounced downwind (northeast of the city) rainfall increase from the city edge into the nearby rural area.

Table 3 notes the differences in mean rainfall and maximum rainfall across different urban sectors. Across the total, rural, urban sectors, and urban edges, the total rainfall decreases for all scenarios, including the NoUrban. However, the difference in maximum precipitation increases with the presence of increasing heterogeneous aerosols. These differences are due to the changes in rain rate. While total precipitation decreases throughout the domain with increased aerosols, some locations near the city center receive over 50% more rainfall due to heavy downbursts. In

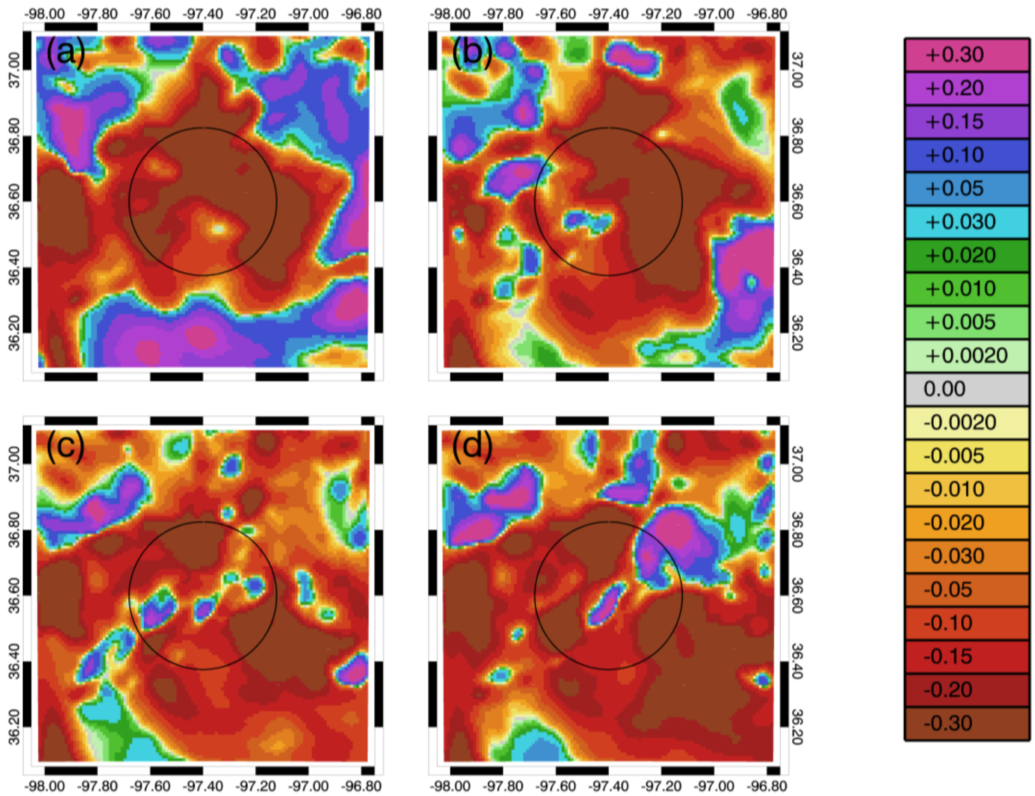

Figure 19. Total precipitation (% of control) difference between each simulation and the control: a) X1, b) X2, c) X3, d) X4. The heterogeneous aerosol field general decreases precipitation in the urban center (a). The edge of the city is indicated by a solid line. As emission rates increase, rainfall increases in the city center, upwind, and downwind for the highest aerosol loading.

the NoUrban case, the decreased precipitation is mostly where the city is located in the control. Rural areas upwind of the city receive increased precipitation due to a lack of extra rain falling in the center from the urban land surface effect. In the emission scenarios, the total rainfall increase at the city edge is due to aerosol effects. Overall, the introduction of heterogeneous aerosol fields leads to results that are different than the pure urban heat island effect and from the effects of spatially homogeneous urban aerosols. The emitting scenarios increase rain rates *where the aerosols are increased*: in the urban center and downwind. While the rain rates and some areas of total rain (e.g. Fig. 19d) increase, the rural areas of the emitting scenarios receive less total precipitation because of the *reduced* aerosols in those areas not being of sufficient concentration to nucleate the deepest convection.

4.2.3 Discussion

The aerosol sensitivity study highlighted many of the general precipitation modifying features of urban areas. The results can be further summarized as follows:

1. Spatially heterogeneous urban aerosols with realistic concentrations (e.g. compared to METROMEX) can be produced in a numerical model by coupling an air quality chemistry model to a cloud microphysics parameterization.
2. The presence of the urban land surface (Control vs NoUrban) increased precipitation in the city center due to increased convective updrafts induced by the UHI. With no city (NoUrban), stratiform rain fell more uniformly over rural areas, leading to locations with more stratiform precipitation, but less overall, due to the decrease in convective rain.
3. The simulated urban aerosol field was approximately coincident with the urban land surface upwind of the city, so the simulated storm interacted with both simultaneously. With sufficient aerosol loading compared to surrounding rural areas (the X2, X3, X4 scenarios), the cloud modified at the upwind edge of the city. This lead to increased precipitation in the city center, and upwind edge in the X3 scenario. The increased precipitation was due to a briefly increased rain rate (Table 3)]. As aerosol loading increased, the time to modify the cloud also increased, so the highest aerosol loading produced increased precipitation over the city and downwind Fig. 19d.
4. The change in precipitation from the emission scenarios corresponded with features of the aerosol indirect effects: a) an increase in cloud droplet concentration, b) a reduction in cloud droplet size and narrowed distribution, and c) increase in cloud liquid water, especially for the heaviest aerosol loading (Fig. 18). These microphysical modifications occurred over the city and persisted downwind, indicating an increase in cloud lifetime.

Characteristically convective precipitation at the surface arises from melted hail or graupel above the freezing level in the clouds. Higher aerosol loading leads to smaller, more numerous cloud droplets with a narrower size distribution compared to lower aerosol loads. The aerosol-cloud interaction increases the amount of cloud water present above supersaturation, enhancing the formation of graupel via riming. When graupel production is increased, the melted graupel or hail leads to heavier rain at the surface, and therefore an overall increase of convective precipitation.

Notably, the enhanced graupel production is progressively delayed by increased aerosol loads, but does occur for all aerosol increases in this study. For stratiform rain, formed primarily via the warm rain process of collision-coallescence, the precipitation effect of high aerosol loads is the opposite: the smaller droplets slow the warm rain process and decrease stratiform rain. In the NoUrban scenario, the decreased aerosol loading has the opposite effects compared to high aerosols with respect to the emission scenarios. Thus another important result is that aerosol loading has an opposite impact on convective versus stratiform precipitation in these simulations.

Total rainwater reaching the surface is slightly increased by mesoscale circulation due to the land-surface heterogeneity *but* is generally reduced by the aerosol effect in this simulation. The areas where increased aerosol emissions lead to more total rain, were entirely due to a brief, but intense, increase in rain rate associated with the initial cloud-aerosol interaction. The increased rainfall was due to intense convective rain falling in a relatively small region of the city and downwind. This highlights the importance of the convective-stratiform rain balance in urban hydrological studies. A burst of convective rain due to urban effects may balance or even exceed the reduction of stratiform rain. However, the heavy convective rain is realized as run-off at the surface. Thus it may not alleviate rainfall deficits or drought as much as a longer, soaking rain would.

The simulation presented to illustrate the model developed for this study has a few shortcomings due to its scope. The RAIL method is necessary for more generalized conclusions because only a single event was simulated. Observed urban rainfall anomalies also exist on a seasonal-to-climatological scale, with individual events exhibiting different types of individual modification. The riming enhancement on graupel is not-monotonic in the sense that in very high CCN concentrations, it will be reduced (Lee et al. 2012). In this study, we did not achieve high enough concentrations for long enough to demonstrate this, but the X4 scenario may be just entering the range of CCN where riming has passed peak enhancement. The gas to particle conversion in the model was instantaneous and did not account for changes in CCN characteristics due to particle aging. Future studies involving the urban module presented in this study will focus on simulations of real cities, in longer time scales, with the additional complexities of aerosol-cloud interaction considered.

Despite the added features to the model simulations presented here, these simulations remain a simplification of urban thunderstorm interaction. The model was developed to simulate observed changes in rainfall to observed urban aerosols via a number of parameterized intermediate processes: changes to cloud formation and precipitation formation via aerosol indirect effects. While the simulation demonstrates some observed effects of the urban sphere, it was assumed that each intermediate step was accurately formulated. Therefore, the results should be interpreted as a *generalized* representation of urban weather, rather than a prescription of the sensitivities of potential weather modification. The model response remains a simplified representation of the non-linear, chaotic coupled system that is urban weather modification.

4.3 Comments on City Shape and Potential Thunderstorm Modification

Given the question "How does city size impact urban rainfall modification?" posed by (4.1, Schmid and Niyogi 2013), a second question was asked in parallel: How does city *shape* impact the same? The short answer to this question is *it probably does not matter* – Almost every urban on Earth is relatively circular unless constrained by topography. Given that coastlines and topography produce vertical circulations at least an order of magnitude greater than the urban effect, the *shape* of the urban footprint does not have an appreciable impact, outside of the topography. In this context, RAIL cannot be used for a generalized city shape.

4.4 References

Changnon, S. A., R. G. Semonin, and F. A. Huff, 1976: A Hypothesis for Urban Rainfall Anomalies. *J. Appl. Meteorol.*, **15**, 544–560, doi:10.1175/1520-0450(1976)015<0544:AHFURA>2.0.CO;2.

Lee, S.-S., G. Feingold, and P. Y. Chuang, 2012: Effect of Aerosol on Cloud–Environment Interactions in Trade Cumulus. *J. Atmos. Sci.*, **69**, 3607–3632, doi:10.1175/JAS-D-12-026.1.

Niyogi, D. and Coauthors, 2011: Urban Modification of Thunderstorms: An Observational Storm Climatology and Model Case Study for the Indianapolis Urban Region *. *J. Appl. Meteorol. Climatol.*, **50**, 1129–1144, doi:10.1175/2010JAMC1836.1.

Oke, T. R., 1973: City size and the urban heat island. *Atmos. Environ.*, **7**, 769–779, doi:10.1016/0004-6981(73)90140-6.

Schmid, P. E., and D. Niyogi, 2013: Impact of city size on precipitation-modifying potential. *Geophys. Res. Lett.*, **40**, 5263–5267, doi:10.1002/grl.50656.

CHAPTER 5. MODELING THE HISTORIC AND CURRENT LA PORTE ANOMALY

The La Porte Anomaly is historically significant as the first well-studied example of urban rainfall modification (Changnon 1980). However, the significant limitations of the original studies relegated some otherwise salient conclusions into uncertainty. Among the limitations were a lack of process-based knowledge of the urban-atmospheric system and the inability to separate the proposed factors influencing rainfall variability. Chapter 2 presented observations showing the continued existence of the rainfall anomaly. This chapter will validate and expand on the observations by simulating the rainfall anomaly in a numerical model.

5.1 Review of Observations

Observations of the evolution of the La Porte Anomaly showed that it was a local, seasonal feature, and linked to forcing from the urban land surface and urban aerosols. As detailed in Chapter 2, the La Porte Anomaly was and continues to be a region of locally higher rainfall downwind of Chicago in Northwest Indiana (NWI). Locally increased rainfall was present at least since the 1930s, possibly peaking as 50% higher seasonal rainfall during the 1950s, apparently "disappearing" during the 1970s, and reemerging from the 1980s to present. Warm season rainfall

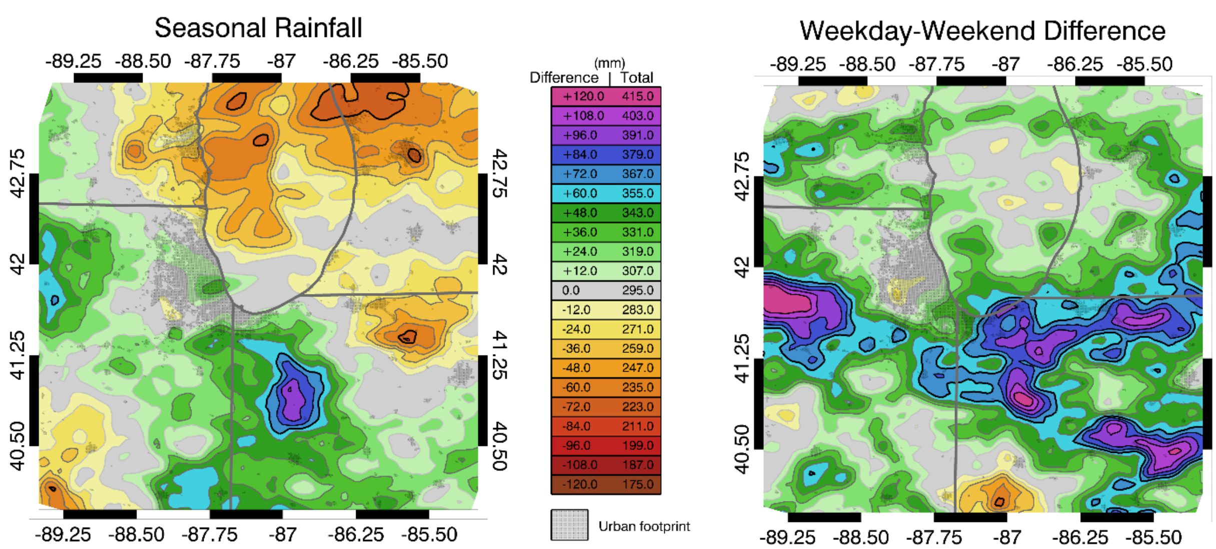

Figure 20. a) Total seasonal rainfall juxtaposed with b) weekday – weekday difference in regional rainfall. Figure corresponds to Fig.2 and Fig. 4c in Chapter 2.

in NWI is broadly 20 – 30% greater than the regional average (Figure 20a). In particular the, the weekday rainfall is up to 50% greater than weekend rainfall in the anomaly region (Figure 20b). Urban modification of rainfall was shown to be independent of wind direction, and the seasonal anomaly peak represents the average of all systems moving across the Chicago urban area. The anomaly was shown to be most prominent on days with local forcing (moderately low CAPE) and high land-atmosphere coupling (low PBL height), indicating the downwind anomaly is forced by the urban land surface interaction with the atmosphere. The weekday-weekend difference in rainfall shows that urban aerosols modifying cloud characteristics is another component, and that the downwind rainfall anomaly exists independent of non-urban features (i.e. Lake Michigan). The significance of the aerosol-cloud interaction is further seen by the suppression of rainfall during the 1970s, the region's most polluted decade ((Lyons and Stedman 1991)). While observations alone can determine the existence of the anomaly, that it is an unambiguously urban feature, and that it is forced by a combination of land-atmosphere and aerosol-cloud interaction, a numerical model simulation is required to separate the individual factors forcing the local rainfall variability.

5.2 Modeling Strategy

Given that the La Porte Anomaly is a supra-seasonal feature, it cannot be approximated though a single precipitation event. The statistical significance of the downwind anomaly increases with the time elapsed during the analysis period. There exist months where a downwind anomaly does not present, but it always appears in a seasonal analysis and becomes most significant in a long-term climatology. In a compromise between adherence to a seasonal simulation and computational speed, the event to simulation the La Porte Anomaly was the rainfall of August 2007. The month featured very high rain totals, which were 200 – 300% average, and thus more typical of an entire warm season than of one month. The increased rainfall was due to a persistent blocking ridge over the southeast United States (NCEI 2007), rather than a climate forcing (i.e. ENSO), so the rainfall over the upper Midwest during that month was comprised of typical warm season thunderstorms. Rainfall was far above average because of more rainfall events, but the

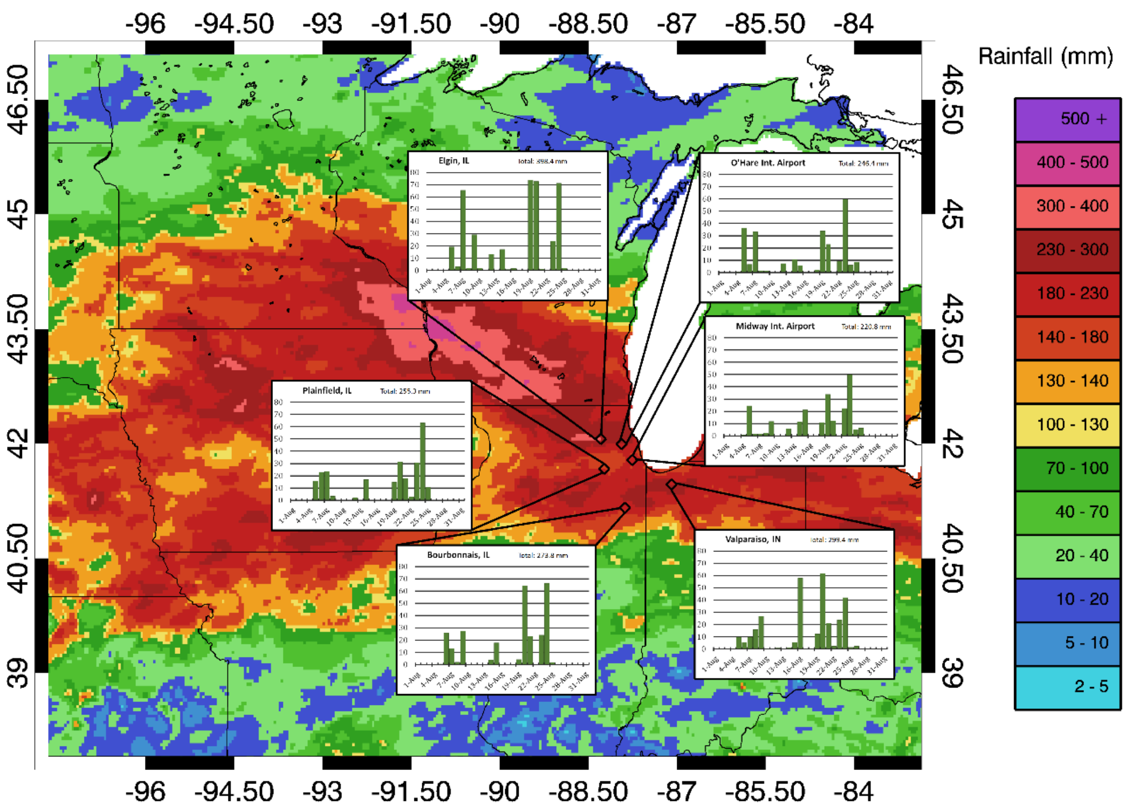

Figure 21. PRISM derived rainfall totals in the upper Midwest during August 2007 with daily rainfall totals from select regional sites.

characteristics of the individual events were not unusual. The downwind rainfall anomaly, while present in NWI, was of typical seasonal prominence[7]. Figure 21 shows the PRISM derived rainfall for August 2007 in the central and upper Midwest (Cumbie-Ward and Boyles 2016).

The goal of the modeling simulations was to examine the combined effects of land-atmosphere and cloud-aerosol interaction as well as separate them into individual factors. In order to accomplish this, the simulations were designed varying the urban land cover based on historical and current land cover observations. The Chicago area has a regional, high-resolution urban land cover map was reliably created in the 1930s (see 5.3), giving a potentially unique opportunity to evaluate its effects on local rainfall variability. The land cover scenarios were defined as the 1932,

[7] Notably, the State of Illinois had “average” August rainfall from the severe drought in the southern part of the state combined with the heavy rainfall in the northern part of the state.

1962, 1992, and 2012 urban land covers, and each of these would be compared to a "Control" of no urban land surface (following the RAIL framework). For the 2012 land cover, aerosol emissions were also simulated with a 2012x0 (homogeneous aerosols), 2012x1 (normal loading), and 2012x2 (double aerosol loading). Table 4 summarizes the land cover and aerosol loading simulations, along with the source of the data.

The urban RAMS model with full surface emissions (Chapter 3) was used to simulate from 3-Aug 2007 to 27-Aug 2007 using NAM reanalysis for the initial conditions and nudging the boundaries every 12 hours. This simulation period enabled sufficient model spinup time, as well as capturing all major rainfall events during the month of August 2007 which produced a season's rainfall in that time span. The 552 hour simulation was run over three nested grids at 32 km – 8 km – 2 km with corresponding time steps of 48 s – 12 s – 3 s, and the Kain-Fritsch convective parameterization enabled on the coarsest model grid. (Figure 22) shows the locations of the nested grids in the model domain. The surface traffic model (3.2.3) found that the emissions for cities much larger than a few kilometers scales to an urban footprint the size of Chicago's metro area.

Table 4. Names and descriptions of each RAMS simulation.

Scenario Name	Land Cover	(Source)	Aerosol Loading
Control	No City		Homogeneous
2012x1	2012	MODIS	x1
2012x2	2012	MODIS	x2
2012x0	2012	MODIS	Homogeneous
1992	1992	NLCD	x1
1962	1962	Extrapolation	x1
1932	1932	CRPA	x1

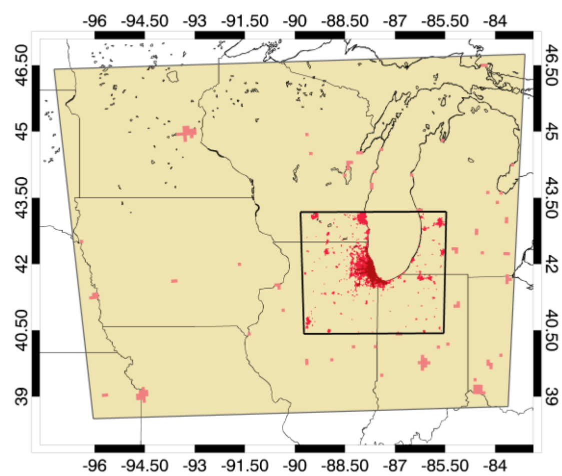

Figure 22. Location of each nest grid within greater model domain.

5.3 Constructing Historic Urban Land Cover

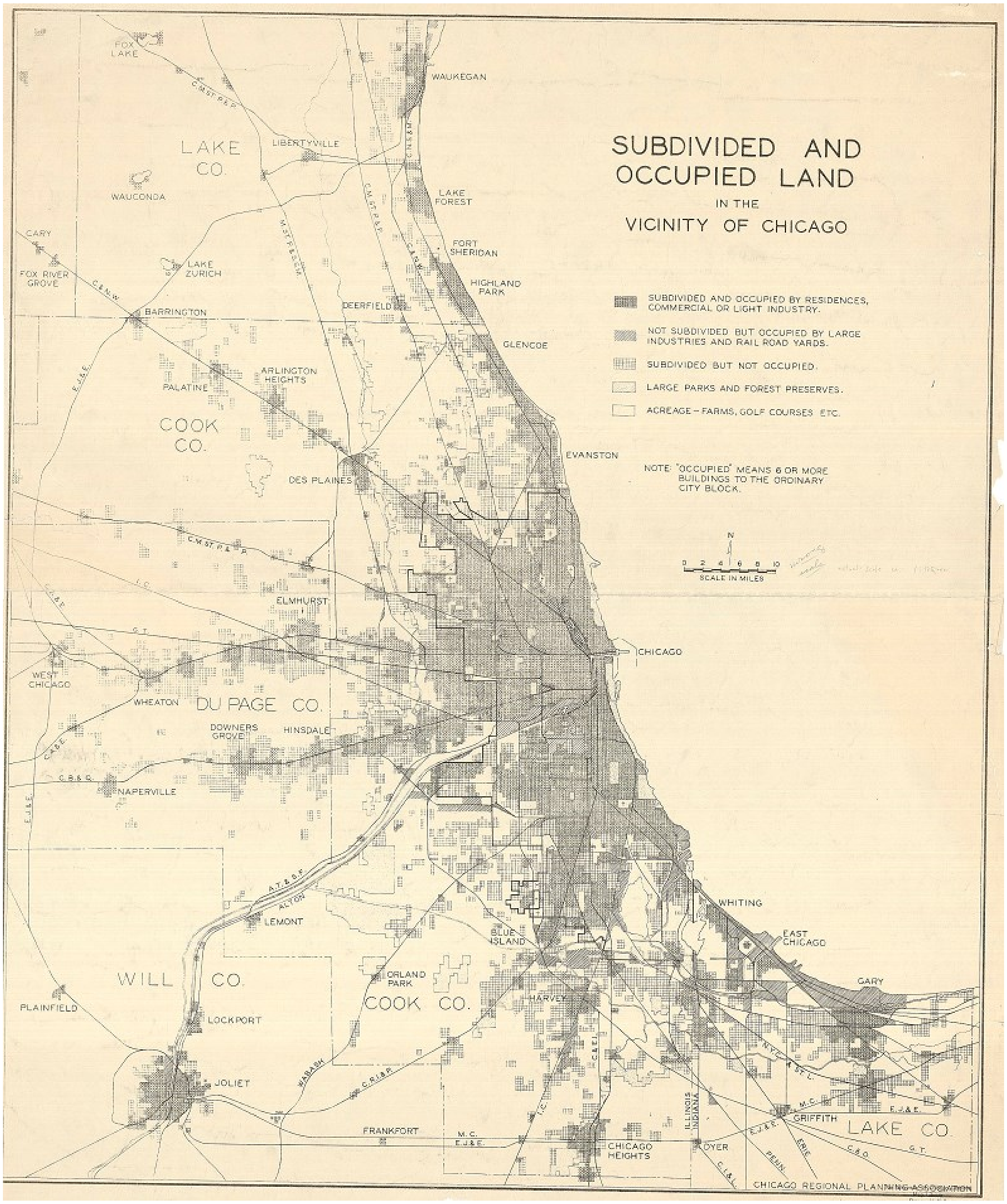

Figure 23. Map of developed land in the Chicago area from c. 1930. The map is undated, the projection is unclear, and the scale is not correct, but the map can be geolocated using railroad intersections which remain at the same location as they were when this map was created.

The study utilized a variety of sources to construct the dated land-cover scenarios described in Table 4. For the “1932” scenario, the land cover was derived from a planning map (Figure 23) showing developed and occupied land for the entire Chicago metro area (CRPA 1930). The map is undated officially, but it was produced in the late 1920s to early 1930s, and the halt in development due to the Great Depression enables it to be valid for any of a few years of the early 1930s. The scale on the map is not correct, however, most of the railroads extant at the time the map was produced still exist at the same location. The map was geolocated using trilateration of each of the railroad intersections with the known coordinates of their current location. The detail of the original map enabled a sub-100 m resolution map of development at the time, but the weather model did not require detail that fine. The 1992 development map was constructed from the 1992 National Land Cover Database analysis of urban development (Fry et al. 2009). The 2012 land cover was constructed from the MODIS land cover classification of urban areas (Friedl and Sulla-Menashe 2015). The 1962 land cover was extrapolated from the 1992 map using a boundary of home age (Sarkar 2011). Figure 24 shows the complete urban map with the 1932 urban land cover being assigned as TEB “Old Urban” and development since then as “Suburban”.

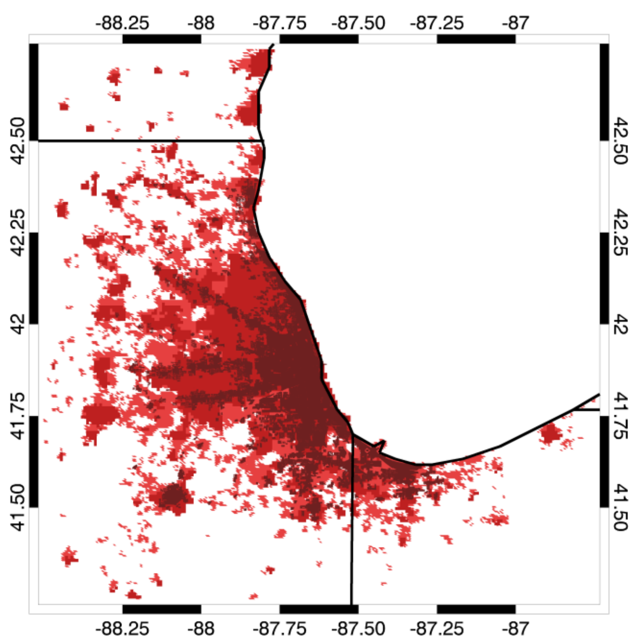

Figure 24. Urbanization factor showing 2012, 1992, and 1932 urban land extent in the Chicago area. For the model, the 1932 was classified as TEB “Old Urban” and urbanization after that was “Suburban”.

5.4 Results

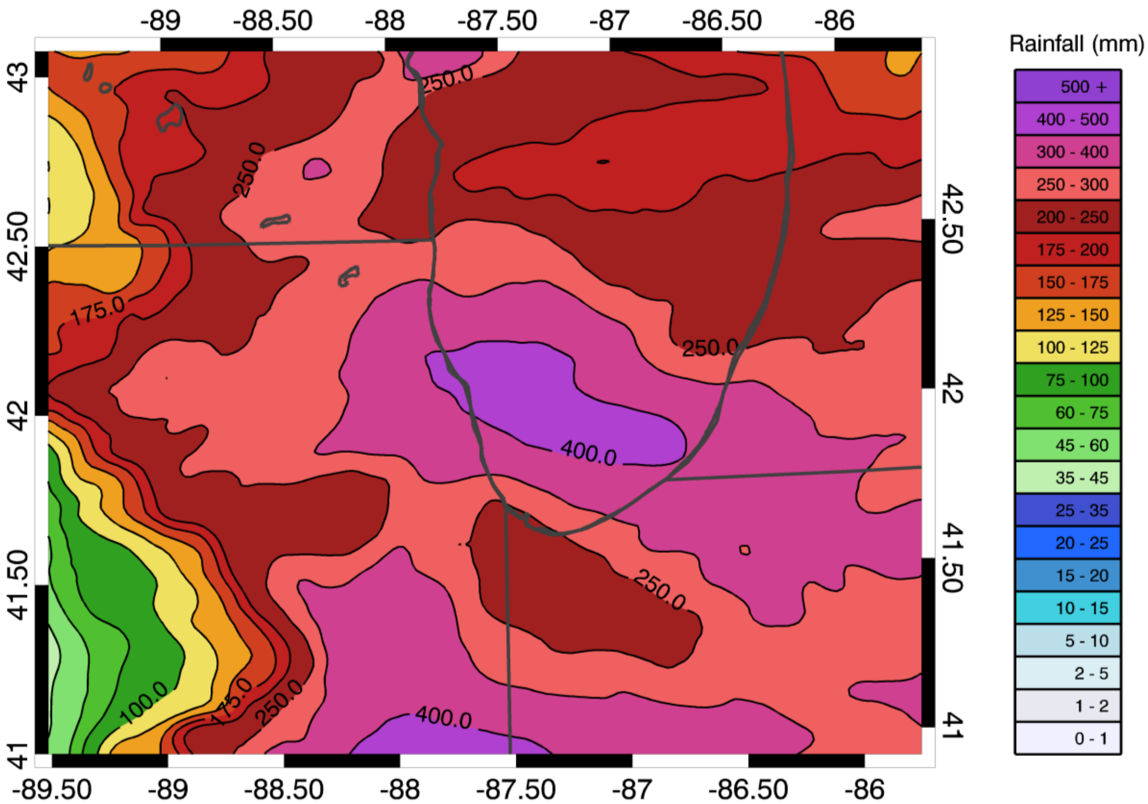

Figure 25. Control (no urban land) results for the seasonal simulation. Rainfall totals are 15 – 20% greater than observation, but the relative distribution compares favorably to the observations.

Based on the RAIL framework, the results of the simulations will be presented as urban-rural comparisons to isolate the individual urban effects. Figure 25 shows the simulation total rainfall for the Control (no urban) simulation. The rainfall variability compares favorably to the PRISM values but simulated rainfall totals are 15 – 20% greater than observed on a regional basis. This wet bias is due to the 2-km grid spacing on the finest model, which for a mesoscale urban model of this type will produce a wet bias. The simulated thunderstorm updrafts are slightly more intense than with a finer grid spacing which leads to larger raindrops. However, the characteristics of individual simulated storms was very reasonable: intensity, duration, and size were realistic and compared favorably to what was observed. The wet bias only became very apparent as the sum of the total seasonal simulation. In the Control, the lack of an urban land surface produces a simulation where downwind rainfall is reduced by the presence of Lake Michigan (ff Notaro et al. 2013), thus simulating a locally reduced rainfall region where the contemporary La Porte Anomaly would have been observed (near 41.5N, -87.25W).

By comparing the land cover simulations to the control, the simulated combined effects of urban rainfall modification can be seen. Figure 27 shows the 1932 rainfall difference from the non-urban simulation. There is a significant rainfall enhancement near the location of La Porte, IN downwind of Chicago. The seasonal 120 mm increase represents an approximately 25-30% regional rainfall enhancement from the total urban effect. By 2012, the 2012x1 simulation (Fig. 26) simulates a more westward downwind peak in rainfall, which agrees with historical observations. There has also appeared a local rainfall enhancement at the upwind edge, which also agree with the observations. The 2012 downwind anomaly represents approximately a 15-20% rainfall enhancement while the upwind anomaly is 20% enhanced. The interim land surface results show the development and migration of both the upwind and downwind anomalies as simulated in the model. In the 1962 simulation (Fig. 29), the upwind enhancement has begun to form, and becomes more complete by the 1992 simulation (Fig. 28). The downwind anomaly in 1962 is its greatest value compared to the regional average: nearly 50%. The 1992 downwind anomaly is less than either than 1962 or 1932 at 20-25%. The overall effects of the changing land surface in time are realized with:

1) Progressive development of an upwind rainfall enhancement between 1932 and 2012.
2) Westward movement of the downwind anomaly

Non-linear change to the intensity of the downwind anomaly. It becomes more pronounced between 1932 and 1962, but gradually decreases in intensity through 1992 to 2012.

The specific aerosol loading effects from the simulation can be determined by comparing the 2012x2 and 2012x0 simulations with the 2012x1. In the same way, the land surface only effects can be seen by comparing the 2012x0 (homogeneous aerosols with urban land) to the non-urban Control. Fig. 31 show the difference between the 2012x0 and the Control: There is a similar magnitude upwind rainfall enhancement to the 2012x1 simulation (15-20%) but a minimal if any

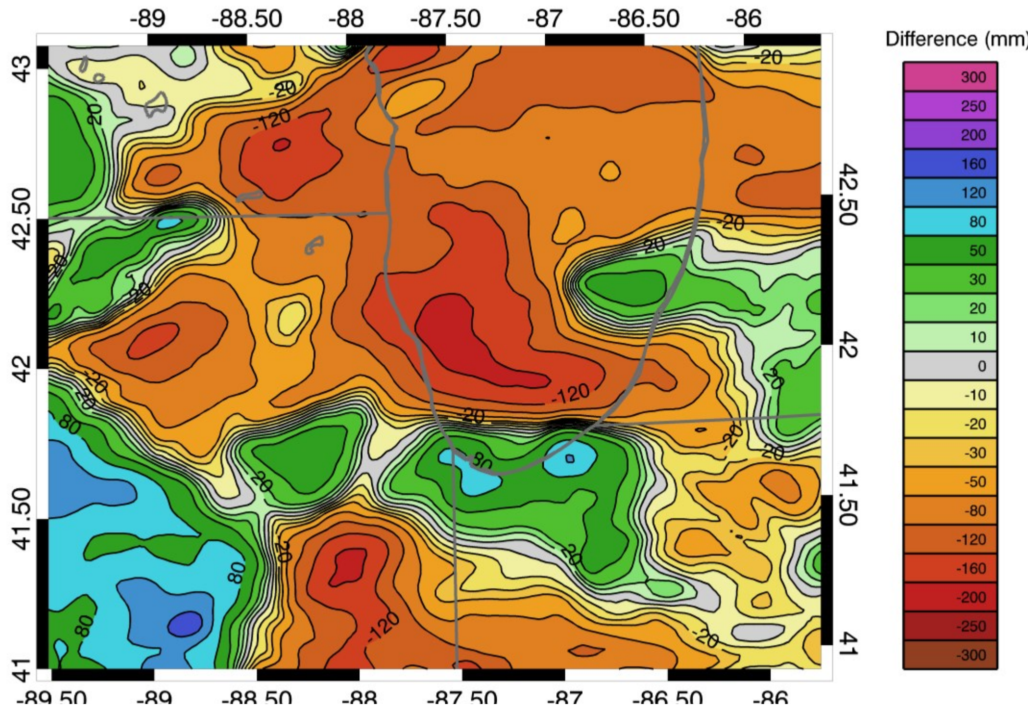

Figure 27. Difference between 1932 simulated rainfall and Control (no urban)

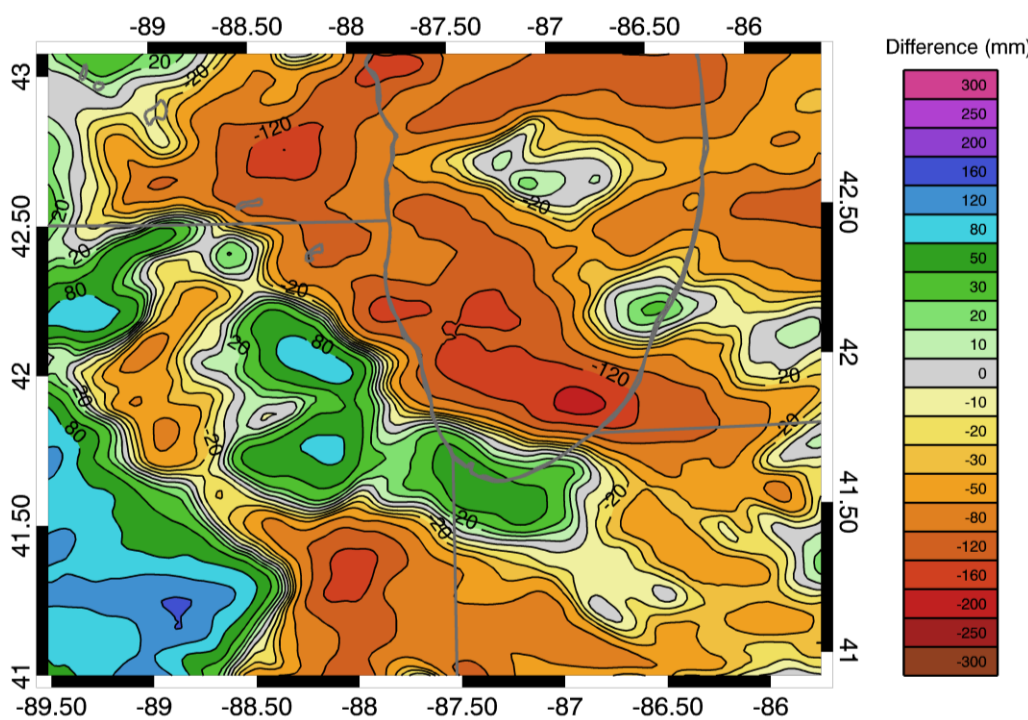

Figure 26. Difference between 2012 simulated rainfall and Control (no urban)

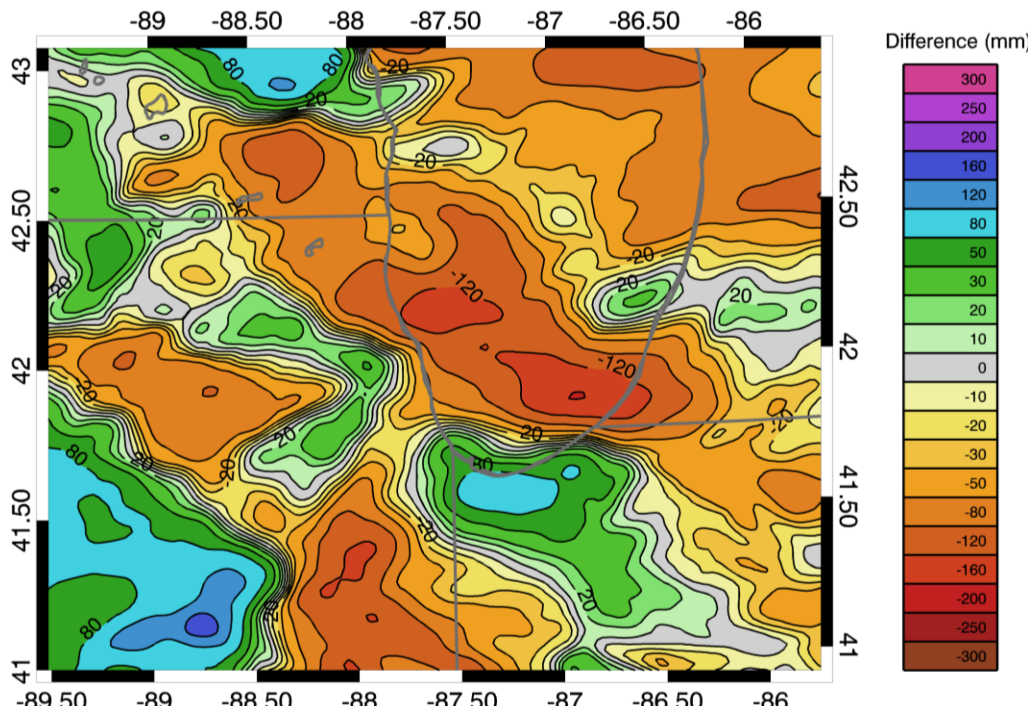

Figure 29. Difference between 1992 simulated rainfall and Control (no urban)

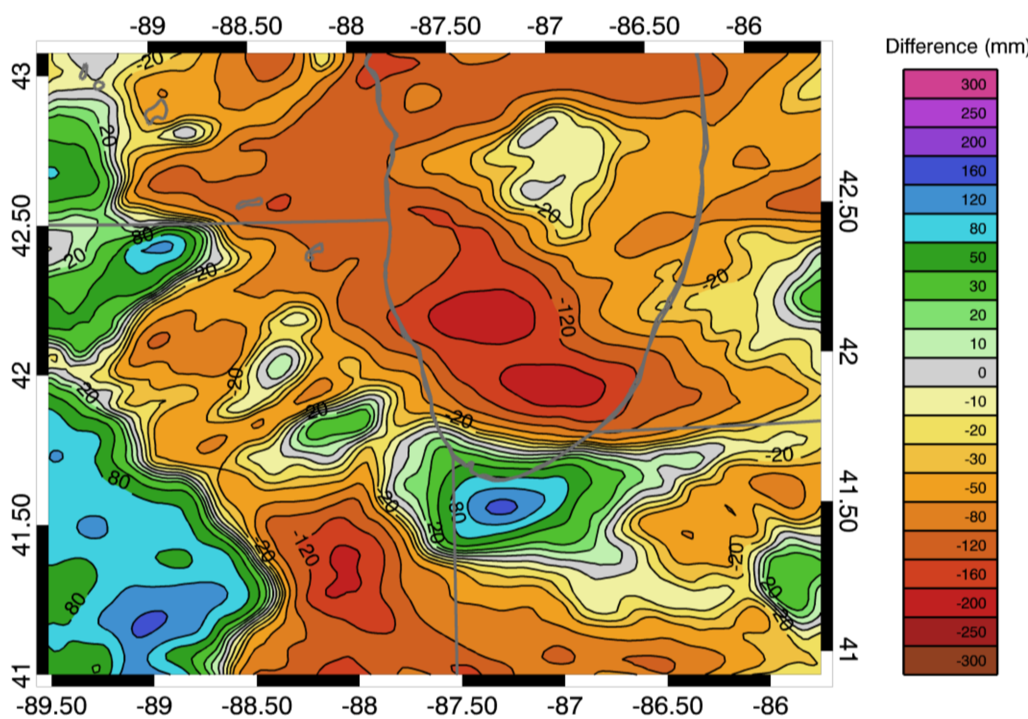

Figure 28. Difference between 1962 simulated rainfall and Control (no urban)

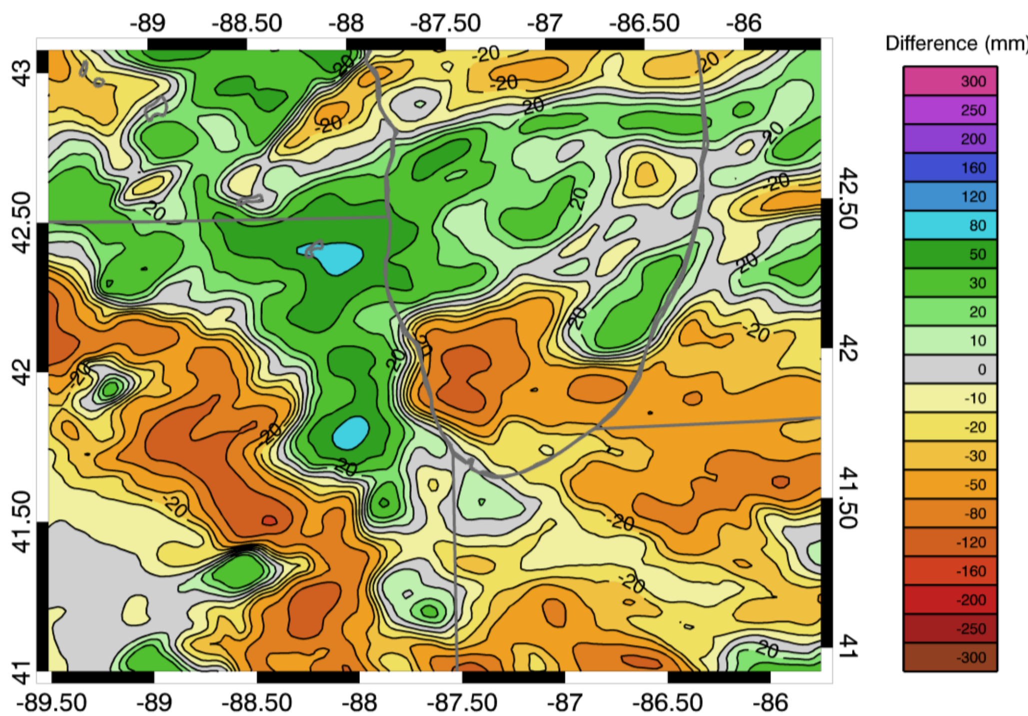

Figure 31. Difference between 2012x0 and Control

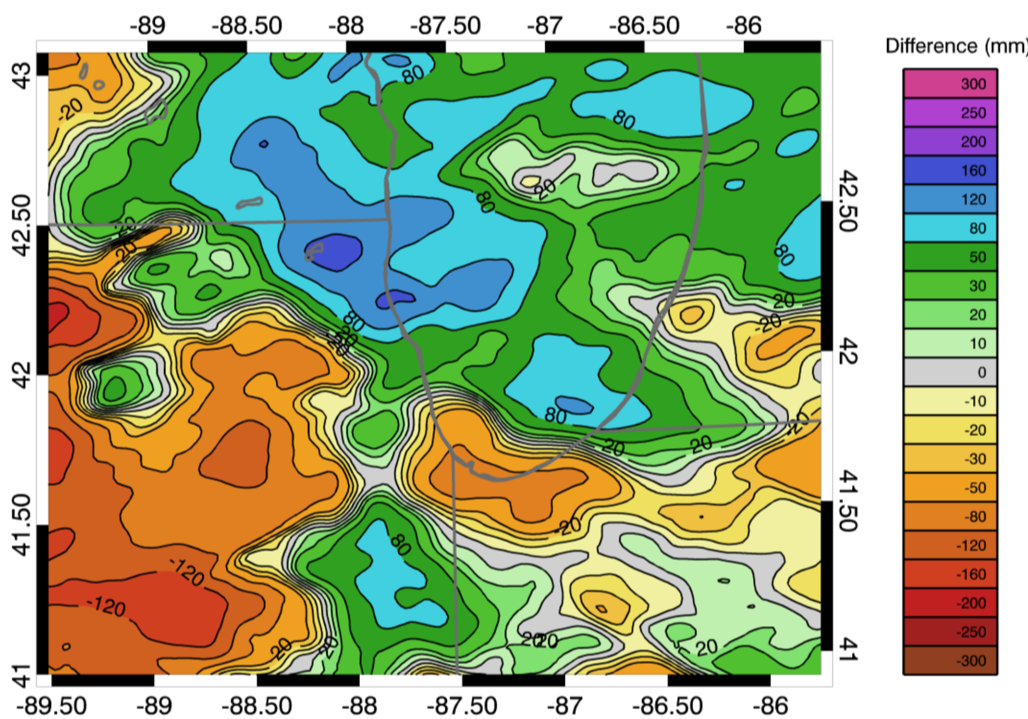

Figure 30. Difference between 2012x0 and 2012x1

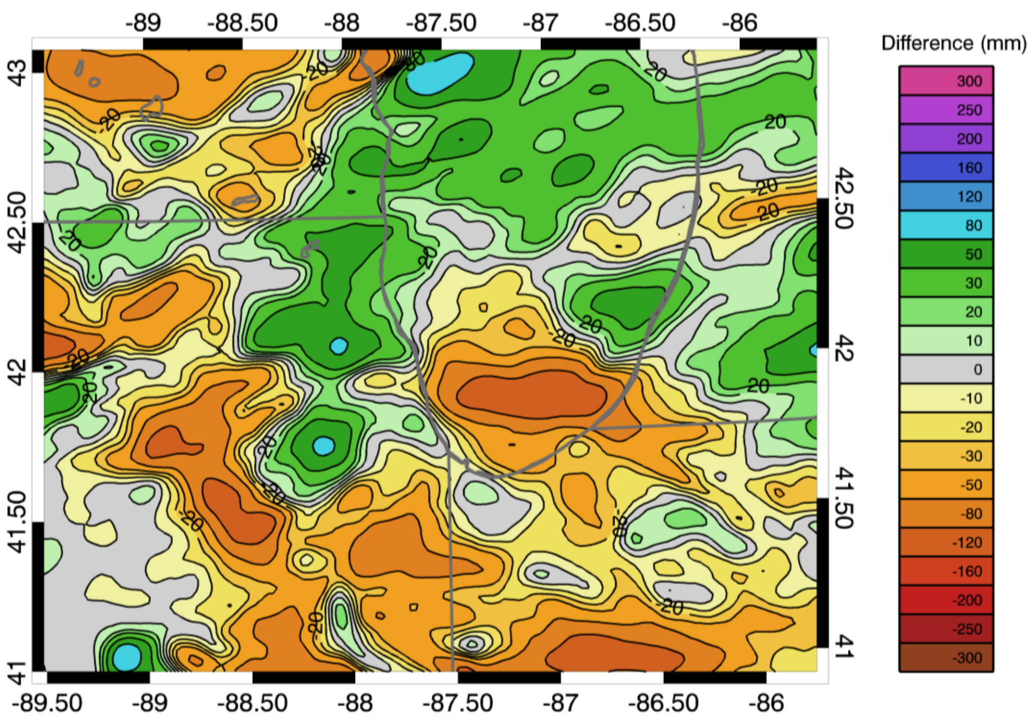

Figure 32. Difference between 2012x2 and 2012x1

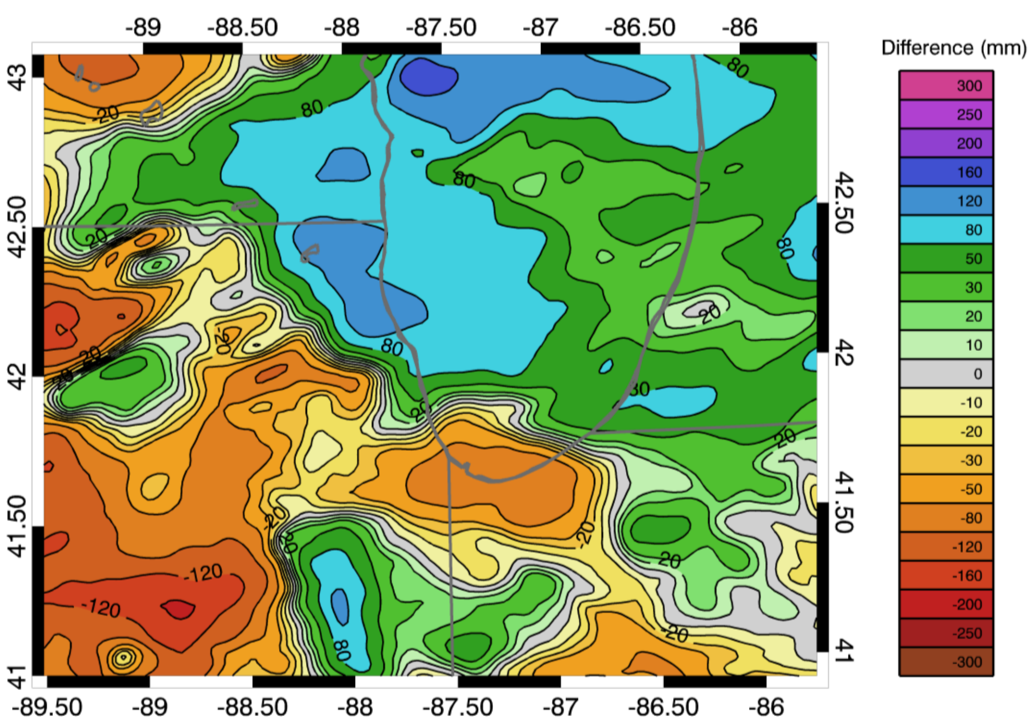

Figure 33. Difference between 2012x2 and Control

significant downwind rainfall enhancement. There is also an increased reduction of rainfall directly to the east of the urban footprint over Lake Michigan. Fig. 30 shows a similar comparison of the aerosol effects between 2012x0 and 2012x1. The homogeneous aerosols produce a simulation with a slightly wetter upwind rainfall enhancement (5-10%) but no downwind enhancement. Finally, Fig. 33 shows the difference between the double aerosol loading 2012x2 and 2012x1. For this, most of the upwind enhancement has disappeared as has much of the downwind enhancement. Fig. 32 corroborates this by showing that there is a decreased upwind enhancement compared to the Control, and the downwind effect is also reduced.

5.5 Discussion

Based on the results of the La Porte Anomaly simulations, the specific land-atmosphere and aerosol-cloud interactions leading to urban thunderstorm modification can be separated. The factors behind the historical variability of the rainfall anomaly are also revealed through the combined effects from the land surface and aerosol effects. The relevant rainfall effects are the location and relative intensity of the downwind rainfall anomaly, the existence and characteristics of upwind rainfall modification, and the changing characteristics of thunderstorms as they pass across the urban environment. The rainfall effects change in time:

- In 1932, there is a downwind anomaly located farthest to the east, that is 25% greater than the Control.
- By 1962, an upwind anomaly has begun to develop, and the downwind anomaly has shifted westward, and is its greatest increase compared to the control: nearly 50% enhancement.
- By 1992, the intensity of the downwind anomaly has decreased to below its 1932 intensity, while the upwind enhancement has increased.
- And by 2012, the downwind rainfall anomaly is 15-20% greater than the control, with a stonger, more significant upwind enhancement.

These results show that the location of the downwind anomaly is related to the location of the upwind edge of Chicago’s urban footprint. The primarily westward suburban expansion between 1932 and present means that an incipient thunderstorm begins modifying at a more westward location and completes that modification at one, thus the location of the downwind anomaly appears to move from east-to-west as the urban area expands. As the upwind edge fills out from ragged development surround rail lines into Chicago to the more continuous urban footprint, there is a more prompt, consistent location for the urban land surface to prompt the beginning of thunderstorm modification.

The aerosol loading scenarios produce two similar results, but with different explanations. By decreasing aerosol loading to homogeneous values, there is still an upwind modification, indicating it is forced from the urban land surface. The increase in downwind rainfall disappears, indicating that it is due to aerosol-cloud interaction. This is similar to observations showing that weekend thunderstorms do not produce increased downwind rainfall. Within the model, the aerosol behavior is consistent with a narrowed cloud droplet distribution which appears in the 2012x1 simulation but not in the 2012x0 simulation. In the 2012x2 simulation, the surface emissions are doubled, and in this scenario the aerosol loading is large enough to completely suppress rainfall enhancement. The 2012x2 cloud characteristics have an extremely narrow cloud droplet distribution wherein rainfall invigoration from enhanced riming does not occur, and thus the downwind rainfall enhancement disappears. The 2012x2 simulations provide a consistent explanation as to how the increased pollution of the 1970s caused the observed La Porte Anomaly to vanish during that decade.

From these results, a more unified explanation of urban thunderstorm modification can be produced. Urban thunderstorm modification occurs as a combination of known land surface and aerosol effects:

1) A thunderstorm approaches the edge of an urban area. There is encounters increased roughness and most importantly a vertical velocity perturbation from the UHI circulation. The more consistent the urban boundary, the stronger the perturbation, and the greater potential for enhanced rainfall at the urban boundary.
2) The cloud water within the urban thunderstorm is temporarily depleted from upwind rainfall enhancement, so there is a local minimum of rainfall. This local minimum is not necessarily at a "city center" but rather depends on the size of the urban footprint and the speed of the thunderstorm as it progresses across the urban area.

3) Throughout the thunderstorm modification process, urban aerosols are changing the cloud properties. Cloud water is reloaded from thunderstorm inflow, but the narrow cloud droplet distribution reduces rainfall efficiency. If the storm passes out of the urban footprint before the aerosol modification to produce heavy rain is complete, the comparable downwind land surface perturbation is reduced as the thunderstorm rainfall has diminished the downwind UHI.
4) In a moderate level of urban aerosol loading, the narrow cloud droplet distribution eventually enhances the growth of cloud graupel via enhanced riming. This ultimately leads to larger rain drops and a "downwind" region of enhanced rainfall. In highly polluted environments, the cloud droplet distribution is too small and narrow to produce enhanced rainfall.

The location of a "downwind" rainfall enhancement is relative to the size of the urban area and the speed of the thunderstorm. The upwind edge of an urban area is a fixed location at a given time. But the total urban rainfall enhancement is time-dependent. Thus, a slower moving thunderstorm could produce a downwind rainfall enhancement over an urban space, while a faster moving thunderstorm produces a rainfall enhancement at a more downwind location. The location of the La Porte Anomaly is fundamentally a seasonal to climatological feature. Individual thunderstorms modify, but the combined local increases and decreases in rainfall intensity may not change the total rainfall a significant amount. The process level modification of individual thunderstorms averaged over a longer time period is what produces the more observable rainfall "anomaly" at the seasonal level. But the simulation indicates that the combination of these processes can be separated and explained in a consistent way.

5.6 References

Changnon, S. A., 1980: More on the La Porte Anomaly: A Review. *Bull. Am. Meteorol. Soc.*, **61**, 702–711, doi:10.1175/1520-0477(1980)061<0702:MOTLPA>2.0.CO;2.

CRPA, 1930: *Subdivided and occupied land in the vicinity of Chicago*. Chicago, 1 map; 84 x 72 cm pp.

Cumbie-Ward, R. V., and R. P. Boyles, 2016: Evaluation of a High-Resolution SPI for Monitoring Local Drought Severity. *J. Appl. Meteorol. Climatol.*, **55**, 2247–2262, doi:10.1175/JAMC-D-16-0106.1.

Friedl, M., and D. Sulla-Menashe, 2015: MCD12Q1 MODIS/Terra+Aqua Land Cover Type Yearly L3 Global 500m SIN Grid V006 [Data set]. doi:10.5067/MODIS/MCD12Q1.006.

Fry, J. A., M. J. Coan, C. G. Homer, D. K. Meyer, and J. D. Wickham, 2009: *Completion of the National Land Cover Database (NLCD) 1992-2001 Land Cover Change Retrofit Product*. 18 pp.

Lyons, C. E., and D. H. Stedman, 1991: *Remote Sensing Enhanced Motor Vehicle Emissions Control for Pollution Reduction in the Chicago Metropolitan Area: Siting and Issue Analysis*. 75p pp.

NCEI, 2007: *State of the Climate: Drought for August 2007*.

Notaro, M., K. Holman, A. Zarrin, E. Fluck, S. Vavrus, and V. Bennington, 2013: Influence of the Laurentian Great Lakes on Regional Climate. *J. Clim.*, **26**, 789–804, doi:10.1175/JCLI-D-12-00140.1.

Sarkar, M., 2011: *How American Homes Vary by the Year They Were Built*. Washington, D.C.,.

CHAPTER 6. A MULTICITY SIMULATION OF A THUNDERSTORM IMPACTING BIRMINGHAM, ALABAMA

This chapter presents a single thunderstorm simulation motivated by the question: How do multiple cities interact together to impact their local and regional climate? More specifically, how far must two cities be separated to be considered independent and distinct in terms of their own local climate? Urban thunderstorm modification impacts both local and regional hydrology. Climate models also require an understanding of whether a local feature such as urban weather modification can be scaled into a regional one (Oleson 2012).

6.1 Introduction

Based on the work presented in Chapter 4 (Schmid and Niyogi 2013), the urban land surface of a city with a certain size (i.e. diameter D) would fully modify a thunderstorm in the time it takes for the perturbation from the surface to be communicated throughout the storm via its updraft. By that reasoning, the thunderstorm becomes "rural" again once the non-urban land surface has communicated through the storm and removes the urban modification characteristics: that is $2D$. So, City B is independent from City A if it is twice the distance away from the size of City A. This reasoning is echoed by conclusions in Niyogi et al. 2011 and Debbage et al. 2015. However, these hypotheses only consider the role of the urban land surface. Based on observation and simulations, urban aerosols are the mechanism which sustain the observed precipitation enhancement as a thunderstorm passes over an urban land surface, and those aerosols can be transported well downwind of their source.

The combined influence of multiple cities has been shown to increase heavy rainfall potential, both within the urban space and downwind. The UHI of a large metropolitan area may propagate downwind to increase rainfall in nearby satellite cities (Wan et al. 2013). And flash flood potential has been shown to be greater in broadly connected megacities (Yeung et al. 2015; Zhang et al. 2011). Urban aerosols can be transported even farther than what the land surface of two connected or disconnected cities. Urban pollution can be detected thousands of kilometers from its source (Koo et al. 2008; Wang et al. 2014), and specific studies have shown direct cloud and precipitation modification at least 500 km from the source of urban aerosols (Finardi et al., 2014). Because of the potential for distant thunderstorm modification via aerosol transport, otherwise disconnected cities within a broader region may influence each other via climate interaction in addition to human transport. This revives the concept of regional and superregional interconnections forming an urban climate archipelago (Sailor et al. 2016; Shepherd et al. 2013).

6.2 Model Setup

On 15-Jun 2009, a bow echo passed directly over Birmingham, Alabama and appeared to split as it crossed the urban area. There was relatively low surface based instability (CAPE < 1000 J·kg^{-1}), making a storm susceptible to urban modification, but the relatively strong mid-level CAPE (3000 J·kg^{-1}) supported a longer lived mesoscale convective system which formed that day. In the early stages of this storm's formation, it had passed over Memphis, Tennessee, 300 km upwind of Birmingham. Based on the storm's formation and track, it could represent an example of two well separated cities modifying the same thunderstorm. Figure 34 shows the observed evolution of the bow echo to be simulated as it formed and moved split over Birmingham.

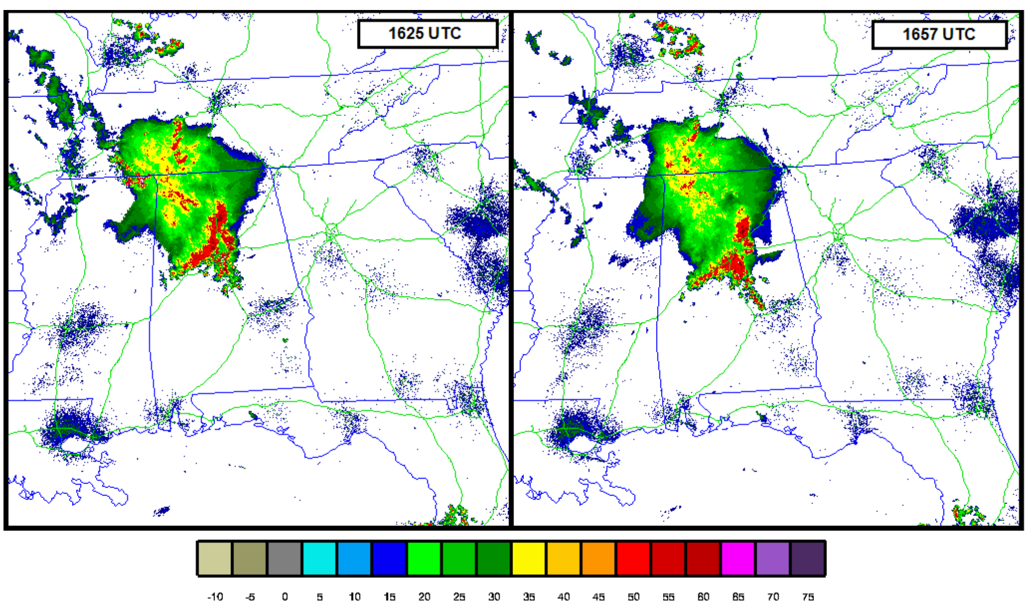

Figure 34. Composite radar showing mesoscale convective system splitting over Birmingham, AL.

To simulate this event, the urban RAMS (Chapter 3) with surface emissions was used with different land surface and aerosol scenarios. NAM reanalysis was used to initialize the model and run it from 14-Jun 2009 at 00UTC to 16-Jun 2009 at 12UTC on three nested grids at 16km – 4km – 1km with corresponding time steps of 24s – 6s – 1s, and the Kain-Fritsch convective parameterization on the coarsest grid. details the aerosol emissions and land surface characteristics of each scenario. The Memphis4 simulation places a second 1km inner grid, also emitting surface aerosols, centered over Memphis, TN. The grid locations and corresponding urban land cover is shown in Figure 35.

Table 5. Scenario names and descriptions

Scenario Name	**Land Cover**	**Aerosol Loading**	**Rural CCN**
Emit x1 (Control)	standard	1.0	500
Emit x1/2	standard	0.5	500
Emit x2	standard	2.0	500
Emit x3	standard	3.0	500
Emit x4	standard	4.0	500
Memphis4	Extra inner grid	1.0	500
Homogeneous	standard	0.0	1500
NoCity	no urban	0.0	1500
NoUrban	no urban	0.0	500

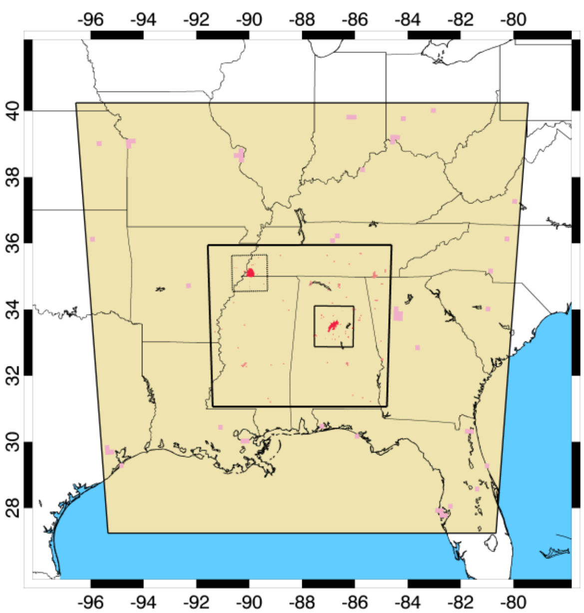

Figure 35. Grid structure and urban footprint for simulations

6.3 Storm Tracking Algorithm

In order to analyze the changing features of a model simulated storm, traveling in space and time, we employed an objective technique to track a storm between two output analyses. Our technique is functionally similar to the Thunderstorm Identification, Tracking, Analysis, and Nowcasting (TITAN) algorithm but specialized for model output rather than observational radar.

1) Storms at timestep t = n, were identified using connected components to label regions where dbZ > 30. Regions smaller than 5 x 5 grid cells were discarded.
2) Following the TITAN algorithm, substorms within each 30+ dbZ region were separated into their own individual cell if they had a peak dbZ greater than 45 (Han et al. 2009).
3) At timestep t = n+1, we employed a hybrid overlap – distance metric to determine what storm at t = n+1 corresponds to a storm at t = n (Lakshmanan and Smith 2010). Unambiguously matched storms were assigned.
4) If there was ambiguity between t = n and t = n+1 for two or more storms, utilized a minimized (but not optimized) cost function technique to determine which storms were matched. The non-optimal technique was necessary as one storm at t = n, can be matched to two or more storms at t = n+1 (splitting), or vice versa (merging).

The storm tracking technique, over 80 model output analyses every 20-min, perform very well compared to subjective human identification. It only missed a single simulated cell merger, one step after formation. The tracking algorithm is essentially a post-processing implementation of TITAN without the need for a “forecast”, because given it is analyzing model output the “future” (t = n+1) is already “known” at the present. The tracking algorithm enabled a one-to-one comparison of the same simulated storm between two different model scenarios.

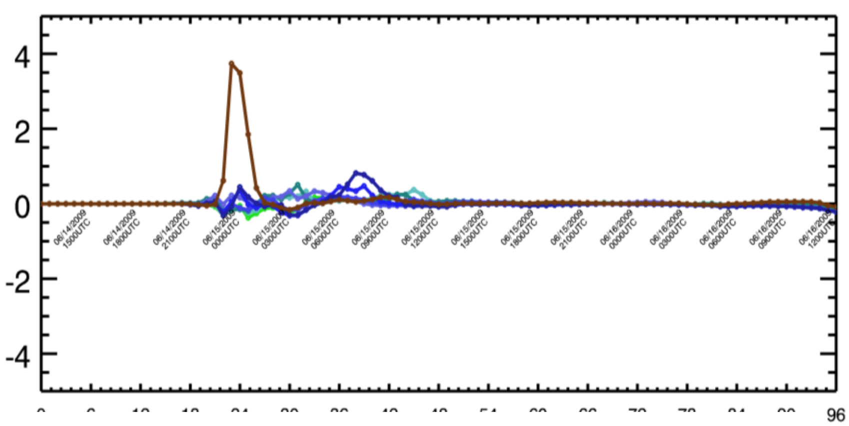

Figure 36. Mean rainfall rate for over the Birmingham urbanization for each scenario. The brown line indicates the Memphis4 simulation.

6.4 Results and Discussion

Most of the scenarios simulated two separate linear storm features. These manifested as a first storm forming earlier than observed, splitting, then forming a second storm which passed over Birmingham 1-3 hours after observed. The Emit x4 scenario produced a completely different regime due to the high aerosol loading diffusing upstream and was dominated by very brief intense storms. The only two scenarios which accurately simulated a single bow echo, which formed near Memphis then split over Birmingham were the Memphis4 and NoCity scenarios. Figure 36 shows how the only storm to have increased rain at the upwind edge of Birmingham was the Memphis4 scenario, where each of the other aerosol loading scenarios produced increased rainfall downwind of the city. The increased rain in the Memphis4 scenario at the upwind edge was what prompted the simulated splitting.

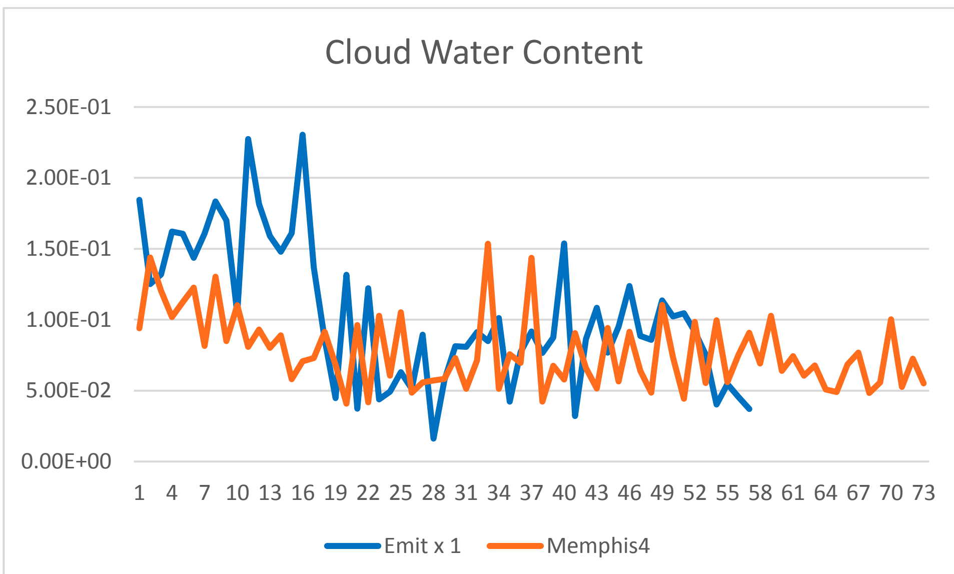

Figure 37. Cloud water content in time for the Control and Memphis4 simulations.

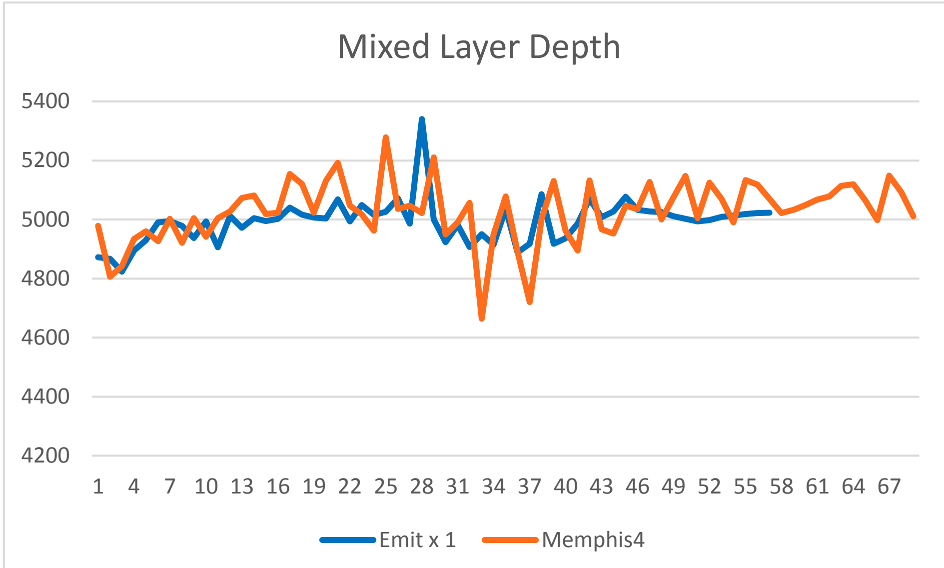

Figure 38. Same as Fig. 37 but for Mixed Layer Depth.

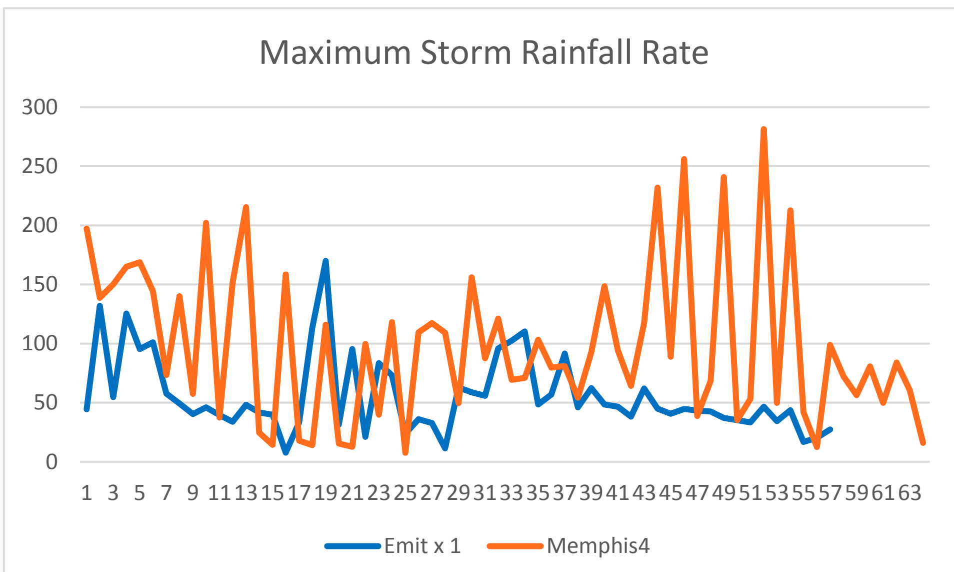

Figure 39 Same as Fig. 37 for maximum storm rainfall rate.

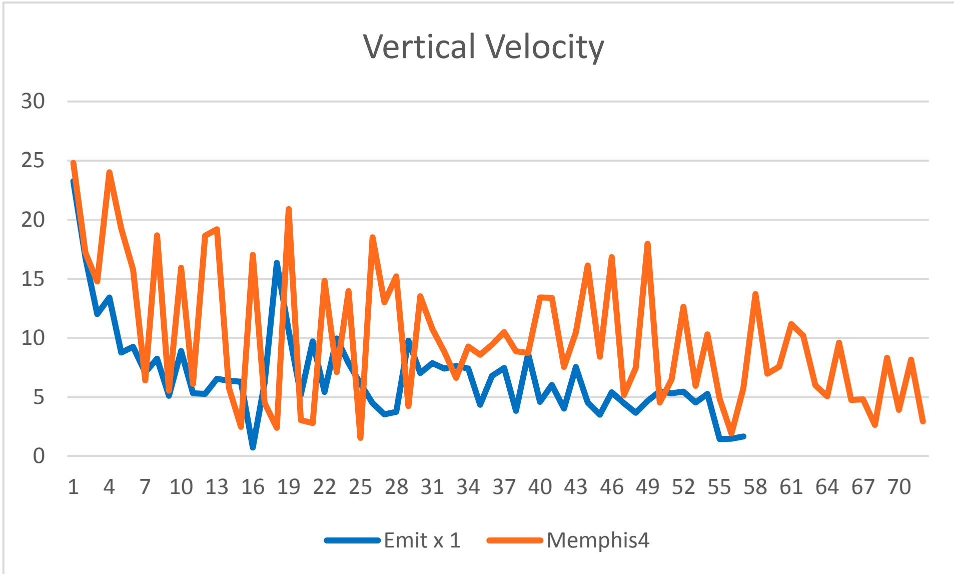

Figure 40 Same as Fig. 37 for vertical velocity.

The storm-centric properties of the Memphis4 simulation demonstrate how it was influenced by its upwind factors. Fig. 38 shows the properties of the Memphis4 storm which passed over Birmingham compared to the same storm simulated by the Control (Emit x1). At the beginning of its evolution, the Memphis4 storm has a lower but more consistent cloud water content due to the higher aerosol loading. The more numerous, but smaller cloud droplets prime the system for modification directly at the upwind edge of the Birmingham urban footprint. At the upwind edge, the vertical velocity perturbation (Hour 35) decreases the mixed layer depth (Fig. 37, 40), characteristic of rapid graupel growth. This is turn increases the rain rate, which rains through the cold pool, splitting the convective system (Fig. 39). This was only simulated in the Memphis4 case because of the upwind aerosol loading.

The results of most of the scenarios were not unexpected as typical behavior of urban thunderstorms, particularly aerosol loaded clouds were simulated as understood. Increasing aerosol emissions from Birmingham produced simulated storms with progressively narrower cloud droplet distributions. These storms modified by delaying the heaviest rainfall, then raining at higher rates, except for Emit x4. Yet none of the simulated storms' sensitivity to splitting came from the direct Birmingham emissions, but rather the upwind aerosol concentrations. The results are significant both from a simulation and regional climatology approach. The urban aerosols provide a connectivity between two distantly separated urban areas. And simulating the features requires an understanding of what is upwind as well as what is present.

6.5 References

Debbage, N., J. McLeod, J. Rackley, L. Zhu, T. L. Mote, and A. J. Grundstein, 2015: The Influence of Point Source Aerosol Emissions on Atmospheric Convective Activity in the Vicinity of Power Plants in Georgia, USA. *Pap. Appl. Geogr.*, **1**, 134–142, doi:10.1080/23754931.2015.1012430.

Han, L., S. Fu, L. Zhao, Y. Zheng, H. Wang, and Y. Lin, 2009: 3D Convective Storm Identification, Tracking, and Forecasting—An Enhanced TITAN Algorithm. *J. Atmos. Ocean. Technol.*, **26**, 719–732, doi:10.1175/2008JTECHA1084.1.

Koo, Y.-S., S.-T. Kim, H.-Y. Yun, J.-S. Han, J.-Y. Lee, K.-H. Kim, and E.-C. Jeon, 2008: The simulation of aerosol transport over East Asia region. *Atmos. Res.*, **90**, 264–271, doi:10.1016/j.atmosres.2008.03.014.

Lakshmanan, V., and T. Smith, 2010: An Objective Method of Evaluating and Devising Storm-Tracking Algorithms. *Weather Forecast.*, **25**, 701–709, doi:10.1175/2009WAF2222330.1.

Niyogi, D. and Coauthors, 2011: Urban Modification of Thunderstorms: An Observational Storm Climatology and Model Case Study for the Indianapolis Urban Region *. *J. Appl. Meteorol. Climatol.*, **50**, 1129–1144, doi:10.1175/2010JAMC1836.1.

Oleson, K., 2012: Contrasts between Urban and Rural Climate in CCSM4 CMIP5 Climate Change Scenarios. *J. Clim.*, **25**, 1390–1412, doi:10.1175/JCLI-D-11-00098.1.

Sailor, D., M. Shepherd, S. Sheridan, B. Stone, L. Kalkstein, A. Russell, J. Vargo, and T. Andersen, 2016: Improving Heat-Related Health Outcomes in an Urban Environment with Science-Based Policy. *Sustainability*, **8**, 1015, doi:10.3390/su8101015.

Schmid, P. E., and D. Niyogi, 2013: Impact of city size on precipitation-modifying potential. *Geophys. Res. Lett.*, **40**, 5263–5267, doi:10.1002/grl.50656.

Shepherd, J. M., T. Andersen, C. Strother, A. Horst, L. Bounoua, C. Mitra, and others, 2013: Urban Climate Archipelagos: A New Framework for Urban Impacts on Climate. *Earthzine*, 1–8.

Wan, H., Z. Zhong, X. Yang, and X. Li, 2013: Impact of city belt in Yangtze River Delta in China on a precipitation process in summer: A case study. *Atmos. Res.*, **125–126**, 63–75, doi:10.1016/j.atmosres.2013.02.004.

Wang, Y. and Coauthors, 2014: Assessing the effects of anthropogenic aerosols on Pacific storm track using a multiscale global climate model. *Proc. Natl. Acad. Sci. U. S. A.*, **111**, 6894–6899, doi:10.1073/pnas.1403364111.

Yeung, J. K., J. A. Smith, M. L. Baeck, G. Villarini, J. K. Yeung, J. A. Smith, M. L. Baeck, and G. Villarini, 2015: Lagrangian Analyses of Rainfall Structure and Evolution for Organized Thunderstorm Systems in the Urban Corridor of the Northeastern United States. *J. Hydrometeorol.*, **16**, 1575–1595, doi:10.1175/JHM-D-14-0095.1.

Zhang, D.-L., Y.-X. Shou, R. R. Dickerson, and F. Chen, 2011: Impact of Upstream Urbanization on the Urban Heat Island Effects along the Washington–Baltimore Corridor. *J. Appl. Meteorol. Climatol.*, **50**, 2012–2029, doi:10.1175/JAMC-D-10-05008.1.

CHAPTER 7. SYNTHESIS, CONCLUSIONS, AND FUTURE RESEARCH DIRECTIONS

The research presented here produces several unifying aspects for understanding urban rainfall modification. For an individual rainfall event, the paradigm by which an urban area modifies precipitation is a maximum-minimum-*likely* maximum distribution through time. At the upwind edge, rainfall from a well-developed thunderstorm increases due to land cover effects from the UHI vertical velocity. As the system progresses, there is locally reduced rainfall from the initial aerosol perturbations in the cloud combined with impacts from urban roughness. Eventually, if aerosol loading is not too intense, the urban aerosols enhance riming in the mixed layer of the cloud and increase rainfall intensity at a later location. This paradigm avoids the use of upwind-central-downwind or similar terminology because of the relative location of those places. "Upwind" is a fixed location: the urban-rural edge first encountered by a precipitating system. The system's modification to decrease and later increase rainfall depends on the speed of the storm as it crosses the urban area. "Downwind" could be anywhere from literally downwind of the urban space in a rural area to the center of the city itself. Numerical model simulations enable us to separate factors to determine the process-based effects behind this urban thunderstorm modification paradigm.

Observing the rainfall modification requires very careful use of regular measurements. Given that an individual thunderstorm undergoes changes to its rainfall rate, precipitation totals cannot necessarily diagnose modification, as certain regional rainfall may not change in quantity but in intensity due to competing rainfall reduction and enhancement. Rainfall rate can be inferred from weather radar, and relative storm intensity can be inferred from lightning strike rate, but other storm properties such as vertical wind velocities and cloud properties are not observed operationally. The overall changes to rainfall patterns by urban areas are best observed at a seasonal to climatology time scale. The La Porte Anomaly's continued existence was reestablished using this technique. But it exists as an average of individual events, and it cannot necessarily be used to determine the providence of an individual thunderstorm. The best practice for observing urban rainfall modification is to separate the seasonal effects from the individual storms: seasonal rainfall distribution affects local hydrology and water budgets, while individual thunderstorm modification impacts regions prone to flash flooding. Knowing the speed and direction of an individual storm as it approaches an urban area can give guidance as to how its modification could impact flood prone areas.

Best practice in numerical modeling urban thunderstorm modification follows observational analysis: individual events should be evaluated from a storm-centric approach, seasonal anomalies should be considered from a regional approach. The research presented here refined a numerical model to include an urban canopy parameterization and urban aerosol cloud interaction. A stated goal for urban modeling is a 100-m simulation of the 2024 Paris Olympics (Masson et al., 2020). Aside from the core model improvements to handle numerical simulations at that resolution, such a model requires direct building energy simulations, spectral bin microphysics for the cloud-aerosol interaction, improved chemistry with direct nucleation, and a sophisticated local climate zone land surface model. Modeling this type of event requires improved surface and remote sensed spatial measurements of aerosol concentrations, and potentially a closed human component of the weather model.

Part of the development of surface emissions in the urban RAMS parameterization involved simulating human behavior: people travel from their homes to work[8], the aerosols produced by their cars enter the atmosphere, modify clouds, and change rain patterns. Closing the loop of this cycle would involve simulating how the people then respond to the modified rainfall. Human behavior in the urban system is an integral component to understanding urban weather. Over 50% of the population lives on 0.6% of the land surface, and the weather modifying effects of that land surface only exist because people have developed it. Understanding and predicting the added risks due to urban rainfall modification is crucial to improving our condition as more people move to urbanized spaces.

[8] May 2020: Ironically, this is not the case because of the current pandemic.